Algebraic combinatorics for computational biology

by

Nicholas Karl Eriksson

B.S. (Massachusetts Institute of Technology) 2001

A dissertation submitted in partial satisfaction of the
requirements for the degree of
Doctor of Philosophy

in

Mathematics

and the Designated Emphasis

in

Computational and Genomic Biology

in the

GRADUATE DIVISION
of the
UNIVERSITY of CALIFORNIA, BERKELEY

Committee in charge:

Professor Bernd Sturmfels, Chair
Professor Lior Pachter
Professor Elchanan Mossel

Spring 2006

The dissertation of Nicholas Karl Eriksson is approved:

Chair Date

Date

Date

University of California, Berkeley

Spring 2006

Algebraic combinatorics for computational biology

Copyright 2006
by
Nicholas Karl Eriksson

Abstract

Algebraic combinatorics for computational biology

by

Nicholas Karl Eriksson
Doctor of Philosophy in Mathematics

University of California, Berkeley

Professor Bernd Sturmfels, Chair

Algebraic statistics is the study of the algebraic varieties that correspond to discrete statistical models. Such statistical models are used throughout computational biology, for example to describe the evolution of DNA sequences. This perspective on statistics allows us to bring mathematical techniques to bear and also provides a source of new problems in mathematics.

The central focus of this thesis is the use of the language of algebraic statistics to translate between biological and statistical problems and algebraic and combinatorial mathematics. The wide range of biological and statistical problems addressed in this work come from phylogenetics, comparative genomics, virology, and the analysis of ranked data. While these problems are varied, the mathematical techniques used in this work share common roots in the field of combinatorial commutative algebra. The main mathematical theme is the use of ideals which correspond to combinatorial objects such as magic squares, trees, or posets. Biological problems suggest new families of ideals, and the study of these ideals can in some cases be useful for biology.

Professor Bernd Sturmfels
Dissertation Committee Chair

To Nirit

Contents

List of Figures

List of Tables

Acknowledgements

Above all, thanks to my advisor, Bernd Sturmfels, from whom I have learned much about the mysterious processes of doing and communicating mathematics. As essentially my second advisor, Lior Pachter has been an excellent guide through the rugged terrain that lies between mathematics and computational biology.

I would not be in this position without a host of mentors and teachers, particularly Jim Cusker and Ken Ono, who started me on this path of studying mathematics. Along the way, it has been a pleasure to learn from my amazing coauthors: Niko Beerenwinkel, Persi Diaconis, Mathias Drton, Steve Fienberg, Jeff Lagarias, Garmay Leung, Kristian Ranestad, Alessandro Rinaldo, Seth Sullivant, and Bernd Sturmfels.

I am grateful for support from the National Science Foundation (grant EF-0331494), the DARPA program *Fundamental Laws in Biology* (HR0011-05-1-0057), and a National Defense Science and Engineering Graduate Fellowship. Due to this support and support from my advisors, I have had the good fortune to travel the world learning and teaching mathematics. From Palo Alto to Spain to Argentina and many places in between, the people I have met on these trips have enriched my mathematical life.

As this thesis depends heavily on computation, I am indebted to the people who have written programs which proved invaluable for my research. In particular, I thank Raymond Hemmecke, whose program `4ti2` was vital for Chapters 2 and 3. Also, thanks to Susan Holmes and Aaron Staple for writing the `R` code used in Chapter 2.

Most importantly, my parents, sister, and wife are each more responsible for my successes than they or I usually realize. They have always supported, accepted, and nourished me in countless ordinary and extraordinary ways.

Chapter 1

Introduction

The main theme of this thesis is the interplay between statistical models and algebraic techniques. More and more, the fields of statistics and biology are generating a wealth of interesting mathematical questions. In return, discrete mathematics provides techniques for the solution of these problems, as well as a theoretical framework from which to ask new questions. From this interplay, the field of *algebraic statistics* has emerged. Its main purpose is the development of computational and theoretical techniques in algebra and combinatorics for applications to practical statistical problems. These techniques supply a valuable mathematical language for the study of computational biology.

Computational biology has been a wonderful source of problems in combinatorics and combinatorial computer science due to the discrete structure of biological objects, notably DNA. For example, counting alignments and counting RNA secondary structures are typical enumerative problems [104]. For other connections between the fields, we note how biology has motivated mathematicians to better understand the structure of the space of trees [16] and how distance measures between signed permutations [41] provide methods for understanding genome rearrangement through evolution.

While biology provides a fount of such interesting questions, it is desirable at the end of the day to better understand real data. And because there is always error in experimental data, this problem requires the use of statistics. Thus, we must form a connection between statistics and mathematics that allows us to use the combinatorial properties of the underlying problems in order to analyze data in a rigorous, robust, and efficient way.

In this thesis, we provide a series of interrelated illustrations of how algebraic combinatorics can be used to increase our understanding of statistical and biological problems. We also demonstrate how biological questions can lead to interesting mathematics. The examples we study are drawn from statistics, phylogenetics, comparative genomics, and virology. The underlying mathematical philosophy is that statistical models can be viewed as algebraic varieties. Our examples draw from a small set of statistical models which we introduce in this chapter: exponential families, phylogenetic models, and Bayesian networks.

In the rest of this introduction, we will briefly outline the new field of algebraic statistics and explain the major algebraic, statistical, and biological ideas that will be used throughout the thesis. We refer the reader to the book [73] for more details.

1.1 Algebraic statistics

Algebraic statistics depends on a set of tools that allow us to translate problems in statistics into algebraic language. We assume the reader is familiar with the basic language of algebraic geometry, namely polynomials, ideals, and varieties. In addition, we will use Gröbner bases throughout the thesis as a computational tool. For a friendly introduction to ideals and Gröbner bases, see [27].

Let X be a discrete random variable taking values in the set $[n] = \{1, 2, \dots, n\}$. We write p_i as shorthand for $\Pr(X = i)$, the probability that X is in state i. Let Δ_{n-1} be the $(n-1)$ dimensional probability simplex, e.g.,

$$\Delta_{n-1} = \{(p_1, \dots, p_n) \in \mathbb{R}^n \mid p_i \geq 0, \quad \sum_{i=1}^{n} p_i = 1\}.$$

We will write Δ for the simplex Δ_{n-1} when the space is understood. A statistical model for X is simply a family of probability distributions $\mathcal{M} \subset \Delta$. We will restrict our attention to statistical models $\mathcal{M}$ which are given as the image of a polynomial parameterization. That is, for every vector of parameters $\theta = (\theta_1, \dots, \theta_d)$ we associate a probability distribution $(p_1(\theta), \dots, p_n(\theta)) \in \Delta$ where $p_1(\theta), \dots, p_n(\theta)$ are polynomials in d unknowns. Given such a polynomial map

$$p\colon \mathbb{R}^d \to \mathbb{R}^n$$
$$\theta = (\theta_1, \ldots, \theta_d) \mapsto (p_1(\theta), p_2(\theta), \ldots, p_n(\theta)),$$

the associated statistical model is given by $\mathcal{M} = p(\Theta)$ where Θ is an appropriate, non-empty, open set in $\mathbb{R}^d$, called the parameter space. If we are concerned with obtaining actual probability distributions via this map, we can either impose constraints on Θ in order to make sure that $p(\Theta) \subset \Delta$, or we can take the model to be $\mathcal{M} = p(\Theta) \cap \Delta$. However, we shall usually ignore this issue and will even assume that the ground field is $\mathbb{C}$ rather than $\mathbb{R}$ in order to work over an algebraically closed field.

A natural question we might ask about a statistical model is what relations among the probabilities $p_1, \ldots, p_n$ are satisfied at all points in the model p. Since p is a polynomial map, these relations are given by polynomials which can be found using Gröbner bases.

Example 1.1. Let X and Y be two binary random variables taking values in $\{0, 1\}$. We place the independence model on X and Y, e.g., $\Pr(X, Y) = \Pr(X)\Pr(Y)$. We write this model in terms of parameters $\alpha = \Pr(X = 0)$ and $\beta = \Pr(Y = 0)$, and we write $p_{ij} = \Pr(X = i, Y = j)$. Then the parameterization is given by

$$\begin{pmatrix} p_{00} & p_{01} \\ p_{10} & p_{11} \end{pmatrix} = \begin{pmatrix} \alpha\beta & \alpha(1-\beta) \\ (1-\alpha)\beta & (1-\alpha)(1-\beta) \end{pmatrix}$$

The following Singular [52] code computes the relations between the p_{ij} which characterize the image of the parameterization.

```
// create rings
  ring A=0,(p00,p01,p10,p11),lp;
  ring B=0,(alpha,beta),lp;
// create ring map A -> B
  map p = A,
          alpha*beta,
          alpha*(1-beta),
          (1-alpha)*beta,
          (1-alpha)*(1-beta);
// compute the kernel of the map
```

```
ideal B0 = 0;
setring A;
preimage(B,p,B0);
```

Singular outputs the following:

```
_[1]=p01*p10+p01*p11+p10*p11+p11^2-p11
_[2]=p00+p01+p10+p11-1
```

The second polynomial is the condition that the probabilities sum to one. The first polynomial doesn't look familiar, but after substituting $p_{11} = 1 - p_{00} - p_{01} - p_{10}$ for one of the factors p_{11} in the term p_{11}^2, we get the determinant of the joint probability matrix $p_{00}p_{11} - p_{01}p_{10}$ as expected. We actually did not need to make this polynomial homogeneous by hand, we could have made the map homogeneous instead and then added in the condition that the probabilities sum to one. Statisticians might recognize this determinant as the odds ratio $\frac{p_{00}p_{11}}{p_{01}p_{10}} = 1$ in the case where all probabilities are non-zero.

Next we give a slightly less trivial example which is a special case of two important classes of statistical models studied in this thesis: phylogenetic models and Bayesian networks.

Example 1.2. Let T be the "claw tree" with three leaves pictured in Figure 1.1. At the root, we have a binary random variable X with distribution (π_0, π_1). We also have binary random variables Y_1, Y_2, Y_3 at the three leaves. Our statistical model $\mathcal{M}$ will encapsulate the assumptions that the leaves are observed, the root is hidden, and the leaves are independent given the root.

This model is given parametrically by giving a root distribution (π_0, π_1) and conditional probabilities $\theta^k_{ji} := \Pr(Y_k = i \mid X = j)$. In terms of these parameters, the joint probabilities are given by

$$\begin{aligned}
p_{000} &= \pi_0\theta^1_{00}\theta^2_{00}\theta^3_{00} + \pi_1\theta^1_{10}\theta^2_{10}\theta^3_{10}, & p_{001} &= \pi_0\theta^1_{00}\theta^2_{00}\theta^3_{01} + \pi_1\theta^1_{10}\theta^2_{10}\theta^3_{11},\\
p_{010} &= \pi_0\theta^1_{00}\theta^2_{01}\theta^3_{00} + \pi_1\theta^1_{10}\theta^2_{11}\theta^3_{10}, & p_{011} &= \pi_0\theta^1_{00}\theta^2_{01}\theta^3_{01} + \pi_1\theta^1_{10}\theta^2_{11}\theta^3_{11},\\
p_{100} &= \pi_0\theta^1_{01}\theta^2_{00}\theta^3_{00} + \pi_1\theta^1_{11}\theta^2_{10}\theta^3_{10}, & p_{101} &= \pi_0\theta^1_{01}\theta^2_{00}\theta^3_{01} + \pi_1\theta^1_{11}\theta^2_{10}\theta^3_{11},\\
p_{110} &= \pi_0\theta^1_{01}\theta^2_{01}\theta^3_{00} + \pi_1\theta^1_{11}\theta^2_{11}\theta^3_{10}, & p_{111} &= \pi_0\theta^1_{01}\theta^2_{01}\theta^3_{01} + \pi_1\theta^1_{11}\theta^2_{11}\theta^3_{11}.
\end{aligned}$$

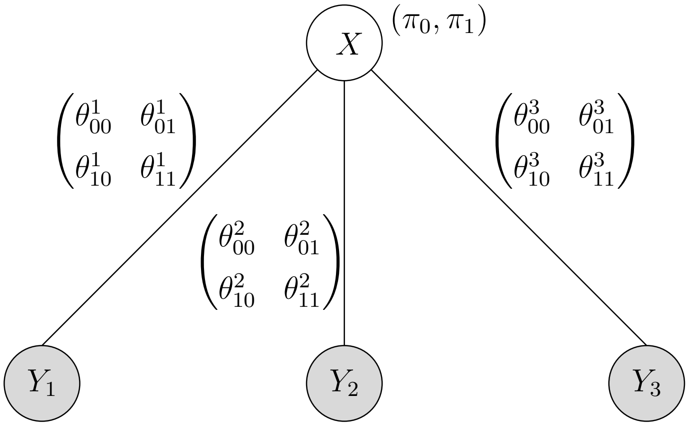
X
(π_0, π_1)
$\begin{pmatrix} \theta^1_{00} & \theta^1_{01} \\ \theta^1_{10} & \theta^1_{11} \end{pmatrix}$
$\begin{pmatrix} \theta^2_{00} & \theta^2_{01} \\ \theta^2_{10} & \theta^2_{11} \end{pmatrix}$
$\begin{pmatrix} \theta^3_{00} & \theta^3_{01} \\ \theta^3_{10} & \theta^3_{11} \end{pmatrix}$
Y_1
Y_2
Y_3

Figure 1.1: A simple statistical model.

We can see (for example, by using Singular) that the image of this map is all of $\mathbb{R}^8$. If we add in the constraints on the parameter space given by $\pi_0 + \pi_1 = 1$ and $\theta^k_{j0} + \theta^k_{j1} = 1$ for $j \in \{0, 1\}$ and $k \in \{1, 2, 3\}$, then we recover the fact that the sum of the joint probabilities is one:

$$p_{000} + p_{001} + p_{010} + p_{011} + p_{100} + p_{101} + p_{110} + p_{111} = 1.$$

However, this puts no additional constraints on the probability distribution.

But if we add the additional constraint that the root distribution is uniform (e.g., $\pi_0 = \pi_1 = \frac{1}{2}$), then we get a non-trivial polynomial invariant of degree 3 with 40 terms that the joint probabilities must satisfy:

$$\begin{gathered} p_{000}^2 p_{111} - p_{000}p_{001}p_{110} + p_{000}p_{001}p_{111} - p_{000}p_{010}p_{101} + p_{000}p_{010}p_{111} - p_{000}p_{011}p_{100} - \\ 2p_{000}p_{011}p_{101} - 2p_{000}p_{011}p_{110} - p_{000}p_{011}p_{111} + p_{000}p_{100}p_{111} - 2p_{000}p_{101}p_{110} + \cdots + \\ p_{011}^2 p_{100} - p_{011}p_{100}^2 - p_{011}p_{100}p_{101} - p_{011}p_{100}p_{110} + p_{011}p_{100}p_{111} - 2p_{011}p_{101}p_{110}. \end{gathered}$$

This resulting model is a hypersurface in the probability simplex Δ_7.

One of the strengths of algebraic statistics is that it allows us to find non-obvious, complicated relations such as this. The challenge, however, is to understand the combinatorial structure of such a polynomial and then to use this knowledge in order to find a meaningful statistical interpretation.

This model is called a naive Bayes model. It is a special case of the phylogenetic models that we will introduce in Section 1.3 and study in Chapters 3, 4, and 5. Phylogenetic models are special cases of Bayesian networks, which will be used in Chapter 6.

1.2 Toric ideals and exponential families

An important special class of polynomial ideals are the *toric ideals*. Toric ideals are prime ideals with a generating set of binomials. Equivalently, they are given by a monomial parameterization. In this section, we provide a brief introduction to the theory of toric ideals and their close relationship to the statistical models called exponential families. See [98] for more details about toric ideals.

Let $\mathcal{A}$ be a $d \times n$ matrix with integer entries written as $\mathcal{A} = (a_{ij}) = (\mathbf{a}_1, \ldots, \mathbf{a}_n) \in \mathbb{Z}^{d \times n}$. This matrix determines a map, $f^{\mathcal{A}}\colon (\mathbb{C}^*)^d \to \mathbb{C}^n$, given by

$$f^{\mathcal{A}}(\theta_1, \ldots, \theta_d) = \left(\prod_{i=1}^{d} \theta_i^{a_{i1}}, \prod_{i=1}^{d} \theta_i^{a_{i2}}, \ldots, \prod_{i=1}^{d} \theta_i^{a_{in}} \right)$$

Definition 1.3. The *toric variety* $X_{\mathcal{A}}$ is the closure of the image of the map $f^{\mathcal{A}}$. If every column of $\mathcal{A}$ has the same sum, we say that $\mathcal{A}$ is homogeneous and that $X_{\mathcal{A}}$ is a projective toric variety.

Definition 1.4. The toric ideal $I_{\mathcal{A}} \subset \mathbb{C}[\mathbf{p}]$ is the vanishing ideal of $X_{\mathcal{A}}$. Alternatively, we can define $I_{\mathcal{A}}$ via the (infinite) generating set

$$I_{\mathcal{A}} = \langle p^{\mathbf{u}} - p^{\mathbf{v}} \mid \mathcal{A}(\mathbf{u} - \mathbf{v}) = 0 \text{ and } \mathbf{u}, \mathbf{v} \in \mathbb{Z}^n_{\geq 0} \rangle.$$

If $\mathcal{A}$ is homogeneous, then the binomials $p^{\mathbf{u}} - p^{\mathbf{v}}$ are homogeneous.

Projective toric varieties correspond to an important subclass of exponential families, the *log-linear* models.

Definition 1.5. The *log-linear model* $\mathcal{M}_{\mathcal{A}}$ associated to $\mathcal{A} = (\mathbf{a}_1, \ldots, \mathbf{a}_n)$ is the probability distribution in Δ_{n-1} defined by

$$P_\theta(X = i) = \frac{1}{Z} e^{\langle \mathbf{a}_i, \theta \rangle} \qquad \text{for } 1 \leq i \leq n, \quad \theta \in \mathbb{R}^d.$$

where $Z = \sum_{i=1}^{n} e^{\langle \mathbf{a}_i, \theta \rangle}$ is a normalizing constant and $\langle , \rangle$ is the standard inner product on $\mathbb{R}^n$.

To see that $I_{\mathcal{A}}$ vanishes on $\mathcal{M}_{\mathcal{A}}$, notice that for $\mathbf{u} = (u_1, \ldots, u_n) \in \mathbb{N}^n$ with $\sum_{i=1}^{n} u_i = N$,

$$p^{\mathbf{u}} = \prod_{i=1}^{n} P_\theta(X = i)^{u_i} = \frac{1}{Z^N} e^{\sum_{i=1}^{n} u_i \langle \mathbf{a}_i, \theta \rangle} = \frac{1}{Z^N} e^{\langle \mathcal{A}\mathbf{u}, \theta \rangle}.$$

Therefore, if $\mathcal{A}\mathbf{u} = \mathcal{A}\mathbf{v}$ and $\mathcal{A}$ is homogeneous, we see that $p^{\mathbf{u}} - p^{\mathbf{v}}$ vanishes on the model $\mathcal{M}_{\mathcal{A}}$. Notice that if we remove the normalizing factor Z^{-1} in the definition of a log-linear model this corresponds to switching to the affine toric variety from the projective one.

Now suppose that we have a series of observations $X^1, \ldots, X^N \in [n]$ that are independent draws from the distribution given by some unknown probability vector p in the model $\mathcal{M}$. For statistical inference about p using the likelihood framework we work with the likelihood function which associates to every $p \in \mathcal{M}$ the probability of observing $X^1, \ldots, X^N$ given the distribution p. This likelihood clearly depends only on the counts $\mathbf{u} \in \mathbb{Z}^n$, where u_i is the number of $X^1, \ldots, X^N$ that equal i. As we saw above, the probability of observing $X^1, \ldots, X^N$ is given by

$$P_\theta(X^1, \ldots, X^N) = \frac{1}{Z^N} e^{\langle \mathcal{A}\mathbf{u}, \theta \rangle}.$$

That is, $\mathcal{A}\mathbf{u}$ is a *sufficient statistic* for the model P_θ.

We can consider P_θ as a distribution on the counts $\mathbf{u}$ by

$$P_\theta(\mathbf{u}) = \binom{N}{u_1, \ldots, u_n} \frac{1}{Z^N} e^{\langle \mathcal{A}\mathbf{u}, \theta \rangle}.$$

This corresponds to forgetting the order of the samples $X^1, \ldots, X^N$. An elementary calculation shows that

$$P_\theta(\mathbf{u} \mid \mathcal{A}\mathbf{u} = \mathbf{t})$$

does not depend on θ, this is true precisely because $\mathcal{A}$ is a sufficient statistic. This property will prove important in Chapter 2 when we wish to sample from the conditional distribution of all data with a fixed sufficient statistic.

We conclude our discussion of toric ideals with a description of how to compute generators for toric ideals using the software `4ti2` [53].

Example 1.6. Let T again be the claw tree with three leaves. We take the same model as in Example 1.2 except we make the root node observed and we require that each edge has the same transition matrix. This is called the the fully observed, homogeneous, binary Markov model on T and will be studied in Chapter 3.

Take the root distribution to be uniform and relax the condition that the transition parameters sum to one. This leaves four parameters which we write θ_{00}, θ_{01}, θ_{10}, and θ_{11}. This is a toric model, since the parameterization $p_{ijkl} = \theta_{ij}\theta_{ik}\theta_{il}$ is monomial (we write p_{ijkl} for the probability that the root is in state i and the leaves are in states j, k, and l). This parameterization corresponds to a 4×16 matrix $\mathcal{A}$ which we save in a file `tree3` in the form

```
4 16
3 2 2 1 2 1 1 0 0 0 0 0 0 0 0 0
0 1 1 2 1 2 2 3 0 0 0 0 0 0 0 0
0 0 0 0 0 0 0 0 3 2 2 1 2 1 1 0
0 0 0 0 0 0 0 0 1 1 2 1 2 2 3
```

For example, column three of $\mathcal{A}$ corresponds to the probability $p_{0010} = \theta_{00}^2\theta_{01}$ of having a tree with a zero at the root and at two of the three leaves. To find a Gröbner basis, run the command `groebner tree3` which produces an output file named `tree3.gro`

```
14 16
-1  1  0  1  0  0  0 -1  0  0  0  0  0  0  0  0
-1  2  0 -1  0  0  0  0  0  0  0  0  0  0  0  0
 0 -1  0  0  1  0  0  0  0  0  0  0  0  0  0  0
 0 -1  0  2  0  0  0 -1  0  0  0  0  0  0  0  0
 0 -1  1  0  0  0  0  0  0  0  0  0  0  0  0  0
 0  0  0 -1  0  0  1  0  0  0  0  0  0  0  0  0
 0  0  0 -1  0  1  0  0  0  0  0  0  0  0  0  0
 0  0  0  0  0  0  0  0 -1  1  0  1  0  0  0 -1
 0  0  0  0  0  0  0  0 -1  2  0 -1  0  0  0  0
 0  0  0  0  0  0  0  0  0 -1  0  0  1  0  0  0
 0  0  0  0  0  0  0  0  0 -1  0  2  0  0  0 -1
 0  0  0  0  0  0  0  0  0 -1  1  0  0  0  0  0
 0  0  0  0  0  0  0  0  0  0  0 -1  0  0  1  0
 0  0  0  0  0  0  0  0  0  0  0 -1  0  1  0  0
```

Each row $\mathbf{w}$ of this matrix corresponds to an element of the Gröbner basis as follows. Write $\mathbf{w}$ in the form $\mathbf{u} - \mathbf{v}$ where $\mathbf{u}, \mathbf{v} \in \mathbb{N}^{16}$. Then the row corresponds to the binomial

$p^{\mathbf{u}} - p^{\mathbf{v}}$. For example, row two gives the relation $p_{0001}^2 - p_{0000}p_{0011}$.

Notice that of the fourteen basis elements, eight are linear (e.g., row three) and six are of degree two (e.g., row one). Modulo the linear relations, algebraic geometers will recognize this variety as being the free join of two copies of the third Veronese embedding of $\mathbb{P}^1$ in $\mathbb{P}^3$.

1.3 Phylogenetic algebraic geometry

In this section, we introduce Markov models on trees, a subject that will be explored further in Chapters 3, 4, and 5. As above, a statistical model on a tree gives an algebraic variety, and these varieties depend in interesting ways on the combinatorics of the trees and of the underlying statistical model. For more details on the algebraic viewpoint on phylogenetics, with many references and open problems, see [45].

The basic object in a phylogenetic model is a tree T which is rooted and has n labeled leaves. Each node of the tree T is a random variable taking values in the alphabet Σ. We write $k = |\Sigma|$ for the number of possible *states*. At the root, the distribution of the states is given by $\pi = (\pi_1, \ldots, \pi_k)$. On each edge e of the tree there is a $k \times k$ transition matrix M_e whose entries are indeterminates representing the probabilities of transition (away from the root) between the states. Typically, the random variables at the interior nodes will be *hidden* and the random variables at the leaves will be *observed*, although we will also consider the case where all nodes are observed in Chapter 3. The entries of the matrices M_e and the vector π are the model parameters. For instance, if T is a binary tree with n leaves then T has $2n-2$ edges, and hence we have $d = (2n-2)k^2 + k$ parameters.

In practice, there will be many constraints on these parameters, usually expressible in terms of linear equations and inequalities, so the set of statistically meaningful parameters is a polyhedron Θ in $\mathbb{R}^d$. For example, one common set of constraints corresponds to making the rows of the transition matrices M_e and the vector π sum to one. Specifying this subset Θ means choosing a *model of evolution*. In the next section we will discuss several models of evolution with different degrees of biological relevance.

At each leaf of T we can observe k possible states, so there are k^n possible joint observations we can make at the leaves. The probability p_σ of making a particular observation $\sigma \in \Sigma^n$ is a polynomial in the model parameters. Hence we get a polynomial map whose coordinates are the polynomials p_σ,

$$\begin{aligned} p\colon \Theta \subset \mathbb{R}^d &\to \mathbb{R}^{k^n} \\ (\theta_1, \ldots, \theta_d) &\mapsto (p_\sigma(\theta) \mid \sigma \in \Sigma^n). \end{aligned}$$

The image of this map is our phylogenetic model.

For every tree and every parameter set Θ, we get such a variety. This leads to a host of interesting algebraic questions. For example: pick Θ and describe the resulting stratification of $\mathbb{R}^{k^n}$ by the varieties for all trees with n leaves.

Example 1.7. Again, let T be the claw tree with three leaves in Figure 1.1. As in Example 1.2 make the root node hidden, and let all the random variables have k states. We fix no constraints on the parameters, so each edge has k^2 parameters associated to it. This model is called the general Markov model. The variety of T is given by

$$X_T = \mathrm{Sec}^k(\mathbb{P}^{k-1} \times \mathbb{P}^{k-1} \times \mathbb{P}^{k-1}),$$

where we write $\mathrm{Sec}^k(V)$ for the k-th secant variety of V (i.e., the variety of all secant $\mathbb{P}^{k-1}$'s to V). To see this, notice that the parameterization consists of one copy of the parameterization of the Segre variety for each value of the hidden state. We have seen this parameterization for $k = 2$ in Example 1.2, where we saw that $\mathrm{Sec}^2(\mathbb{P}^1 \times \mathbb{P}^1 \times \mathbb{P}^1) = \mathbb{P}^7$.

1.4 Genomics and phylogenetics

Phylogenetics is the field of biology concerned with resolving the evolutionary relationships among and between organisms. With the recent explosion of genomic data, the focus of phylogenetics has been on understanding models of DNA evolution and using these models to infer ancestral relationships. Standard phylogenetic techniques fall broadly into two classes: distance based and character based. Distance methods rely on estimating pairwise distances between species and then try to find a tree which gives similar distances. The most common example of this method is neighbor joining [83]. Character based methods start with a *multiple alignment* (defined below) and typically perform model selection in some family of statistical models of evolution. For example, likelihood or parsimony methods are character based. We believe that algebraic statistics provides an interesting new viewpoint on character based tree construction techniques.

In this section, we describe some of the basic biological facts needed to understand phylogenetic models and then delve into the practical side of the algebraic statistics of these models. See the books [46, 86] for introductions to the mathematical and algorithmic sides of the field of phylogenetics.

The basic genetic information of an organism is (almost always) carried in the form of DNA, a double helix consisting of two complementary polymers bound together. The four nucleotides that form DNA come in two types: the purines (`A` and `G`) and the pyrimidines (`C` and `T`). The two strands of the double helix are joined together via the base pairings `A` to `T` (via 2 hydrogen bonds) and `C` to `G` (via 3 hydrogen bonds).

Since each cell typically contains a copy of the DNA of the organism, DNA copying occurs frequently. Several types of errors are possible during the replication of DNA. Single bases can mutate, or large pieces of DNA can separate and become reattached, possibly at another position, possibly in the opposite direction. These are just some of the events that occur over the course of evolution.

In order to understand the relationships of various species from DNA data, we must find sections of DNA in each species which we believe share a common ancestor. This problem is called orthology mapping, and can be solved using software such as `mercator` [32]. After orthologous regions are identified, they must be *aligned* using a program such as `MAVID` [18]. The starting point for phylogenetic algorithms is a multiple sequence alignment, as pictured in Figure 1.2. We will write an alignment as a set of n strings of equal length from the alphabet Σ. In Figure 1.2, $\Sigma = \{\mathtt{A}, \mathtt{C}, \mathtt{G}, \mathtt{T}, \mathtt{-}\}$.

The standard assumption in character-based phylogenetics is that evolution happens independently at each point in the genome. We explore this assumption in Chapter 5, searching for parts of the genome with extreme and unexpected correlation between adjacent sites. However, the independence assumption makes the problem of phylogenetics much easier since then the columns of the alignment can be considered as independent, identically distributed samples.

In this manner, an alignment of n species gives an observed probability dis-

```
platypus    1 --------------------------------------------------
mouse       1 AGTGTGTCTCGTCGTGCCTACTTTCAGGACGAGAGCAGGTGAGTGTTGAT
human       1 AGTGAGACACGACGAGCCTACTATCAGGACGAGAGCAGGAGAGTGATGAT

platypus    1 --------CTCTGCGGCGTTCGTCTCGGGTGGGTTGGGGGTGGGGGTGT
mouse      51 GAGTTGCGCTCTGCGACGTTCATCTCGAGTGAGTTAGAAAGTGAAGGTAT
human      51 GAGTAGCGCACAGCGACGATCATCACGAGAGAGTAAGAA-----------

platypus   43 GGCGCAAGGTGTGAAGCACGACGACGATCTACGACGAGCGAGTGATGAGA
mouse     101 AACACAAGGTGTGA----------------------AGGCAGTGATGA--
human      90 --------------------------------------GCAGTGATGA--

platypus   93 GTGATGAGCGACGACGAGCACTAGAAGCGACGACTACTATCGACGAGCAG
mouse     127 -TGTAGAGCGACGA-GAGCAC----AGCGGCGG-----------------
human     100 -TGTAGAGCGACGA-GAGCAC----AGCGGCGA-----------------

platypus  143 CCGAGATGATGATGAAAGAGAGAGAA--------------
mouse     154 -------GATGATATATCTAGGAGGATGCCCAATTTTTTT
human     127 -----------CTACTACTAGG------------------
```

Figure 1.2: A multiple alignment of 3 DNA sequences from platypus, mouse and human. The numbers refer to the current position in each sequence at the beginning of each line.

tribution $p_{i_1,\dots,i_n} \in \Delta_{|\Sigma|^n-1}$. For example, the alignment in Figure 1.2 is of length 240 and corresponds to the probability distribution on all strings in $\{\mathtt{A},\mathtt{C},\mathtt{G},\mathtt{T},\mathtt{-}\}^3$ given by $(p_{\mathtt{AAA}}, p_{\mathtt{AAC}}, p_{\mathtt{AAG}}, p_{\mathtt{AAT}}, \dots, p_{\mathtt{---}}) = (\frac{9}{240}, 0, 0, \frac{1}{240}, \dots, 0)$. That is, of the 240 columns in the alignment, there are 9 columns with the pattern AAA, etc. We would like to discover which tree topology best explains such a data point using a suitable statistical model. Of course there is only one tree topology for our three leaf example.

As we have seen above, a statistical model in phylogenetics is given by constraints on the parameter space. If there are no constraints, this is the general Markov model, studied in Chapter 4, in which each entry of each transition matrix is an independent parameter. A much simpler model is known as the Jukes-Cantor model, where each transition matrix has two parameters: one for the diagonal entries, one for the off-diagonal entries. More complicated models such as the Kimura two- and three-parameter models (see [73, Figure 4.7] for a full list) take into account the structure of DNA to better weigh different types of mutations.

Phylogenetic models are usually stated in the language of continuous time Markov chains. In this language, the specification of a model involves constraining the entries of a *rate matrix* Q and then taking, for an edge of length t, the transition matrix to be e^{tQ}. Beware that if the tree is allowed to have only one rate matrix, then these continuous models are typically only subsets of the algebraic models described above and are not generally algebraic varieties.

If we fix a model of evolution, then every tree with n leaves gives rise to an algebraic variety. The study of *phylogenetic invariants* consists of the determination of a set of generators for the ideals of such varieties. For many of the algebraic phylogenetic models, authors have worked on finding the phylogenetic invariants. We do not attempt a comprehensive review of these results, but refer the reader to a sample of the original papers [22, 59, 91, 92, 2, 3, 97].

To say that the data comes from the model for a specific tree means that the polynomials defining this variety will all vanish on the data point. Our hope is that the algebraic geometry of phylogenetic models can provide some clue regarding which tree to pick, given this data point.

In practical terms, there are two problems with this approach. First the phylogenetic invariants are not known for many models, although progress has been made in this direction. Second, since the data is not perfect, the phylogenetic invariants will not evaluate to zero. Furthermore, since the generators of an ideal are not canonically defined, the results of the evaluation will depend on which set of generators is chosen. In Chapter 4, we present methods for the *general Markov model* that avoid these two problems by using as generators certain rank conditions on *flattenings* of the data.

1.5 Outline of the thesis

Chapter 2 is devoted to an application of toric ideals to the problem of sampling from discrete exponential families, which is one of the founding problems in algebraic statistics. In Chapter 3, the theme of toric ideals is picked up again, this time in the context of the simplified phylogenetic model that we introduced in Example 1.6. A more general, realistic phylogenetic model is studied in Chapter 4. We show how the algebraic properties of this model can be used to build phylogenetic trees. These are the first practical methods for tree construction using phylogenetic invariants and we hope they can provide motivation for how algebraic statistics can be used in practice.

In Chapter 5, we study genomic sequences which are perfectly preserved at extreme evolutionary distances. This provides an example of how comparative genomics can help derive the function of genomic elements. We also apply our phylogenetic models to quantify the evolutionary significance of these highly-conserved elements. Finally, in Chapter 6 we again study evolution, but this time in the very specialized case in which the organism is under severe pressure and can evolve in only one direction. The set of possible genotypes is modeled as a distributive lattice and Bayesian networks are used to study evolution proceeding up this lattice. We are concerned with the risk that the organism escapes from the selective pressure, which is the probability that it evolves to the top of the lattice before becoming extinct. This risk depends on the combinatorics of the lattice.

Chapter 2

Markov bases for noncommutative analysis of ranked data

In this chapter, we give a general methodology for studying group valued data where the summary we are interested in is given by a representation of the group. In particular, we analyze in detail the case of ranked data. Our main example of ranked data is the case of an election where every voter was asked to rank the five candidates.

Our methods depend on two tools. First, we show how Fourier analysis and representation theory can be used to obtain descriptive statistics of group-valued data. In the case of ranked data, this gives in particular a description of how likely a voter would be to rank a given pair of candidates in a given pair of positions. Second, in order to calibrate these methods, we show how to use Markov chain Monte Carlo techniques to sample from group-valued data with a fixed summary. In order to run a Markov chain, a set of moves (a *Markov basis*) is needed. We calculate this basis using the theory of toric ideals and show how symmetry can be very helpful in these calculations. The material in this chapter comes from the paper [37], with Persi Diaconis.

We believe that these methods can be useful in computational biology. For example, suppose we want to understand how the fitness of an organism depends on the order of certain genes in its genome. Understanding this dependence can lead to a picture of the regulatory network for these genes. The function that assigns a fitness value to each ordering of the genes is called a *fitness landscape*. This fitness landscape can be analyzed using the methods discussed in this chapter in order to understand how the position of a pair of genes affects the total fitness.

From the perspective of [11], a fitness landscape corresponds to a triangulation of a certain polytope that encodes the space of genotypes. In our case, this polytope is the Birkhoff polytope. It would be interesting to study the relationship between the triangulations of the Birkhoff polytope obtained from fitness landscapes and the spectral analysis presented in this chapter.

2.1 Election data with five candidates

Table 2.1 shows the results of an election. A population of 5738 voters was asked to rank five candidates for president of a national professional organization. The table shows the number of voters choosing each ranking. For example, 29 voters ranked candidate 5 first, candidate 4 second, . . . , and candidate 1 last, resulting in the entry $54321 = 29$. Table 2.2 shows a simple summary of the data: the proportion of voters ranking candidate i in position j. For example, 28.0% of the voters ranked candidate 3 first and 23.1% of the voters ranked candidate 3 last.

Table 2.2 is a natural summary of the 120 numbers in Table 2.1, but is it an adequate summary? Does it capture all of the signal in the data? In this paper, we develop tools to answer such questions using Fourier analysis and algebraic techniques.

In Section 2.2, we give a general exposition of how noncommutative Fourier analysis can be used to analyze group valued data with summary given by a representation ρ. In order to use Markov chain Monte Carlo techniques to calibrate the Fourier analysis, we define an exponential family and toric ideal (as introduced in Section 1.2) associated to a finite group G and integer representation ρ. A generating set of the toric ideal can be used to run a Markov chain to sample from data on the group. For example, the 14 moves in Table 2.3 allow us to randomly sample from the space of data on S_5 with fixed first order summary (Table 2.2).

For example, the first entry in Table 2.2 corresponds to the move that adds one to both of the 53412 and 54321 entries of the data and subtracts one from both the 53421 and 54312 entries. Notice that this move does not change the first order summary.

Ranking	# votes	Ranking	# votes	Ranking	# votes	Ranking	# votes
54321	29	43521	91	32541	41	21543	36
54312	67	43512	84	32514	64	21534	42
54231	37	43251	30	32451	34	21453	24
54213	24	43215	35	32415	75	21435	26
54132	43	43152	38	32154	82	21354	30
54123	28	43125	35	32145	74	21345	40
53421	57	42531	58	31542	30	15432	40
53412	49	42513	66	31524	34	15423	35
53241	22	42351	24	31452	40	15342	36
53214	22	42315	51	31425	42	15324	17
53142	34	42153	52	31254	30	15243	70
53124	26	42135	40	31245	34	15234	50
52431	54	41532	50	25431	35	14532	52
52413	44	41523	45	25413	34	14523	48
52341	26	41352	31	25341	40	14352	51
52314	24	41325	23	25314	21	14325	24
52143	35	41253	22	25143	106	14253	70
52134	50	41235	16	25134	79	14235	45
51432	50	35421	71	24531	63	13542	35
51423	46	35412	61	24513	53	13524	28
51342	25	35241	41	24351	44	13452	37
51324	19	35214	27	24315	28	13425	35
51243	11	35142	45	24153	162	13254	95
51234	29	35124	36	24135	96	13245	102
45321	31	34521	107	23541	45	12543	34
45312	54	34512	133	23514	52	12534	35
45231	34	34251	62	23451	53	12453	29
45213	24	34215	28	23415	52	12435	27
45132	38	34152	87	23154	186	12354	28
45123	30	34125	35	23145	172	12345	30

Table 2.1: American Psychological Association (APA) voting data: the number of voters that ranked the 5 candidates in a given order.

	Rank				
Candidate	1	2	3	4	5
1	18.3	26.4	22.8	17.4	14.8
2	13.5	18.7	24.6	24.6	18.3
3	28.0	16.7	13.8	18.2	23.1
4	20.4	16.9	18.9	20.2	23.3
5	19.6	21.0	19.6	19.2	20.3

Table 2.2: First-order summary: The proportion of voters who ranked candidate i in position j. This is a scaled version of the Fourier transform of Table 2.1 at the permutation representation.

In Section 2.4 we show how this basis (Table 2.3) was computed — either using Gröbner bases or by utilizing symmetry. We describe extensive computations of the basis for ranked data on at most 6 objects. From these computations, we conjecture that the toric ideal for S_n is generated in degree 3. In Section 2.5, we show that this ideal for S_n is generated in degree $n-1$, improving a result of [39], and we describe the degree 2 moves. Finally, in Section 2.6, we apply these methods to analyze the data in Table 2.1 and an example from [35].

2.2 Fourier analysis of group valued data

Let G be a finite group (in our example, $G = S_5$). Let $f\colon G \to \mathbb{Z}$ be any function on G. For example, if $g_1, g_2, \ldots, g_N$ is a sample of points chosen from a distribution on G, take $f(g)$ to be the number of sample points g_i that are equal to g. We view f interchangeably as either a function on the group or an element of the group ring $\mathbb{Z}[G]$. Recall that a map $\rho\colon G \to GL(V_\rho)$ is a matrix representation of G if $\rho(st) = \rho(s)\rho(t)$ for all $s, t \in G$. The dimension d_ρ of the representation ρ is the dimension of V_ρ as a $\mathbb{C}$-vector space. We say that a ρ is integer-valued if $\rho_{ij}(g) \in \mathbb{Z}$ for all $g \in G$ and for all $1 \leq i, j \leq d_\rho$. We denote the set of irreducible representations of G by $\hat{G}$.

An analysis of $f(g)$ may be based on the Fourier transform. The Fourier transform of f at ρ is

$$\hat{f}(\rho) = \sum_{g \in G} f(g)\rho(g). \tag{2.1}$$

The Fourier transform at all the irreducible representations $\rho \in \hat{G}$ determines f through

Move	Number	Move	Number
$\begin{bmatrix}53412\\54321\end{bmatrix} - \begin{bmatrix}53421\\54312\end{bmatrix}$	450	$\begin{bmatrix}45231\\54312\end{bmatrix} - \begin{bmatrix}45312\\54231\end{bmatrix}$	600
$\begin{bmatrix}54123\\54231\\54312\end{bmatrix} - \begin{bmatrix}54132\\54213\\54321\end{bmatrix}$	200	$\begin{bmatrix}53412\\54123\\54231\end{bmatrix} - \begin{bmatrix}53421\\54132\\54213\end{bmatrix}$	3600
$\begin{bmatrix}45123\\54231\\54312\end{bmatrix} - \begin{bmatrix}45132\\54213\\54321\end{bmatrix}$	200	$\begin{bmatrix}45123\\53412\\54231\end{bmatrix} - \begin{bmatrix}45132\\53421\\54213\end{bmatrix}$	7200
$\begin{bmatrix}43512\\54123\\54231\end{bmatrix} - \begin{bmatrix}43521\\54132\\54213\end{bmatrix}$	3600	$\begin{bmatrix}43512\\53241\\54123\end{bmatrix} - \begin{bmatrix}43521\\53142\\54213\end{bmatrix}$	3600
$\begin{bmatrix}45231\\52341\\53412\end{bmatrix} - \begin{bmatrix}45312\\52431\\53241\end{bmatrix}$	7200	$\begin{bmatrix}45132\\52341\\53412\end{bmatrix} - \begin{bmatrix}45312\\52431\\53142\end{bmatrix}$	3600
$\begin{bmatrix}34512\\45123\\53241\end{bmatrix} - \begin{bmatrix}34521\\45213\\53142\end{bmatrix}$	600	$\begin{bmatrix}34521\\45213\\53142\end{bmatrix} - \begin{bmatrix}35142\\43521\\54213\end{bmatrix}$	600
$\begin{bmatrix}35142\\43521\\54213\end{bmatrix} - \begin{bmatrix}35241\\43512\\54123\end{bmatrix}$	600	$\begin{bmatrix}34521\\45312\\52143\end{bmatrix} - \begin{bmatrix}35142\\42513\\54321\end{bmatrix}$	1440

Table 2.3: A Markov basis for S_5 with 29890 moves in 14 symmetry classes.

	S^5	$S^{4,1}$	$S^{3,2}$	$S^{3,1,1}$	$S^{2,2,1}$	$S^{2,1,1,1}$	$S^{1,1,1,1,1}$
d_ρ^2	1	16	25	36	25	16	1
Data	2286	298	459	78	27	7	0

Table 2.4: Squared length (divided by 120) of the projection of the APA data (Table 2.1) into the 7 isotypic subspaces of S_5.

the Fourier inversion formula

$$f(g) = \frac{1}{|G|} \sum_{\rho \in \hat{G}} d_\rho \operatorname{Tr}(\hat{f}(\rho)\rho(g^{-1})), \tag{2.2}$$

which can be rewritten as $f(g) = \sum_{\rho \in \hat{G}} f|_{V_\rho}(g)$, where

$$f|_{V_\rho}(g) = \frac{d_\rho}{|G|} \sum_{h \in G} \chi_\rho(h) f(gh). \tag{2.3}$$

This decomposition shows the contributions to f from each of the irreducible representations of G. For example, if a few of the $f|_{V_\rho}$ are large, we can analyze these components in order to understand the structure of f. See [34, 35] for background, proofs, and previous literature.

Example 2.1. This analysis is most familiar for the cyclic group C_n where it becomes the discrete Fourier transform

$$\hat{f}(j) = \sum_{k=0}^{n-1} f(k) e^{-2\pi ijk/n}, \qquad f(k) = \frac{1}{n} \sum_{j=0}^{n-1} \hat{f}(j) e^{2\pi ikj/n} \tag{2.4}$$

In (2.4), if a few of the $\hat{f}(j)$ are much larger than the rest, then f is well understood as approximately a sum of a few periodic components.

For the symmetric group S_n, the permutation representation assigns permutation matrices $\rho(\pi)$ to permutations π. Thus, if $f(\pi)$ is the number of rankers choosing π, $\hat{f}(\rho)$ is a $n \times n$ matrix with (i, j) entry the number of rankers ranking item i in position j (as in Table 2.2). The irreducible representations of S_5 are indexed by the seven partitions of five and are written as S^λ where λ is a partition of 5. For our data, (2.2) gives a decomposition of f into 7 parts. Table 2.4 shows the lengths of the projection of Table 2.1 onto the seven isotypic subspaces of S_5.

	Ranks									
Candidates	1,2	1,3	1,4	1,5	2,3	2,4	2,5	3,4	3,5	4,5
1,2	-137	-20	18	140	111	22	4	6	-97	-46
1,3	476	-88	-179	-209	-147	-169	-160	107	128	241
1,4	-189	51	113	24	-9	98	99	-65	23	-146
1,5	-150	57	47	45	43	49	56	-48	-53	-48
2,3	-42	84	19	-61	30	-16	82	-76	-39	72
2,4	157	-20	-43	-25	-93	-76	-56	8	38	112
2,5	22	-44	7	15	-117	69	25	62	99	-138
3,4	-265	-7	72	199	39	140	85	19	-52	-233
3,5	-169	10	88	70	78	44	47	-51	-36	-80
4,5	296	-24	-142	-130	-5	-163	-128	38	-9	267

Table 2.5: Second order summary for the APA data.

The largest contribution to the data occurs from the trivial representation S^5. We call the projection onto $S^5 \oplus S^{4,1}$ the first order summary; it was shown in Table 2.2 above. We see that the projection onto $S^{3,2}$ is also sizable while the rest of the projections are relatively negligible. This suggests a data-analytic look at the projection into $S^{3,2}$. Table 2.5 shows this projection in a natural coordinate system. This projection is based on the permutation representation of S_5 on unordered pairs $\{i, j\}$. Table 2.5 is an embedding of a 25 dimensional space into a 100 dimensional space so that its coordinates are easy to interpret. See [35] for further explanation.

The largest number in Table 2.5 is 476 in the $\{1, 3\}, \{1, 2\}$ position corresponding to a large positive contribution to ranking candidates one and three in the top two positions. There is also a large positive contribution for ranking candidates four and five in the top two positions. Since Table 2.5 gives the projection of f onto a subspace orthogonal to $S^5 \oplus S^{4,1}$, the popularity of individual candidates has been subtracted out. We can see the “hate vote” against the pair of candidates one and three (and the pair four and five) from the last column. Finally, the negative entries for e.g., pairs one and four, one and five, three and four, three and five show that voters don’t rank these pairs in the same way.

The preceding analysis is from [35] which used it to show that noncommutative spectral analysis could be a useful adjunct to other statistical techniques for data analysis. The data is from the American Psychological Association — a polarized group of academicians and clinicians who are on very uneasy terms (the organization almost split in two just after this election). Candidates one and three are in one camp, candidates four and five from the other. Candidate two seems to be disliked by both camps. The winner of the election depends on the method of allocating votes. For example, the Hare system or plurality voting would elect candidate three. However, other widely used voting methods (Borda's sum of ranks or Coomb's elimination system) elect candidate one. For details and further analysis of the data, see [93].

2.3 Exponential families

To explain the perturbation analysis in Section 2.6, it is useful to consider a simple exponential model for group-valued data.

Definition 2.2. Let ρ be a n dimensional, integer-valued representation of a finite group G. Then the exponential family of G and ρ is given by the family of probability distributions on G

$$P_\Theta(g) = Z^{-1} e^{\mathrm{Tr}(\Theta\rho(g))} \tag{2.5}$$

where the normalizing constant is $Z = \sum_{g \in G} e^{\mathrm{Tr}(\Theta\rho(g))}$ and Θ is a $n \times n$ matrix of parameters to be chosen to fit the data.

For example let $G = S_n$ and ρ be the usual permutation representation. Then if Θ is the zero matrix, P_Θ is the uniform distribution. If $\Theta_{1,1}$ is nonzero and $\Theta_{i,j}$ is zero otherwise, the model P_Θ corresponds to item one being ranked first with special probability, the rest ranked randomly. Such models have been studied by [88, 102, 35]. See [63] for a book-length treatment of models for permutation data. In the notation of Section 1.2, this exponential family is characterized by a $d_\rho^2 \times |G|$ matrix $\mathcal{A}$ with columns given by $\mathbf{a}_g = \rho(g)$.

From the Darmois-Koopman-Pitman Theorem [38, Theorem 3.1], we deduce

Proposition 2.3. *The model (2.5) has the property that a sufficient statistic for Θ based on data $f(\pi)$ is the Fourier transform $\hat{f}(\rho)$. Furthermore, (2.5) is the unique model characterized by this property.*

Definition 2.4. Given a finite group G and an integer valued representation ρ of dimension d_ρ define the toric ideal of G at ρ as $I_{G,\rho} = \ker(\phi_{G,\rho})$, where

$$\begin{aligned} \phi_{G,\rho}\colon \mathbb{C}[x_g \mid g \in G] &\longrightarrow \mathbb{C}[t_{ij}^{\pm 1} \mid 1 \le i,j \le d_\rho] \\ x_g &\longmapsto \prod_{1\le i,j\le d_\rho} t_{ij}^{\rho_{ij}(g)}. \end{aligned}$$

This ideal is the vanishing ideal of the exponential family from Definition 2.2. It will be our main object of study in Sections 2.4 and 2.5.

Remark 2.5. For representations which are not integer valued, the previous construction does not work. However, these representations give rise to lattice ideals as follows. Let G be a finite group and $\rho\colon G \to GL(V)$ be a d_ρ dimensional complex representation. Then extend ρ linearly to a map $\rho\colon \mathbb{Z}[G] \to GL(V)$. The kernel of ρ is a lattice in $\mathbb{Z}[G]$ which we write as $\mathcal{L}_{G,\rho} = \ker\rho$. Let $I_{G,\rho}$ be the associated lattice ideal. That is, $I_{G,\rho}$ is the ideal in $\mathbb{C}[x_g \mid g \in G]$ corresponding to all additive relations between $\rho(g)$ for $g \in G$.

We believe that this family of toric and lattice ideals arising from group representations is deserving of further study. In particular, while this paper analyzes the group S_n and the permutation representation $S^n \oplus S^{n-1,1}$, it could be interesting to analyze the representation $S^{n-2,2}$ corresponding to the second order summary.

As suggested by [48], tests of goodness of fit of the model (2.5) should be based on the conditional distribution of the data f given the sufficient statistic $\hat{f}(\rho)$. Since $\hat{f}(\rho)$ is a sufficient statistic, it is easy to see that the conditional distribution is given by

$$P_\Theta(f|\hat{f}(\rho)) = w^{-1}\prod_{\sigma\in G}\frac{1}{f(\sigma)!}, \quad \text{where} \quad w = \sum_{\substack{g\in\mathbb{Z}[G] \\ \hat{g}(\rho)=\hat{f}(\rho)}}\prod_{\sigma\in G}\frac{1}{g(\sigma)!}. \tag{2.6}$$

Observe that the conditional distribution in (2.6) is free of the unknown parameter Θ, this is a consequence of the fact that $\hat{f}(\rho)$ is a sufficient statistic, as noted in Section 1.2.

The original justification for the Fourier decomposition is model free (non-parametric). The first order summary in Table 2.2 is a natural object to look at and the second order summary was analyzed because of a sizable projection to $S^{3,2}$ in Table 2.4. It is natural to wonder if the second order summary is real or just a consequence of finding patterns in any set of numbers. To be honest, the APA data is not a sample (those 5,972 who choose to vote are likely to be quite different from the bulk of the 100,000 or so APA members). If the first order summary is accepted "as is", the largest probability model for which $\hat{f}(\rho)$ captures all the structure in the data is the exponential family (2.5). It seems natural to use the conditional distribution of the data given $\hat{f}(\rho)$ as a way of perturbing things. The uniform distribution on data with fixed $\hat{f}(\rho)$ is a much more aggressive perturbation procedure. Both are computed and compared in Section 2.6.

2.4 Computing Markov bases for permutation data

To carry out a test based on Fisher's principles, we use Markov chain Monte Carlo to draw samples from the distribution (2.6).

Definition 2.6. A *Markov basis* for a finite group G and a representation ρ is a finite subset of "moves" $g_1, \ldots, g_B \in \mathbb{Z}[G]$ with $\hat{g}_i(\rho) = 0$ such that any two elements in $\mathbb{N}[G]$ with the same Fourier transform at the representation ρ can be connected by a sequence of moves in that subset.

In [39] it was explained how Gröbner basis techniques could be applied to find such Markov bases.

Proposition 2.7. *A generating set of $I_{G,\rho}$ (see Definition 2.4) is a Markov basis for the group G and the representation ρ.*

We will write I_{S_n} for our main example, the ideal of S_n with the permutation representation ρ. The representation $\rho \colon \mathbb{N}[S_n] \to \mathbb{N}^{n^2}$ sends an element of S_n to its permutation matrix. The elements $\mathbf{b} \in \mathbb{N}^{n^2}$ with $\rho^{-1}(\mathbf{b})$ non-empty are the *magic squares*, that is, matrices with non-negative integer entries such that all row and column sum are equal. We write an element $\pi_1 + \cdots + \pi_m \in \mathbb{N}[S_n]$ as a tableau $\begin{bmatrix} \pi_1(1) & \ldots & \pi_1(n) \\ \vdots & & \vdots \\ \pi_m(1) & \ldots & \pi_m(n) \end{bmatrix}$.

In this notation, a Markov basis element is written as a difference of two tableaux. For example, the degree 2 element of the Markov basis for S_5, $\begin{bmatrix} 13452 \\ 14325 \end{bmatrix} - \begin{bmatrix} 13425 \\ 14352 \end{bmatrix}$, corre-

S_3 Move	Number	S_4 Move	Number
$\begin{bmatrix}123\\231\\312\end{bmatrix} - \begin{bmatrix}132\\213\\321\end{bmatrix}$	1	$\begin{bmatrix}1234\\2143\end{bmatrix} - \begin{bmatrix}1243\\2134\end{bmatrix}$	18
		$\begin{bmatrix}2314\\2431\\4123\end{bmatrix} - \begin{bmatrix}2134\\2413\\4321\end{bmatrix}$	144
		$\begin{bmatrix}1324\\2134\\3214\end{bmatrix} - \begin{bmatrix}1234\\2314\\3124\end{bmatrix}$	16

Table 2.6: Markov bases for S_3 and S_4 and the size of their symmetry classes.

sponds to adding one to the entries 13452 and 14325 in Table 2.1 and subtracting one from the entries 13425 and 14352.

At the time of writing [39], finding a Gröbner basis for I_{S_5} was computationally infeasible. Due to an increase in computing power and the development of the software `4ti2` [53], we were able to compute a Gröbner and a minimal basis of I_{S_5}.

This computation involved finding a Gröbner basis of a toric ideal involving 120 indeterminates. It took `4ti2` approximately 90 hours of CPU time on a 2GHz machine and produced a basis with 45,825 elements. The Markov basis had 29890 elements, 1050 of degree 2 and 28840 of degree 3, see Tables 2.3 and 2.7. Using `4ti2`, we have also computed Markov bases of the ideals I_{S_n} for $n = 3$ and $n = 4$, they are shown in Table 2.6.

Although the calculation for S_6 is currently not possible using Gröbner basis methods, there is a natural group action that reduces the complexity of this problem. The group $S_n \times S_n$ acts on $\mathbb{N}^{n^2}$ by permuting rows and columns. If we permute the rows and columns of a magic square, we still have a magic square, therefore, this action lifts to a group action on the Markov basis of I_{S_n}. In terms of tableaux, one copy of S_n acts by permuting columns of the tableau, the other acts by permuting the labels in the tableau. We have calculated orbits under this action; notice that the symmetrized bases are remarkably small (Table 2.7).

To calculate a Markov basis for I_{S_6}, we had to construct the fiber over every magic square with sum at most 5 (by Theorem 2.10) and then pick moves such that every fiber is connected by these moves [98, Theorem 5.3]. For degrees 2 and 3 this was relatively straightforward (e.g., there are 20,933,840 six by six magic squares with sum 3). For these degrees, we constructed all squares and then calculated orbits of the group action and calculated the fiber for each orbit (there were 11 orbits in degree 2 and 103 in degree 3).

However, there are 1,047,649,905 six by six magic squares of degree 4 and 30,767,936,616 of degree 5 [7], so complete enumeration was not possible. Instead, we first randomly generated millions of magic squares with sums 4 or 5 using another Markov chain. We broke these down into orbits, keeping track of the number of squares we had found. For example, we needed to generate 30 million squares of degree 5 to find a representative for each orbit. We were left with 2804 orbits for degree 4 and 65481 orbits for degree 5. For degree 5, the proof of Theorem 2.10 shows that we only need to consider magic squares with norm squared less that 50, leaving 13196 orbits to check. The fibers were calculated by a depth first search with pruning. Remarkably, the computation showed that I_{S_6} is generated in degree three.

Theorem 2.8. *The ideal I_{S_n} is minimally generated by 57,150 binomials of degree two and 7,056,420 binomials of degree three. The degree two generators form seven orbits under the action of $S_6 \times S_6$; the degree three generators form 51 orbits under this action.*

The entire calculation for S_6 took about 2 weeks, with the vast majority of the time spent calculating orbits of degree 5 squares. Our data and code (in perl) are available for download at `http://math.berkeley.edu/~eriksson`. The code could be easily adapted to calculate other Markov bases with a good degree bound and a large symmetry group. Our calculations (see Table 2.7) suggest the following conjecture:

Conjecture 2.9. *The ideal I_{S_n} is generated in degree 3.*

2.5 Structure of the toric ideal I_{S_n}

Theorem 6.1 of [39] shows that every reverse lexicographic Gröbner basis of I_{S_n} has degree at most n. By considering only minimal generators and not a full Gröbner basis, we are able to strengthen this degree bound.

	Degree 2		Degree 3		Degree 4		Degree 5		Degree 6	
n	all	sym	all	sym	all	sym	all	sym	all	sym
3	0	0	1	1						
4	18	1	160	2	0	0				
5	1050	2	28840	12	0	0	0	0		
6	57150	7	7056240	51	0	0	0	0	0	0
7	3567690	12	?	?	?	?	?	?	?	?

Table 2.7: Number of generators and symmetry classes of generators by degree in a Markov basis for I_{S_n}.

Theorem 2.10. *The ideal I_{S_n} is generated in degree $n-1$ for $n > 3$.*

Proof. Since we know that I_{S_n} is generated in degree n, we need to show that the fibers over all magic squares with sum n are each connected by moves of degree $n-1$ or less. Let S and T be tableaux in $\rho^{-1}(\mathbf{b})$, where $\mathbf{b}$ is a magic square with sum n. Suppose that the first row of S and the first row of T differ in exactly k places. Then we claim that there is a degree $k+1$ move that can be applied to S to get a tableau $S' \in \rho^{-1}(\mathbf{b})$ with the same first row as T.

To change the first row of S to make it agree with the first row of T, we have to permute k elements of the first row of S. But to remain in the fiber, this means we must also permute (at most) k other rows of S. For example, if the first row of S is $123\ldots n$ and the first row of T is $213\ldots n$, we would also have to pick the row of S with a 2 in the first column and the row with a 1 in the second column. Once we have picked the (at most) k rows of S that must be changed, it follows from Birkhoff's theorem [100, Theorem 5.5] that we can change these k rows and the first row to make a new tableau $S' \in \rho^{-1}(\mathbf{b})$ that agrees with T in one row.

We applied a degree $k+1$ move and are left with S' and T being connected by a degree $n-1$ move, so as long as we have $k+1 \leq n-1$, we are done. That is, for every pair (S,T) of tableaux in a degree n fiber, we must show that there is a row of S and a row of T that differ in at most $n-2$ places.

Given such a pair (S,T), introduce an $n \times n$ matrix M where the entries M_{ij} are the number of entries that row i of S and row j of T agree. Notice that if $M_{ij} \geq 2$, we have rows i in S and j in T that differ in at most $n-2$ places and are done.

Suppose that row i of S is $(\pi_i(1),\ldots,\pi_i(n))$. The row sum $\sum_{j=1}^{n} M_{ij}$ counts the total number of times that $\pi_i(j)$ appears in column j for each j. This is exactly $\sum_{k=1}^{n} \mathbf{b}(k, \pi(k))$. Summing over all rows, we see that every entry of $\mathbf{b}$ gets counted its cardinality number of times. That is,

$$\sum_{1 \le i,j \le n} M_{ij} = \sum_{1 \le i,j \le n} \mathbf{b}(i,j)^2 = ||\mathbf{b}||^2$$

Now since each row of $\mathbf{b}$ sums to n, we have that $||\mathbf{b}||^2 \geq n^2$, with equality only if $\mathbf{b}(i,j) = 1$ for all i, j. Notice that if $||\mathbf{b}||^2 > n^2$, then one of the M_{ij} must be larger than 1, and we are done.

Therefore, we only have to consider the fiber over $\mathbf{b}_1 = \begin{pmatrix} 1 & 1 & \dots & 1 \\ \vdots & & & \vdots \\ 1 & 1 & \dots & 1 \end{pmatrix}$. Elements of this fiber are tableaux such that every row and every column is a permutation of $\{1, \dots, n\}$ ("Latin squares"). Two tableaux are connected by a degree $n-1$ move if they have a row in common. We claim that if $n > 3$, this graph is connected. (Note that for $n = 3$, there are two components and a degree 3 move for S_3, see Table 2.7.)

For fixed $\nu \in S_n$, the set T_ν of all tableaux in $\rho^{-1}(\mathbf{b}_1)$ that have ν as a row is connected by definition. Form the graph G_n where the vertices are elements $\nu \in S_n$ and there is an edge between λ and ν if λ and ν occur in a tableau together. Then if this graph is connected, the whole fiber over $\mathbf{b}_1$ is connected by degree $n-1$ moves.

First, we claim that λ and ν occur together in a tableau if and only if λ is a derangement with respect to ν (i.e., if λ and ν are disjoint from each other). The derangement condition is clearly necessary. Sufficiency follows from Birkhoff's theorem: if λ is a derangement with respect to ν, then the square $\mathbf{b}_1 - \rho(\lambda) - \rho(\nu)$ has non-negative entries and row and column sums $n-2$, therefore, it it the sum of $n-2$ permutation matrices. Thus, G_n is the graph where two permutations are connected by an edge when they are disjoint.

Now note that $[1, 2, \dots, n-2, n-1, n]$ and $[3, 4, \dots, n, 1, 2]$ are connected in G_n since the second is a cyclic shift of the first. Then, if $n > 3$, $[3, 4, \dots, n, 1, 2]$ and $[1, 2, \dots, n-2, n, n-1]$ are also connected. Thus $[1, 2, \dots, n]$ and $[1, 2, \dots, n-2, n, n-1]$ are connected, so applying transpositions keeps us in the same connected component of G_n. But S_n is generated by transpositions, so G_n is connected and therefore $\rho^{-1}(\mathbf{b}_1)$ is connected by moves of degree $n-1$. □

Theorem 2.10 gives rise to the question of whether there exists a Gröbner basis of degree $n-1$ for I_{S_n}.

Definition 2.11. Let I be an ideal in m unknowns, and let $C[\omega]$ be the equivalence class of vectors in $\mathbb{R}^m$ that give the same Gröbner basis as ω, i.e.,

$$C[\omega] = \left\{\omega' \in \mathbb{R}^m \mid in_{\omega'}(g) = in_{\omega}(g) \text{ for all } g \in \mathcal{G}\right\},$$

where $\mathcal{G}$ is the reduced Gröbner basis of I with respect to ω. Then the *Gröbner fan* of I, denoted $GF(I)$ is the set of closed cones $\overline{C[\omega]}$ for all $\omega \in \mathbb{R}^m$.

Remark 2.12. We attempted to find the entire Gröbner fan for $n = 4$ using the software packages `CaTS` [57] and `gfan` [56]. This computation failed for both programs after several weeks due to excessive memory usage of over 3 GB. However, before failing, we were able to calculate 805,671 Gröbner bases with `CaTS` and 2,973,312 Gröbner bases with `gfan`. Every one of these Gröbner bases contained elements of degree 4, in contrast with the Markov basis of degree 3. Furthermore, our Gröbner basis for S_5 contained degree 5 elements. Therefore, it is possible that the degree n Gröbner basis of [39] is the Gröbner basis of smallest degree.

While I_{S_n} is difficult to compute, it is easy to classify the degree 2 part of the Markov basis.

Proposition 2.13. *Let $D_2(n)$ be the number of degree 2 moves, up to symmetry, in a Markov basis for S_n. Then*

$$D_2(n) = D_2(n-1) + \sum_{k=2}^{\lfloor \frac{n}{2} \rfloor} (2^{k-1}-1)[q^{n-2k}] \prod_{i=1}^{k} \frac{1}{1-q^i},$$

where $[q^j](\sum a_i q^i) := a_j$. For example, $D_2(9) = 47$.

Proof. First assume that all entries of the magic square $\mathbf{b}$ are either 1 or 0. Then the squares with non-trivial $\rho^{-1}(\mathbf{b})$ are those that can be put in a block diagonal form with $k \geq 2$ blocks and each block of size at least 2. Such a magic square has a fiber of size 2^{k-1}, corresponding to choosing, for each block, an orientation of the two permutations that sum to that block (since the order of the rows in a tableau don't matter, there

	S^5	$S^{4,1}$	$S^{3,2}$	$S^{3,1,1}$	$S^{2,2,1}$	$S^{2,1,1,1}$	$S^{1,1,1,1,1}$
Data	2286	298	459	78	27	7	0
Hypergeometric	2286	298	16	19	10	6	0
Uniform	2286	298	511	672	436	295	25
Bootstrap	2286	303	469	93	37	13	1

Table 2.8: Squared length (divided by 120) of the projection of the APA data into the 7 isotypic subspaces of S_5. Also, the averages of this projection for 100 random draws for three perturbations.

are only $k-1$ such choices). Therefore, we need $2^{k-1}-1$ moves to make such a fiber connected. It is a standard fact [90, Chapter 1] that the number of partitions of n into k blocks each of size at least 2 (denoted $p_2(n;k)$) satisfies

$$\sum_{n\geq 0} p_2(n;k)q^n = q^{2k}\prod_{i=1}^{k}\frac{1}{1-q^i}$$

If a magic square contains a 2, it can be thought of as coming from $D_2(n-1)$ in a unique way (up to symmetry). □

2.6 Statistical analysis of the election data

In order to run a Markov chain fixing $\hat{f}(\rho)$ on data f, we use the Markov basis $\{g_1,\ldots,g_B\}$ as calculated above. Then, starting from f, choose i uniformly in $\{1,2,\ldots,B\}$ and choose $\epsilon=\pm 1$ with probability 1/2. If $f+\epsilon g_i \geq 0$ (coordinate-wise), the Markov chain moves to $f+\epsilon g_i$. Otherwise, the Markov chain stays at f. This gives a symmetric connected Markov chain on the data sets with a fixed value of $\hat{f}(\rho)$. As such, it has a uniform stationary distribution. To get a sample from the hypergeometric distribution (2.6), the Metropolis algorithm or the Gibbs sampler can be used [62].

Given a symmetrized basis, we can still perform a random walk. Pick, at random, an element g of $S_n \times S_n$. Pick a move from the symmetrized basis at random, apply g to it (permuting columns and renaming entries), then use the resulting move in the Markov chain. This again gives a symmetric Markov chain that converges to the uniform distribution.

In this section, we apply the Markov basis for S_5 to analyze Table 2.1. The second and third rows of Table 2.8 show the average sum of squares for 100 samples from

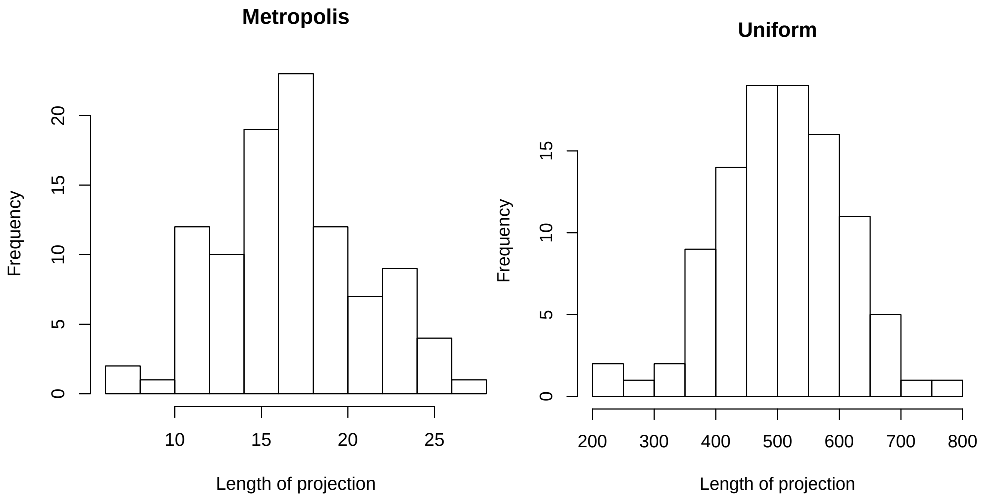

Figure 2.1: Distribution of the length of the projection to $S^{3,2}$ with the Metropolis and uniform random walks.

the hypergeometric distribution (2.6) (row 2) and from the uniform distribution (row 3) with $\hat{f}(\rho)$ fixed. Both sets of numbers are based on a Markov chain simulation using a symmetrized version of the minimal basis. In each case, starting from the original data set, the chain was run 10,000 steps and the current function recorded. From here, the chain was run 10,000 further steps, and so on until 100 functions were recorded. While the running time of 10,000 steps is arbitrary, wide variation in the running time did not appreciably change the results.

A histogram of the 100 values of the length of the projection into $S^{3,2}$ under each distribution is shown in Figure 2.1. These show some of variability but nothing exceptional. The histograms for the other projections are very similar.

Consider first the hypergeometric distribution leading to row 2 of Table 2.8 and Figure 2.1. A natural test of goodness of fit of the model (2.5) for the APA data may be based on the conditional distribution of the squared length of the projection of the data into $S^{3,2}$. From the random walk under the null model, this should be about 15 ± 5. For the actual data, this projection is 459. This gives a definite reason to reject the null model. Our look at the data projected into $S^{3,2}$ and the analysis that emerged in Section 2.2 confirms this conclusion.

In [36], the uniform distribution of the data conditional on a sufficient statistic was suggested as an antagonistic alternative to the null hypothesis when the data strongly rejects a null model. The idea is to help quantify if the data is really far from the null, or practically close to the null and just rejected because of a small deviation but a large sample size [36]. From Figure 2.1, we see that the actual projected length 459 is roughly typical of a pick from the uniform. This affirms the strong rejection of (2.5) and points to a need to look at the structure of the higher order projection on its own terms.

An appropriate stability analysis was left open in [35]. If the data in Table 2.1 were a sample from a larger population, the sampling variability adds noise to the signal. How stable is the analysis above to natural stochastic perturbations? One standard approach is shown in the last row of Table 2.8. This is based on a boot-strap perturbation of the data in Table 2.1. Here, the votes of all 5972 rankers are put in a hat and a sample of size 5972 is drawn from the hat with replacement to give a new data set. The sum of squares decomposition is repeated. This resampling step (from the original population) was repeated 100 times. The entries in the last row of Table 2.8 show the average squared length of these projections. We see that they do not vary much from the original sum of squares. While not reported here, the boot-strap analogue of the second order analysis in Table 2.8 was quite stable. We conclude that sampling variability is not an important issue for this example.

2.7 Statistical analysis of an S_4 example

In [39] an S_4 example was analyzed. However, the data was analyzed using only the uniform distribution, which only tells half of the story. The analysis under hypergeometric sampling gives an important supplement. Briefly, a sample of 2262 German citizens were asked to rank order the desirability of four political goals:

1. Maintain order;

2. Give people more say in government;

3. Fight rising prices;

4. Protect freedom of speech.

1234	137	2134	48	3124	330	4123	21
1243	29	2143	23	3142	294	4132	30
1324	309	2314	61	3214	117	4213	29
1342	255	2341	55	3241	69	4231	52
1423	52	2413	33	3412	70	4312	35
1432	93	2431	59	3421	34	4321	27

Table 2.9: The number of German citizens who ranked the four political goals in a given order.

	Rank			
Goal	1	2	3	4
1	875	279	914	194
2	746	433	742	341
3	345	773	419	725
4	296	777	187	1002

Table 2.10: First order summary for the S_4 ranked data in Table 2.9.

The data appears in Table 2.9 and the first order summary in Table 2.10. The sizes of the projections for the data and the random walks appear in Table 2.11. We have corrected a typographical error in the data in [39], the 2431 entry should be 59.

The projection of the data into the second order subspace $S^{2,2}$ has squared length 268. The boot-strap analysis (Line 4 in Table 2.11) shows this is stable under sampling perturbations. The hypergeometric analysis (line 2 of Table 2.11) suggests that for the specific data, relatively large projections onto the second order space are typical, even if the first order model holds. This is quite different than the previous example. Still, the observed 268 is sufficiently much larger than 169 that a look at the second order projection is warranted. The uniform analysis points to the actual projection

	S^4	$S^{3,1}$	$S^{2,2}$	$S^{2,1,1}$	$S^{1,1,1,1}$
Data	462	381	268	49	4
Metropolis	462	381	169	37	8
Uniform	462	381	277	228	80
Bootstrap	462	381	269	56	7

Table 2.11: Length of the projections onto the five isotypic subspaces for the S_4 data and three perturbations.

being typical, this again suggests a serious look at the second order projection.

Remark 2.14. We note that the software package `LattE` [28] can be used to count how many data sets have a given first order summary. For our S_4 example (Table 2.9), these correspond to lattice points inside a convex polytope with 6285 vertices in $\mathbb{R}^{24}$. `LattE` quickly computes that there are 11606690287805167142987310121 (approximately 10^{28}) elements of $\mathbb{N}[S_4]$ with the same first order summary as our S_4 example. However, `LattE` was unable to compute this number for the S_5 data (Table 2.1).

Chapter 3

Toric ideals of homogeneous phylogenetic models

In this chapter, we consider the fully observed homogeneous phylogenetic model That is to say, every node of the tree is an observed, binary random variable and the transition probabilities are given by the same matrix on each edge of the tree. The ideal of invariants of this model is a toric ideal, returning to a major theme from Chapter 2.

We are able to compute the Gröbner basis and minimal generating set for this ideal for trees with up to 11 nodes. These are the first non-trivial Gröbner bases calculations in $2^{11} = 2048$ indeterminates. We conjecture that there is a quadratic Gröbner basis for binary trees, but that generators of degree n are required for certain non-binary trees on n nodes. The polytopes associated with these toric ideals display interesting finiteness properties. We describe the polytope for an infinite family of binary trees and conjecture (based on extensive computations) that there is a universal bound on the number of vertices of the polytope of a binary tree. This polytope is meaningful statistically — it solves the problem of *parametric inference*. Parametric inference solves the maximum a posteriori inference problem for all model parameters simultaneously. See [33] for an example of parametric inference applied to the biological problem of sequence alignment.

It should be noted that since all nodes are observed, the invariant calculations will not themselves be useful for phylogenetics. Furthermore, the homogeneous model is not very biologically relevant. However, the fully observed homogeneous model is particularly attractive due to the small number of parameters and the toric structure.

The material in this chapter comes from [43].

3.1 Homogeneous phylogenetic models

In this chapter we consider the homogeneous Markov model on a tree T where all transition matrices are equal, all nodes are binary and observable, and the root has uniform distribution. We write $A = \begin{pmatrix} \theta_{00} & \theta_{01} \\ \theta_{10} & \theta_{11} \end{pmatrix}$ for the transition matrices. Let $\rho(v)$ denote the parent of $v \in T$.

The probability of observing i at a node v is computed from the parent of v by

$$P(X_v = i) = \theta_{0i} P(X_{\rho(v)} = 0) + \theta_{1i} P(X_{\rho(v)} = 1).$$

We are interested in the algebraic relations satisfied by the joint distribution

$$p_{i_1 i_2 \ldots i_n} := P(X_1 = i_1, \ldots, X_n = i_n).$$

Writing the joint distribution in terms of the model parameters $\theta_{00}, \theta_{01}, \theta_{10}, \theta_{11}$, we have

$$p_{i_1 i_2 \ldots i_n} = \prod_{j=2}^{n} \theta_{i_{\rho(j)} i_j} \tag{3.1}$$

where the nodes of the tree are labeled 1 to n starting with the root. That is, the probability of observing a certain labeling of the tree is the product of the θ_{ij} that correspond to the transitions on all edges of the tree. The indeterminates θ_{ij} parameterize a toric variety of dimension 4 in $\mathbb{R}^{2^n}$. We let I_T be the corresponding toric ideal, called the ideal of phylogenetic invariants. In the notation of [98], the toric ideal I_T is specified by the 4 by 2^n configuration $\mathcal{A}_T$, where the column $\mathbf{a}_i$ consists of the exponent vector of the θ_{ij} in (3.1). We order the rows $(\theta_{00}, \theta_{01}, \theta_{10}, \theta_{11})$. Let P_T be the convex hull of the columns of $\mathcal{A}_T$.

We are interested in two questions from [72]. First, which relations on the joint probabilities $p_{i_1 \ldots i_n}$ does the model imply? This problem is solved by giving generators of the ideal of invariants I_T.

In Section 3.2, we study the generators of this ideal. Our main accomplishment is the computation of Gröbner and Markov bases for all binary trees with 11 nodes. These are computations in 2048 indeterminates, which we believe to be the largest number of indeterminates yet in a Gröbner basis calculation. We also calculate generating sets for all trees on at most 9 nodes. Based on this evidence, we conjecture that if T is binary, then the ideal I_T has a quadratic generating set. However, our calculations suggest that relations of degree n are necessary to generate I_T for certain trees with n nodes.

Our second goal is to determine, given a labeling of the tree T, if we can identify parameters θ_{ij} such that the labeling is the most likely among all labelings. This problem is solved by computing the normal fan of the toric variety in the sense of [50].

In Section 3.3, we study this normal fan and the polytope P_T. Our main result, Theorem 3.7, is an explicit description of the polytope P_T for an infinite family of binary trees. For this family, P_T always has 8 vertices and 6 facets which we characterize. We also present extensive calculations of P_T for various trees and conjecture that there is a bound on the number of vertices of P_T as T ranges over all binary trees.

Example 3.1. Let T be a path with 3 nodes. Then

$$\mathcal{A}_T = \begin{pmatrix} 2 & 1 & 0 & 0 & 1 & 0 & 0 & 0 \\ 0 & 1 & 1 & 1 & 0 & 1 & 0 & 0 \\ 0 & 0 & 1 & 0 & 1 & 1 & 1 & 0 \\ 0 & 0 & 0 & 1 & 0 & 0 & 1 & 2 \end{pmatrix},$$

the polytope P_T is three dimensional with seven vertices and six facets. The toric ideal of the path of length 3 is generated by 6 binomials

$$\begin{aligned} I_T = \langle & p_{101} - p_{010},\ p_{001}p_{100} - p_{000}p_{010}, \\ & p_{011}p_{100} - p_{001}p_{110},\ p_{011}p_{110} - p_{010}p_{111}, \\ & p_{001}^2 p_{111} - p_{000}p_{011}^2,\ p_{100}^2 p_{111} - p_{000}p_{110}^2 \rangle. \end{aligned}$$

3.2 Toric ideals

The toric ideals I_T are homogeneous, since all monomials in (3.1) have the same degree $n-1$. Thus they define projective toric varieties Y_T.

Recall that a projective toric variety given by a configuration $\mathcal{A} = (\mathbf{a}_1, \dots, \mathbf{a}_k)$ is covered by the affine toric varieties given by $\mathcal{A} - \mathbf{a}_i$. An affine toric variety defined by a configuration $\mathcal{B}$ is said to be smooth if the semigroup $\mathbb{N}\mathcal{B}$ is isomorphic to $\mathbb{N}^r$ for some r [99, Lemma 2.2].

Proposition 3.2. *The projective toric variety Y_T of a binary tree T is not smooth.*

Proof. Recall that the columns of the configuration $\mathcal{A}_T$ are indexed by 0/1-labelings of the tree T. Look at the affine chart $I_{\mathcal{A}-\mathbf{a}_{0\dots0}}$, where $\mathbf{a}_{0\dots0}$ corresponds to the all zero tree. On this chart, write $\tilde{\mathbf{a}}_i = \mathbf{a}_i - \mathbf{a}_{0\dots0}$. The cone $\mathbb{R}_{\geq 0}(\mathcal{A} - \mathbf{a}_{0\dots0})$ is simplicial, with extreme rays coming from the following labelings of the tree: let $10\dots0$ be the tree with a 1 at the root and zeros everywhere else, $0\dots01$ be the tree with a 1 at a single leaf and zeros everywhere else, and $1\dots1$ be the tree with all ones. That is, three generators of the semigroup are

$$\begin{aligned}\tilde{\mathbf{a}}_{10\dots0} &= (n-3, 0, 2, 0) - \mathbf{a}_{0\dots0} = (-2, 0, 2, 0)\\ \tilde{\mathbf{a}}_{0\dots01} &= (n-2, 1, 0, 0) - \mathbf{a}_{0\dots0} = (-1, 1, 0, 0)\\ \tilde{\mathbf{a}}_{1\dots1} &= (0, 0, 0, n-1) - \mathbf{a}_{0\dots0} = (-n+1, 0, 0, n-1)\end{aligned}$$

Now it is easy to check that, for example, the point $\tilde{\mathbf{a}}_* = (-n+1, 0, 2, n-3)$ does not lie in the semigroup generated by the three previous elements. Furthermore, this point comes from the labeling of a tree (the tree with all labels one except for 2 sibling leaves, their parent, and a single other leaf who are labeled zero). Thus it lies in the configuration $\mathcal{A} - \mathbf{a}_{0\dots0}$, so the semigroup requires at least 4 generators. Therefore, $\mathbb{N}(\mathcal{A} - \mathbf{a}_{0\dots0})$ is not isomorphic to $\mathbb{N}^3$ and so the toric variety Y_T is not smooth. □

Using `4ti2` [53], Gröbner and Markov bases for the ideal I_T were computed for all trees with at most 9 nodes as well as selected trees with 10 and 11 nodes. This took about 6 weeks of computer time in total on a 2GHz computer. The computations in 2048 variables (trees with 11 nodes) each took as long as a week and required over 2 GB of memory.

Details about the Markov bases for all binary trees with at most 11 nodes are shown in Table 3.1. These computations lead us to make the following conjectures.

Tree	Degree of I_T	#Minimal generators	Max degree of generator
	4	4	2
	28	79	2
	92	441	2
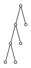	96	561	2
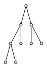	210	2141	2
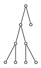	220	2068	2
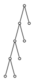	210	2266	2
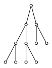	412	7121	2
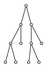	404	7131	2
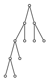	400	7137	2
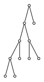	412	7551	2
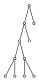	412	7551	2
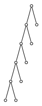	404	7561	2

Table 3.1: Degree of I_T, number of minimal generators, and maximum degree of a generator of I_T for binary trees.

Conjecture 3.3. *The toric ideal corresponding to a binary tree is generated in degree 2. More generally, if every non-leaf node of the tree has the same number of children d (for $d \geq 2$), the toric ideal is generated in degree 2.*

Conjecture 3.4. *There exists a quadratic Gröbner basis for the toric ideal of a binary tree.*

Using the Gröbner Walk [24] implementation in `magma`, we have computed thousands of Gröbner bases for random term orders for the smallest binary trees. It doesn't seem to be possible to compute the entire Gröbner fan for these examples with `CaTS` [57], but the random computations have yielded some information: Conjecture 3.4 is true for the binary tree with 5 nodes, in fact, there are at least 4 distinct quadratic Gröbner bases for this tree. Analysis of these bases lends some optimism towards Conjecture 3.4. However, for the binary trees on 7 nodes, computation of over 1000 Gröbner bases did not find a quadratic basis. The best basis found contained quartics and some bases even contained relations of degree 29.

Another nice family of toric ideals is given by I_T for T a path of length n. Table 3.2 presents data for Markov bases of paths that leads us to conjecture that this family also has well behaved ideals.

Conjecture 3.5. *The toric ideal corresponding to a path is generated in degree 3, with $2n-4$ generators of degree 3 needed.*

Unfortunately, the toric ideal of a general tree doesn't seem to have such simple structure. For $n \leq 9$, the trees with highest degree minimal generators are those of the form 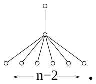. These trees require generators of degree n.

3.3 Viterbi polytopes

In this section, we are interested in the following problem. Given any observation $(i_1, \ldots, i_n)$ of the tree, which matrices $A = (\theta_{ij})$ make $p_{i_1 \ldots i_n}$ maximal among the coordinates of the distribution p?

# of nodes	Degree of I_T	#Minimal generators	Max degree	Number of deg 3
3	6	6	3	2
4	19	32	3	4
5	36	102	3	6
6	61	259	3	8
7	90	540	3	10
8	127	1041	3	12
9	168	1842	3	14
10	217	3170	3	16
11	270	5286	3	18

Table 3.2: Degree of I_T, size of Markov basis, maximum degree of a minimal generator, and number of degree 3 generators for paths.

To solve this problem, transform to logarithmic coordinates $x_{ij} = -\log(\theta_{ij})$. Then the condition that $p_{i_1 \ldots i_n} > p_{l_1 \ldots l_n}$ for all $(l_1, \ldots l_n) \in \{0,1\}^n$ is translated into the the linear system of inequalities

$$x_{i_1 i_2} + \cdots + x_{i_{\rho(n)} i_n} > x_{l_1 l_2} + \cdots + x_{l_{\rho(n)} l_n}$$

for all $(l_1, \ldots l_n) \in \{0,1\}^n$. The set of solutions to these inequalities is a polyhedral cone. For most values of $i_1, \ldots, i_n$, this cone will be empty. Those sequences $i_1, \ldots, i_n$ for which the cone is maximal are called *Viterbi* sequences. The collection of the cones, as $(i_1, \ldots, i_n)$ varies, is the normal fan of the polytope P_T, where P_T is the convex hull of the columns of $\mathcal{A}_T$.

Notice that P_T is a polytope in $\mathbb{R}^4$. However, since all the monomials in (3.1) are of degree $n-1$, we see that this polytope is actually contained in $n-1$ times the unit simplex in $\mathbb{R}^4$. Thus, P_T is actually a 3 dimensional polytope. We call P_T the *Viterbi* polytope.

The polytopes P_T show remarkable finiteness properties as T varies. Since P_T is defined as the convex hull of 2^n vectors, it would seem that it could have arbitrarily bad structure. However, as it is contained in $n-1$ times the unit simplex, it can be shown that there are at most $O(n^{1.5})$ integral points in P_T.

Example 3.6. Eric Kuo has shown [58] that if T is a path with n nodes, then P_T has only two combinatorial types for $n > 3$, depending only on the parity of n. The polytope

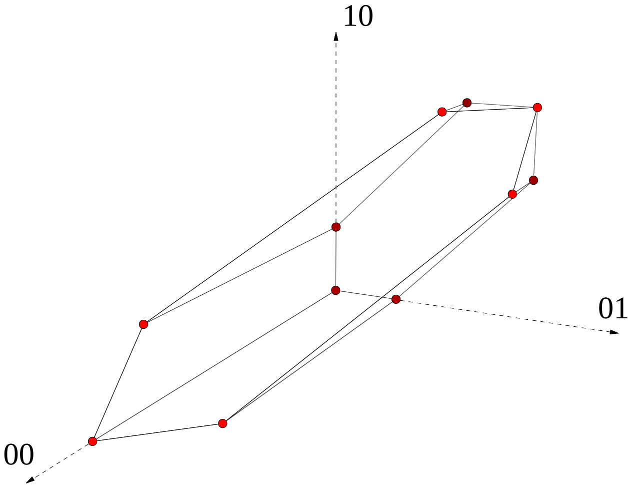

Figure 3.1: The Viterbi polytope of a path with 7 nodes, after projecting onto the first three coordinates (x_{00}, x_{01}, x_{10}).

for the path with 7 nodes is shown in Figure 3.1. Think of this picture as roughly a tetrahedron with the vertex corresponding to all 0 → 1 transitions and the vertex with all 1 → 0 transitions both sliced off. These two inequalities come from the fact that for a path, the number of 0 → 1 and the number of 1 → 0 transitions can differ by at most one.

Two facts from Example 3.6 are important to remember. First, the structure of the polytope is related more to the topology of the tree than the size of the tree. Second, there is a distinction between even and odd length paths. We call a binary tree *completely odd* if the tree has all leaves at an odd distance from the root. For example, the tree 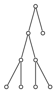 is completely odd.

Theorem 3.7. *Let T be a completely odd binary tree with more than three nodes. The associated polytope P_T always has the same combinatorial type with 8 vertices and 6 facets (see Figure 3.2).*

Proof. First, we derive six inequalities that are satisfied by any binary tree, deriving a "universal" polytope for binary trees. Then we show that a completely odd binary tree has labelings that give us all vertices of the "universal" polytope.

Thinking of the polytope space as the log space of the parameters θ_{ij}, we write $\mathbb{R}^4$ with coordinates $b_{00}, b_{01}, b_{10}, b_{11}$. Since P_T lies in $n-1$ times the unit simplex in $\mathbb{R}^4$, we have $b_{00} + b_{01} + b_{10} + b_{11} = n - 1$ and the 4 inequalities $b_{ij} \geq 0$. We claim that any binary tree T satisfies two additional inequalities

$$\frac{b_{00} - b_{01}}{2} + b_{10} \leq \frac{n+1}{2}, \tag{3.2}$$

$$\frac{b_{11} - b_{10}}{2} + b_{01} \leq \frac{n+1}{2}. \tag{3.3}$$

We prove (3.2), the second inequality follows by interchanging 1 and 0.

Fix a labeling of the binary tree. We claim that the left hand side of (3.2) counts the net number of zeros that are "created" while moving down the tree, that is, it counts the number of leaves that are zero minus one if the root is labeled zero. Pick a non-leaf of the tree which is labeled "0". It has two children. If both are "0", then this node contributes 2 to $b_{00} - b_{01}$. If both are "1", then this node contributes -2 to $b_{00} - b_{01}$. If one is "0" and one is "1", then the node doesn't contribute. We think of a "0" node with two "0" children as having created a new zero and a "0" node with two "1" children as having deleted a zero. Therefore we see that the term $(b_{00} - b_{01})/2$ counts the net number of zeros created as children of "0" nodes. Similarly, if a non-leaf is labeled "1", then its contribution to b_{10} counts the number of new zeros in the children.

Since there are $\frac{n+1}{2}$ leaves in a binary tree, there can be at most $\frac{n+1}{2}$ zeros created, so (3.2) holds. Notice that the labelings that lie on this facet are exactly those with a one at the root and all zeros at the leaves.

These six inequalities and the equality $b_{00} + b_{01} + b_{10} + b_{11} = n - 1$ define a three dimensional polytope in $\mathbb{R}^4$. It is straightforward to compute that there are eight vertices of this polytope:

$$\begin{gathered}
(n-1, 0, 0, 0), \quad (n-3, 0, 2, 0) \\
\left(\frac{n-3}{2}, \frac{n+1}{2}, 0, 0\right), \quad \left(0, \frac{2n}{3}, \frac{n-3}{3}, 0\right) \\
\left(0, \frac{n-3}{3}, \frac{2n}{3}, 0\right), \quad \left(0, 0, \frac{n+1}{2}, \frac{n-3}{2}\right) \\
(0, 2, 0, n-3), \quad (0, 0, 0, n-1)
\end{gathered}$$

Six of these vertices occur in any binary tree: a tree with all zeros gives the $(n-1,0,0,0)$ vertex, a tree with a one at the root and zeros elsewhere gives $(n-3,0,2,0)$, and a tree with ones at the leaves and zeros elsewhere gives $(\frac{n-3}{2},\frac{n+1}{2},0,0)$. Interchanging 1 and 0 gives three more vertices. However, the remaining two vertices aren't obtained by all binary trees.

The vertex $(0,\frac{n-3}{3},\frac{2n}{3},0)$ lies on the facet defined by (3.2), so we know it must have a one at the root, all zeros at the leaves, and the labels must alternate going down the tree since there are no zero to zero or one to one transitions. This means that this vertex is representable by a labeled tree if and only if the tree has all leaves at an odd depth from the root. Notice that this implies that n must be divisible by 3 for the tree to be completely odd. Finally, if $n > 3$ is odd and divisible by 3, then $n \geq 9$ and one checks that the eight vertices are distinct.

See Figure 3.2 for a picture of the polytope and a Schlegel diagram with descriptions of the labelings on the facets and at the vertices. □

In the case where T is binary but not completely odd, the polytope shares 6 vertices with this universal polytope, but the remaining 2 vertices are either not integral or not realizable. However, the polytope still shares much of the boundary with the universal polytope, so it is perhaps realistic to expect that the polytope for a general binary tree behaves well. Table 3.3 shows data from computations for all binary trees with at most 23 nodes. The maximum number of vertices of P_T appears to grow very slowly with the size of the tree.

Although binary trees seem to generally have polytopes with few vertices, arbitrary trees are not so nice. For example, Figure 3.3 shows a tree with 15 nodes that has a polytope with 34 vertices.

Table 3.4 shows data for all trees on at most 15 nodes. It appears that the maximum number of vertices for the polytope of an arbitrary tree of size n grows approximately as $2n$. Notice that the tree with all leaves at depth 1 has P_T a tetrahedron, giving the unique minimum number, 4, of vertices for all trees.

Conjecture 3.8. *There is a bound on the number of vertices of P_T if T is a binary tree. However, for an arbitrary tree, the number of vertices of P_T is unbounded.*

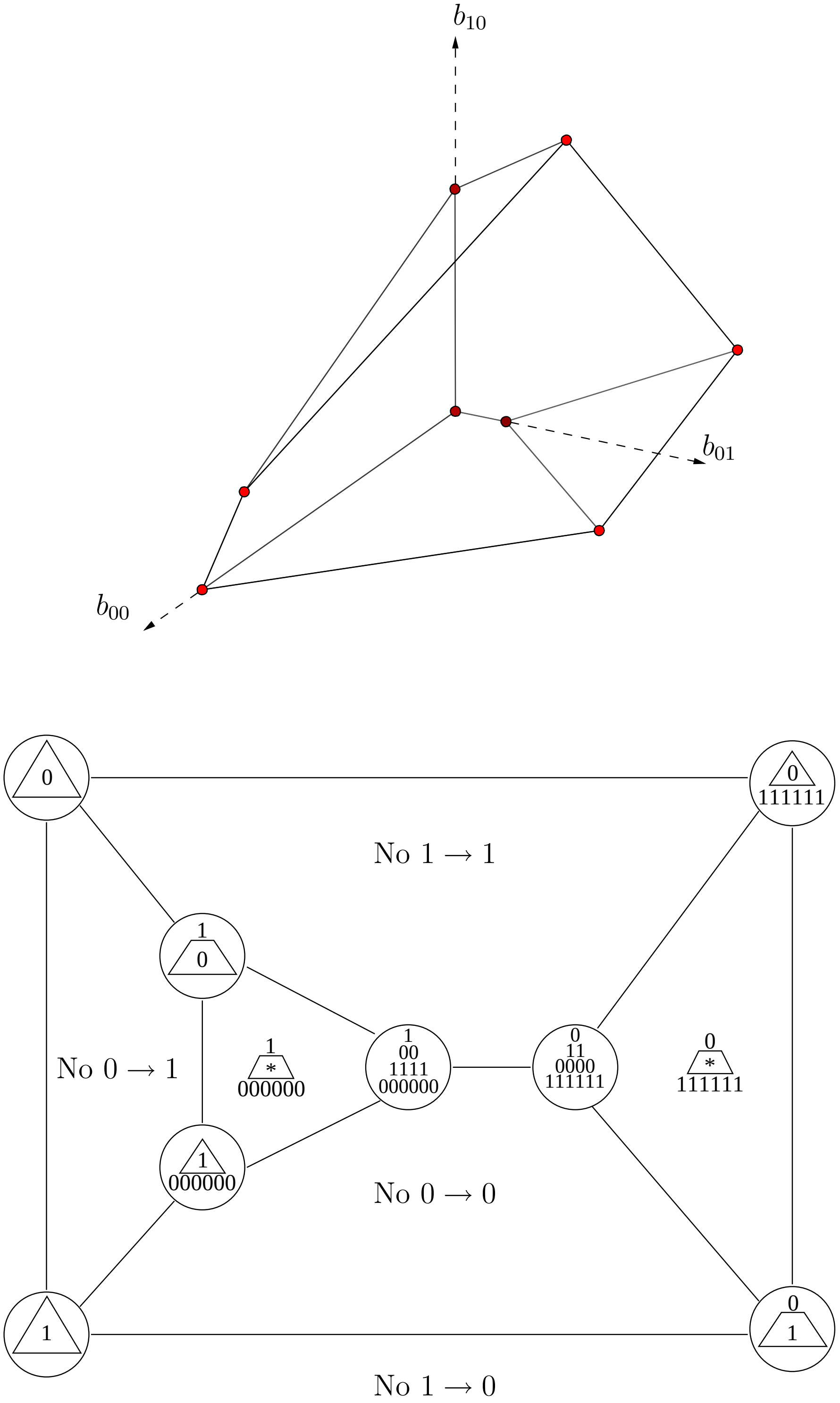

Figure 3.2: The polytope of the completely odd binary tree and a Schlegel diagram of this polytope with facets and vertices labeled.

Number of nodes	Number of binary trees	Min vertices	Max vertices	Ave vertices
3	1	4	4	4
5	1	7	7	7
7	2	8	10	9
9	3	8	13	11.33
11	6	10	14	11.66
13	11	11	13	11.91
15	23	8	16	14.35
17	46	12	17	13.82
19	98	10	20	14.65
21	207	8	19	14.8
23	451	10	20	15.6

Table 3.3: Minimum, maximum and average number of vertices of P_T over all binary trees with at most 23 nodes.

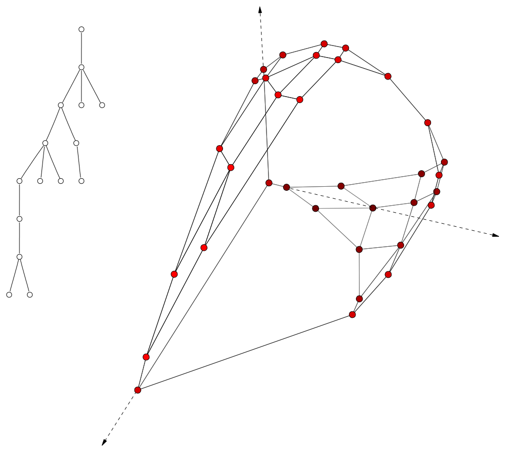

Figure 3.3: A tree T with 15 nodes where P_T has 34 vertices, 58 edges, and 26 facets.

Number of nodes	Number of trees	Min vertices	Max vertices	Ave vertices
3	2	4	7	5.5
4	4	4	8	7
5	9	4	11	8
6	20	4	14	9.7
7	48	4	15	10.75
8	115	4	20	12.59
9	286	4	21	13.67
10	719	4	22	15.42
11	1842	4	25	16.60
12	4766	4	28	18.3
13	12486	4	31	19.5
14	32973	4	32	19.75
15	87811	4	34	22.6

Table 3.4: Minimum, maximum and average number of vertices of P_T over all trees with at most 15 nodes

We conclude with a description of an algorithm to quickly compute P_T. Notice that the naive method involves taking the convex hull of 2^n points, but this can certainly be improved, since there are many duplicates. The *polytope propagation algorithm* of [71] can be used to calculate P_T in polynomial time in the number of nodes. This powerful algorithm can be used to perform *parametric inference* for many statistical models of interest to computational biologists. In our case, the algorithm depends on the observation that P_T can be rewritten roughly as the Minkowski sum of P_{T_1} and P_{T_2}, where T_1 and T_2 are the left and right subtrees of the root (after splitting into 8 subcases depending on the labels of the root and its children). This can be applied recursively down the tree to give a polynomial time algorithm.

Chapter 4

Tree construction using singular value decomposition

In this chapter, we present a new, statistically consistent algorithm for phylogenetic tree construction that uses the algebraic theory of statistical phylogenetic models as introduced in Section 1.4 and studied in Chapter 3. Our basic tool is *Singular Value Decomposition* (SVD) from numerical linear algebra.

Starting with an alignment of n DNA sequences, we show that SVD allows us to quickly decide whether a split of the taxa occurs in their phylogenetic tree, assuming only that evolution follows a tree Markov model. Using this fact, we have developed an algorithm to construct a phylogenetic tree by computing only $O(n^2)$ SVDs.

We have implemented this algorithm in `C++` using the `SVDLIBC` library (available at `http://tedlab.mit.edu/~dr/SVDLIBC/`) and have done extensive testing with simulated and real data. The algorithm is fast in practice on trees with 20–30 taxa.

We begin by describing the general Markov model and then show how to flatten the joint probability distribution along a partition of the leaves in the tree. We give rank conditions for the resulting matrix; most notably, we give a set of new rank conditions that are satisfied by non-splits in the tree. Armed with these rank conditions, we present the tree-building algorithm, using SVD to calculate how close a matrix is to a certain rank. Finally, we give experimental results on the behavior of the algorithm with both simulated and real-life (ENCODE) data. The material in this chapter comes from the book chapter [44].

4.1 The general Markov model

We assume that evolution follows a tree Markov model, as introduced in Section 1.4, with evolution acting independently at different sites of the genome. We do not assume that the transition matrices for the model are stochastic. Furthermore, we do not assume the existence of a global rate matrix.

This model is called the general Markov model. It is a more general model than any in the Felsenstein hierarchy [73, pg. 154]. The main results in this chapter therefore hold no matter what model of evolution one works with.

Under the general dogma that statistical models are algebraic varieties, the polynomials (called "phylogenetic invariants") defining the varieties are of great interest. Phylogenetic invariants have been studied extensively since [59, 22]. Linear invariants for the Jukes–Cantor model have been used to infer phylogenies on four and five taxa; see [85]. Sturmfels and Sullivant finished the classification of the invariants for group-based models [97]; see [21] for an application of these invariants for constructing trees on four taxa. Invariants for the general Markov model have been studied in [2, 3].

The main problem with invariants is that there are exponentially many polynomials in exponentially many variables to test on exponentially many trees. Because of this, they are currently considered impractical by many and have only been applied to small problems. However, we solve the problem of this combinatorial explosion by only concentrating on invariants which are given by rank conditions on certain matrices, called "flattenings".

4.2 Flattenings and rank conditions

Recall that a *split* $\{A, B\}$ in a tree is a partition of the leaves obtained by removing an edge of the tree. We will say that $\{A, B\}$ is a *partition* of the set of leaves if it is not necessarily a split but merely a disjoint partition of the set of leaves into two sets.

Throughout, all trees will be assumed to be binary with n leaves. We let m

denote the number of states in the alphabet Σ. Usually $m = 4$ and $\Sigma = \{A, C, G, T\}$ or $m = 2$ and $\Sigma = \{0, 1\}$. We will write the joint probabilities of an observation on the leaves as $p_{i_1 \ldots i_n}$. That is, $p_{i_1 \ldots i_n}$ is the probability that leaf j is observed to be in state i_j for all $j \in \{1, \ldots, n\}$. We write P for the entire probability distribution.

Although the descriptions of tree-based models in this book all deal with rooted trees, we will mostly consider unrooted tree models, which are equivalent to them for the general Markov model; see [3] for details on this technical point. Our tree-building algorithm constructs an unrooted tree, additional methods would be required to find the root.

Definition 4.1. A *flattening* along a partition $\{A, B\}$ is the $m^{|A|}$ by $m^{|B|}$ matrix where the rows are indexed by the possible states for the leaves in A and the columns are indexed by the possible states for the leaves in B. The entries of this matrix are given by the joint probabilities of observing the given pattern at the leaves. We write $\mathrm{Flat}_{A,B}(P)$ for this matrix.

Example 4.2 (Flattening a partition on 4 taxa)**.** Let T be a tree with 4 leaves and let $m = 4$, $\Sigma = \{\texttt{A,C,G,T}\}$. The partition $\{1, 3\}, \{2, 4\}$ flattens to the 16×16 matrix $\mathrm{Flat}_{\{1,3\},\{2,4\}}(P)$ where the rows are indexed by bases of taxa 1 and 3 and the columns by bases of taxa 2 and 4:

$$\mathrm{Flat}_{\{1,3\},\{2,4\}}(P) = \begin{array}{c|ccccccc|}
 & \texttt{AA} & \texttt{AC} & \texttt{AG} & \texttt{AT} & \texttt{CA} & \texttt{CC} & \ldots \\
\texttt{AA} & p_{\texttt{AAAA}} & p_{\texttt{AAAC}} & p_{\texttt{AAAG}} & p_{\texttt{AAAT}} & p_{\texttt{ACAA}} & p_{\texttt{ACAC}} & \cdots \\
\texttt{AC} & p_{\texttt{AACA}} & p_{\texttt{AACC}} & p_{\texttt{AACG}} & p_{\texttt{AACT}} & p_{\texttt{ACCA}} & p_{\texttt{ACCC}} & \cdots \\
\texttt{AG} & p_{\texttt{AAGA}} & p_{\texttt{AAGC}} & p_{\texttt{AAGG}} & p_{\texttt{AAGT}} & p_{\texttt{ACGA}} & p_{\texttt{ACGC}} & \cdots \\
\texttt{AT} & p_{\texttt{AATA}} & p_{\texttt{AATC}} & p_{\texttt{AATG}} & p_{\texttt{AATT}} & p_{\texttt{ACTA}} & p_{\texttt{ACTC}} & \cdots \\
\texttt{CA} & p_{\texttt{CAAA}} & p_{\texttt{CAAC}} & p_{\texttt{CAAG}} & p_{\texttt{CAAT}} & p_{\texttt{CCAA}} & p_{\texttt{CCAC}} & \cdots \\
\vdots & \vdots & \vdots & \vdots & \vdots & \vdots & \vdots & \vdots
\end{array}.$$

Next we define a measure of how close a general partition of the leaves is to being a split. If A is a subset of the leaves of T, we let T_A be the subtree induced by the leaves in A. That is, T_A is the minimal set of edges needed to connect the leaves in A.

Definition 4.3. Suppose that $\{A, B\}$ is a partition of $[n]$. The *distance* between the partition $\{A, B\}$ and the nearest split, written $e(A, B)$, is the number of edges that occur in $T_A \cap T_B$.

Notice that $e(A, B) = 0$ exactly when $\{A, B\}$ is a split. Thus $e(A, B)$ gives a measure of how close $\{A, B\}$ is to being a split.

Consider $T_A \cap T_B$ as a subtree of T_A. Color the nodes in $T_A \cap T_B$ red, the nodes in $T_A \setminus (T_A \cap T_B)$ blue. Say that a node is *monochromatic* if it and all of its neighbors are of the same color. We let $\operatorname{mono}(A)$ be the number of monochromatic red nodes. That is:

Definition 4.4. Define $\operatorname{mono}(A)$ as the number of nodes in $T_A \cap T_B$ that do not have a node in $T_A \setminus (T_A \cap T_B)$ as a neighbor.

See Figure 4.1 for an example of $e(A, B)$ and $\operatorname{mono}(A)$. Our main theorem ties together how close a partition is to being a split with the rank of the flattening associated to that partition.

Theorem 4.5. *Let $\{A, B\}$ be a partition of $[n]$, let T be a binary, unrooted tree with leaves labeled by $[n]$, and assume that the joint probability distribution P comes from a Markov model on T with an alphabet with m letters. Let*

$$\mathcal{P}(A, B) = \min\left(e(A, B) + 1 - \operatorname{mono}(A), e(A, B) + 1 - \operatorname{mono}(B), |A|, |B|\right). \tag{4.1}$$

Then the generic rank of the flattening $\operatorname{Flat}_{A,B}(P)$ is given by $m^{\mathcal{P}(A,B)}$.

Proof. We claim that $\operatorname{Flat}_{A,B}(P)$ can be thought of as the joint distribution for a simple graphical model. Pick all the nodes that are shared by the induced subtrees for A and B: call this set R. If R is empty, then $\{A, B\}$ is a split; in that case let R be one of the vertices of the edge separating A and B. Notice that $|R| = e(A, B) + 1$. Think of these vertices as a single hidden random variable, which we will also call R, with $m^{|R|} = m^{e(A,B)+1}$ states. Group the states of the nodes in A together into one $m^{|A|}$-state observed random variable; similarly the nodes in B are grouped into a $m^{|B|}$-state random variable. Then create the graphical model with one hidden $m^{|R|}$-state random variable and two descendent observed variables with $m^{|A|}$ and $m^{|B|}$ states. Notice that $\operatorname{Flat}_{A,B}(P)$ is the joint distribution for this model. See Figure 4.1 for an example.

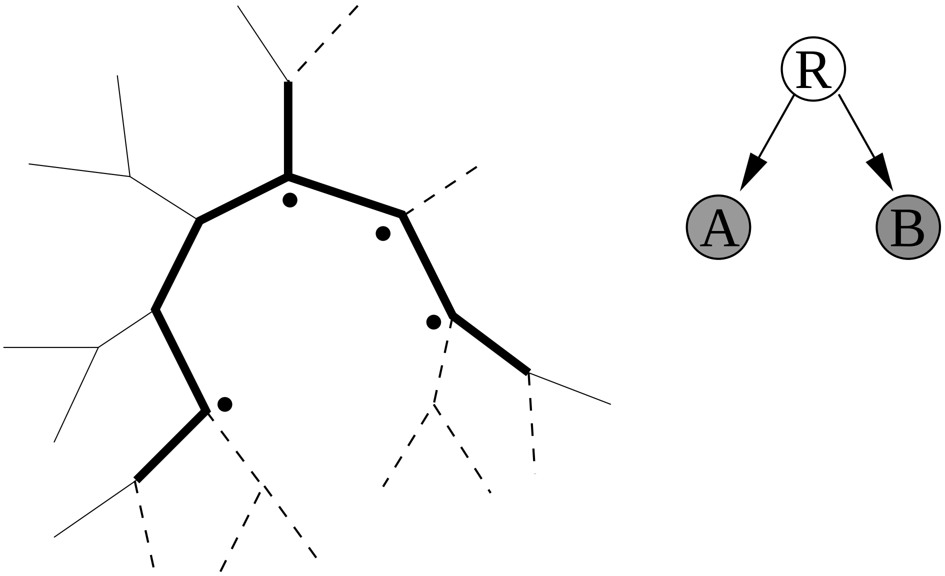

Figure 4.1: Determining the rank of $\mathrm{Flat}_{A,B}(P)$ where $\{A, B\}$ is not a split. If A is given by the 8 dashed leaves and B by the 7 solid leaves, then $e(A, B) = 8$ (shown in bold) and $\mathrm{Flat}_{A,B}(P)$ is the joint distribution for a 3-state graphical model where the root R has m^9 states and the descendents A and B have m^8 and m^7 states, respectively. Here $\mathrm{mono}(B) = 4$ (indicated by the dots), so the $m^9 \times m^8$ matrix M_A has rank $m^{9-4} = m^5$, which is the rank of $\mathrm{Flat}_{A,B}(P)$.

Furthermore, the distribution for this simplified model factors as

$$\mathrm{Flat}_{A,B}(P) = M_A^{\mathrm{T}} \operatorname{diag}(\pi(R)) M_B \tag{4.2}$$

where $\pi(R)$ is the distribution of R and M_A and M_B are the $m^{|R|} \times m^{|A|}$ and $m^{|R|} \times m^{|B|}$ transition matrices. That is, the (i,j)th entry of M_A is the probability of transitioning from state i at the root R to state j at A.

To say the tree distribution factors as (4.2) just means that

$$\mathrm{Prob}(A = i, B = j) = \sum_k \mathrm{Prob}(R = k)\,\mathrm{Prob}(A = i \mid R = k)\,\mathrm{Prob}(B = j \mid R = k).$$

Notice that all of the terms in this expression can be written as polynomials in the edge parameters (after choosing a rooting). Therefore the rank of $\mathrm{Flat}_{A,B}(P)$ is at most $m^{\min(|R|,|A|,|B|)}$.

However, the matrices in this factorization do not necessarily have full rank. For example, if one of the nodes in R has only neighbors that are also in R, then the $m^{|R|} \times m^{|A|}$ transition matrices from R to A have many rows that are the same, since the transition from a state of R to a state of A does not depend on the value of this one node. More generally, if a node of R has no neighbors in $T_A \setminus (T_A \cap T_B)$, then the entries of the transition matrix M_A do not depend on the value of this node. But the entries do depend on the values of all other nodes of R (that is, those with neighbors in $T_A \setminus (T_A \cap T_B)$). So R really behaves like a model with $m^{|R|-\mathrm{mono}(A)}$ states on the transition to A and $m^{|R|-\mathrm{mono}(B)}$ states for the transition to B. There are enough parameters so that after canceling out these equal rows, all other rows are linearly independent. Therefore, the rank of M_A is $\min\left(m^{|R|-\mathrm{mono}(A)}, m^{|A|}\right)$ (and similarly for M_B). □

Remark 4.6. We note that $\mathcal{P}(A,B)$ is related to the parsimony score for the tree with leaves in A in state 0 and leaves in B in state 1. First notice that all the nodes in $T_A \setminus (T_A \cap T_B)$ need to be in state 0 and the nodes in $T_B \setminus (T_A \cap T_B)$ need to be in state 1 to obtain a parsimonious tree. Therefore, we are just left with the nodes in $T_A \cap T_B$ to decide. If we set all the nodes in $T_A \cap T_B$ to be in state 1, then $e(A,B) + 1 - \mathrm{mono}(A)$ is the parsimony score, since this quantity is the number of nodes of $T_A \cap T_B$ that have a node in $T_A \setminus (T_A \cap T_B)$ as a neighbor. The case where the nodes in $T_A \cap T_B$ are in state 0 gives parsimony score $e(A, B) + 1 - \text{mono}(B)$. In many cases, one of these two labelings is the most parsiminous. However, there are trees which have a parsimony score which is lower than $\mathcal{P}(A, B)$. For example, trees with large clusters of monochromatic nodes for both A and B will tend to have low parsimony scores but relatively large $\mathcal{P}(A, B)$.

Theorem 4.5 gives rise to a well-known corollary upon noticing that if $\{A, B\}$ is a split, then $e(A, B) = 0$ (see [3], for example).

Corollary 4.7. *If $\{A, B\}$ is a split in the tree, the generic rank of $\text{Flat}_{A,B}(P)$ is m.*

A partial converse of Corollary 4.7 will be used later.

Corollary 4.8. *If $\{A, B\}$ is not a split in the tree, and we have $|A|, |B| \geq 2$ then the generic rank of $\text{Flat}_{A,B}(P)$ is at least m^2.*

Proof. Since we have $|A|, |B| \geq 2$, we must show that the two other exponents in (4.1) are at least 2. That is, we have to show that $e(A, B) + 1 - \text{mono}(A) \geq 2$ (the case for B is symmetric). This term counts the number of nodes in $T_A \cap T_B$ that are directly connected to a part of T_A outside of $T_A \cap T_B$. Since $\{A, B\}$ is not a split, we know that $|T_A \cap T_B| = e(A, B) + 1 \geq 2$. Consider $T_A \cap T_B$ as a subtree with at least 2 nodes of T_A. The only way for all but one of these nodes to be isolated from the rest of the tree is to have the two consist of a leaf and its parent. However, this is impossible since $\{A, B\}$ is a disjoint partition of the set of leaves, so $T_A \cap T_B$ contains no leaves. □

Example 4.9. In Example 4.2, the 16×16 matrix $\text{Flat}_{\{1,3\},\{2,4\}}(P)$ has rank 4 if the split $\{\{1, 3\}, \{2, 4\}\}$ occurs in the tree, otherwise, it has rank 16.

In fact, if $m = 2$, it has recently been shown [4] that the rank conditions in Corollary 4.7 generate the ideal of invariants for the general Markov model. However, they do not suffice if $m = 4$, since in that case a polynomial of degree 9 lies in the ideal of invariants (see [95, 51]) but this polynomial is not generated by the degree 5 rank conditions (see [60]).

4.3 Singular value decomposition

Singular Value Decomposition provides a method to compute the distance between a matrix and the nearest rank k matrix. In this section, we briefly introduce the basic properties of SVD for real matrices. See [30] for a thorough treatment.

Definition 4.10. A *singular value decomposition* of a $m \times n$ matrix A (with $m \geq n$) is a factorization $A = U\Sigma V^{\mathrm{T}}$ where U is $m \times n$ and satisfies $U^{\mathrm{T}}U = I$, V is $n \times n$ and satisfies $V^{\mathrm{T}}V = I$ and $\Sigma = \operatorname{diag}(\sigma_1, \sigma_2, \ldots, \sigma_n)$, where $\sigma_1 \geq \sigma_2 \geq \cdots \geq \sigma_n \geq 0$ are called the *singular values* of A.

Definition 4.11. Let a_{ij} be the (i,j)th entry of A. The *Frobenius norm*, written $\|A\|_{\mathrm{F}}$, is the root-sum-of-squares norm on $\mathbb{R}^{m \cdot n}$. That is,

$$\|A\|_{\mathrm{F}} = \sqrt{\sum a_{ij}^2}.$$

The L_2 *norm* (or operator norm), written $\|A\|_2$, is given by

$$\|A\|_2 = \max_{\substack{x \in \mathbb{R}^n \\ x \neq 0}} \left\{ \frac{\|Ax\|}{\|x\|} \right\},$$

where $\|x\|$ is the usual root-sum-of-squares vector norm.

The following is Theorem 3.3 of [30]:

Theorem 4.12. *The distance from A to the nearest rank k matrix is*

$$\min_{\operatorname{Rank}(B)=k} \|A - B\|_{\mathrm{F}} = \sqrt{\sum_{i=k+1}^{m} \sigma_i^2}$$

in the Frobenius norm and

$$\min_{\operatorname{Rank}(B)=k} \|A - B\|_2 = \sigma_{k+1}$$

in the L_2 norm.

One way of computing the singular values is to compute the eigenvalues of $A^{\mathrm{T}}A$; the singular values are the square roots of these eigenvalues. Therefore, general techniques for solving the real symmetric eigenvalue problem can be used to compute the SVD. These various methods, both iterative and direct, are implemented by many software packages for either sparse or general matrices. We will discuss the computational issues with SVD after we describe how to use it to construct phylogenetic trees.

4.4 Tree-construction algorithm

Now that we know how to tell how close a matrix is to being of a certain rank, we can test whether a given split comes from the underlying tree or not by using the SVD to tell how close a flattening matrix is to being rank m. However, since there are exponentially many possible splits, we must carefully search through this space. Following a suggestion by S. Snir, we do this by building the tree bottom up, at each step joining cherries together, in a method reminiscent of neighbor-joining.

It is an interesting open question whether the additional information in Theorem 4.5 about non-splits that are almost splits can be harnessed to produce an improved algorithm.

Algorithm 4.13 (Tree construction with SVD)**.**
Input: A multiple alignment of genomic data from n species, from the alphabet Σ with m states.
Output: An unrooted binary tree with n leaves labeled by the species.

Initialization: Compute empirical probabilities $p_{i_1 \dots i_n}$. That is, count occurrences of each possible column of the alignment, ignoring columns with characters not in Σ. Store the results in a sparse format.

Loop: For k from n down to 4, perform the following steps.

For each of the $\binom{k}{2}$ pairs of species compute the SVD for the split $\{\{\text{pair}\}, \{\text{other } k-2 \text{ species}\}\}$. Pick the pair whose flattening is closest to rank m according to the Frobenius norm and join this pair together in the tree. That is, consider this pair as a single element when picking pairs at the next step.

Proposition 4.14. *Algorithm 4.13 runs in time $O(n^3L^4)$ for an input of length L for n species.*

Proof. Notice that although each flattening is of exponential size (i.e., of size $m^{|A|} \times m^{|B|}$), these matrices must be very sparse. If an alignment is of length L, at most L entries of the flattening are non-zero. Furthermore, while constructing the flattening, we can throw out all rows and columns which consist of all zeros. This operation does not take any additional time beyond the $O(nL)$ time it takes to construct the flattening and it does not change the singular value decomposition. Computing exactly all singular values of an $\alpha \times \beta$ matrix takes $O(\alpha^2\beta + \alpha\beta^2)$ time (see [30]). In our case, $\alpha, \beta \leq L$, so this gives a factor of $O(L^3)$.

Finally, we need to compute $O(n^2)$ SVDs. At the first step, we compute an SVD $\binom{n}{2}$ times. At each subsequent step, we only need to compute those splits involving the pair that we just joined together. Thus we compute $(n-2)+(n-3)+\cdots+3 = \binom{n-1}{2}-3$ total SVDs after the first step for $\binom{n}{2} + \binom{n-1}{2} - 3 = (n-1)^2 - 3$ SVD computations in total. □

Proposition 4.14 shows that our algorithm runs in polynomial time in the input size. Although the exponents in the polynomials are fairly large, there is some cause for optimism. Lanczos iterative methods (cf. Chapter 7 of [30]) allow singular values to be computed iteratively, one at a time, starting with the largest. Therefore we don't need to compute all singular values, only those which are larger than some error bound (all singular values could be computed to break ties, if necessary). These iterative methods run much faster than exact methods. However, it is an open question about how large L must be as a function of n in order to reliably construct the tree using this method — it may turn out that L must be exponential in n.

Since we will be comparing the SVD from different sized splits, we need to compute distances in the Frobenius norm, which does not change as the dimensions of the matrices change (as long as the number of entries is constant). This means that we should compute all singular values. But in practice, the singular values typically decrease very quickly, so it suffices to compute only the largest singular values to estimate the Frobenius norm to good accuracy.

By exploiting the sparsity and only computing singular values until they become sufficiently small, we find that we are able to very quickly compute the SVD for flattenings coming from trees with at most 31 leaves with binary data ($m = 2$) and up to 15 leaves with DNA data ($m = 4$). This limitation is due to limits on the size of array indices in `SVDLIBC` and can probably be exceeded. Furthermore, there are approximation algorithms for SVD that could possibly make very large problems practical [49].

Theorem 4.15. *Algorithm 4.13 is statistically consistent. That is, as the probability*

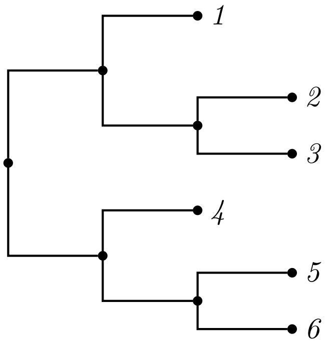

Figure 4.2: The 6-taxa tree constructed in Example 4.16.

distribution converges to a distribution that comes from the general Markov model on a binary tree T, the probability that Algorithm 4.13 outputs T goes to 1.

Proof. We must show that the algorithm picks a correct split at each step; that is, as the empirical distribution approaches the true distribution, the probability of choosing a bad split goes to zero. By Corollary 4.7, we see that a true split will lead to a flattening that approaches a rank m matrix, while Corollary 4.8 shows that other partitions will approach a matrix of rank at least m^2 (except for partitions where one set contains only one element; however, these are never considered in the algorithm). Therefore, as the empirical distribution approaches the true one, the distance of a split from rank m will go to zero while the distance from rank m of a non-split will not. □

Example 4.16. We begin with an alignment of DNA data of length 1000 for 6 species, labeled $1, \ldots, 6$, simulated from the tree in Figure 4.2 with all branch lengths equal to 0.1. For the first step, we look at all pairs of the 6 species. The score column is the distance in the Frobenius norm from the flattening to the nearest rank 4 matrix:

```
Partition        Score
2 3 | 1 4 5 6    5.8374
5 6 | 1 2 3 4    6.5292
1 2 | 3 4 5 6    20.4385
1 3 | 2 4 5 6    20.5153
4 6 | 1 2 3 5    23.1477
4 5 | 1 2 3 6    23.3001
1 4 | 2 3 5 6    44.9313
```

```
3 4 | 1 2 5 6   52.1283
2 4 | 1 3 5 6   52.6763
1 6 | 2 3 4 5   52.9438
1 5 | 2 3 4 6   53.1727
3 6 | 1 2 4 5   59.5006
3 5 | 1 2 4 6   59.7909
2 6 | 1 3 4 5   59.9546
2 5 | 1 3 4 6   60.3253
picked split 1 4 5 6 | 2 3
tree is 1 4 5 6 (2,3)
```

After the first step, we see that the split $\{\{2,3\},\{1,4,5,6\}\}$ is the best, so we join nodes 2 and 3 together in the tree and continue. Notice that the scores of the partitions roughly correspond to how close they are to being splits:

```
Partition       Score
1 2 3 | 4 5 6   5.8534
5 6 | 1 2 3 4   6.5292
4 6 | 1 2 3 5   23.1477
4 5 | 1 2 3 6   23.3001
1 4 | 2 3 5 6   44.9313
2 3 4 | 1 5 6   45.1427
1 6 | 2 3 4 5   52.9438
2 3 6 | 1 4 5   53.0300
1 5 | 2 3 4 6   53.1727
2 3 5 | 1 4 6   53.3838
picked split 1 2 3 | 4 5 6
tree is 4 5 6 (1,(2,3))
```

After the second step, we join node 1 to the $\{2,3\}$ cherry and continue:

```
Partition       Score
5 6 | 1 2 3 4   6.5292
4 6 | 1 2 3 5   23.1477
4 5 | 1 2 3 6   23.3001
picked split 1 2 3 4 | 5 6
tree is 4 (1,(2,3)) (5,6)

Final tree is (4,(1,(2,3)),(5,6))
```

We have found the last cherry, leaving us with 3 remaining groups which we join together to form an unrooted tree.

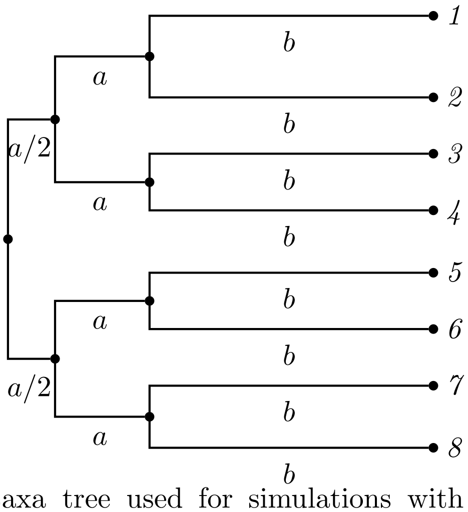

Figure 4.3: The eight-taxa tree used for simulations with $(a, b) = (0.01, 0.07)$ and $(0.02, 0.19)$.

4.5 Building trees with simulated data

The idea of simulation is that we first pick a tree and simulate a model on that tree to obtain aligned sequence data. Then we build a tree using Algorithm 4.13 and other methods from that data and compare the answers to the original tree.

We used the program `seq-gen` [78] to simulate data of various lengths for the tree in Figure 4.3 with the two sets of branch lengths given in Figure 4.3. This tree was chosen as a particularly difficult tree [96, 70].

We simulated DNA data under the general reversible model (the most general model supported by `seq-gen`). Random numbers uniformly distributed between 1 and 2 were chosen on each run for the six rate matrix parameters. The root frequencies were all set to 1/4.

Next, the data was collapsed to binary data (that is, `A` and `G` were identified, similarly `C` and `T`). We used binary data instead of DNA data because of numerical instability with SVD using the much larger matrices from the DNA data. It should be noted that Algorithm 4.13 performed better on binary data than on DNA data. This may be due to the instability, but it may also be because the rank conditions define the entire ideal for binary data.

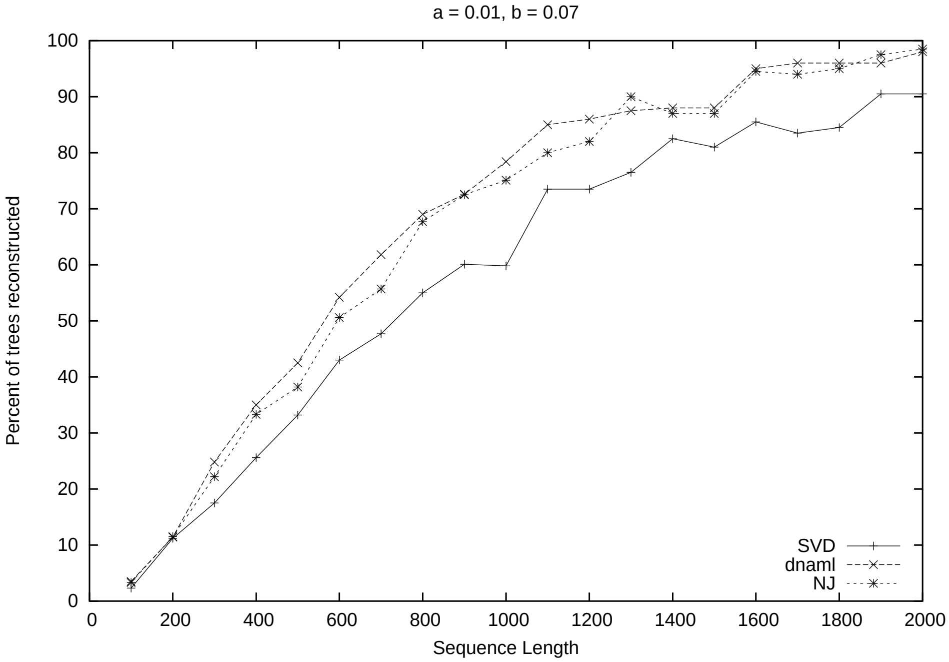

Figure 4.4: Percentage of trees reconstructed correctly (for the 8-taxa tree with branch lengths $(a, b) = (0.01, 0.07)$) using our SVD algorithm and two `PHYLIP` packages.

We ran all tests using our Algorithm 4.13 as well as two algorithms from the `PHYLIP` package [47]: neighbor-joining and a maximum likelihood algorithm (`dnaml`). We used Jukes–Cantor distance estimation for neighbor-joining and the default settings for `dnaml`. All three algorithms took approximately the same amount of time, except for `dnaml`, which slowed down considerably for long sequences.

Figures 4.4 and 4.5 show the results of the simulations. Each algorithm was run 1000 times for each tree and sequence length. While SVD performed slightly worse than the others, it showed very comparable behavior. It should be noted that SVD constructs trees according to a much more general model than the other two methods, so it should be expected to have a higher variance.

4.6 Building trees with real data

For data, we use the October 2004 freeze of the ENCODE alignments. For detailed information on these, see [26] and Chapter 5.

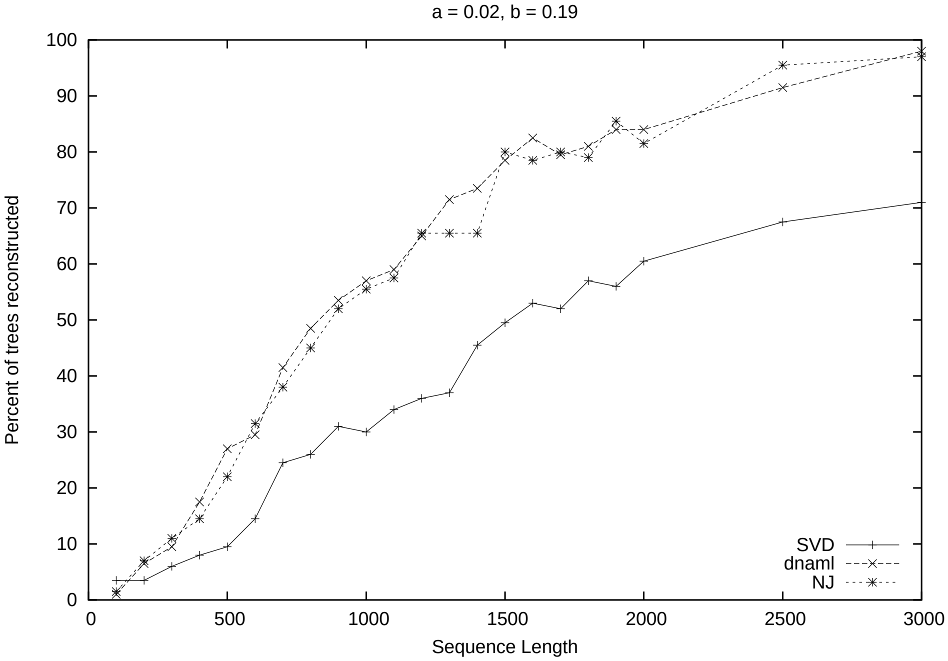

Figure 4.5: Percentage of trees reconstructed correctly (for the 8-taxa tree with branch lengths $(a, b) = (0.02, 0.19)$) using our SVD algorithm and two `PHYLIP` packages.

	SVD		`dnaml`	
	Ave. distance	% correct	Ave. distance	% correct
All	2.06	5.8	3.29	2.9
Gene	1.93	10.3	3.21	0.0
Exon	2.43	21.4	3.0	3.5

Table 4.1: Comparison of the SVD algorithm and `dnaml` on data from the ENCODE project. Distance between trees is given by the symmetric distance, % correct gives the percentage of the regions which had the correct tree reconstructed.

As in [1], we restricted our attention to 8 species: human, chimp, galago, mouse, rat, cow, dog, and chicken. We processed each of the 44 ENCODE regions to obtain 3 data sets. First, for each region, all of the ungapped columns were chosen. Second, within each region, all ungapped columns that corresponded to RefSeq annotated human genes were chosen. Third, we restricted even further to only the human exons within the genes. Bins without all 8 species and bins with less than 100 ungapped positions in the desired class were removed from consideration. This left us with 33 regions for the entire alignment, and 28 for both the gene and exon regions, of lengths between 302 and over 100000 base pairs. See [1] for a more thorough discussion of these data sets.

As is discussed in [1], tree construction methods that use genomic data usually misplace the rodents on the tree. See Figure 4.6 for the correct tree and the tree with the rodents misplaced. The reasons for this are not entirely known, but it could be because tree construction methods generally assume the existence of a global rate matrix for all the species. However, rat and mouse have mutated faster than the other species. Our method does not assume anything about the rate matrix and thus is promising for situations where additional assumptions beyond the Markov process of evolution at independent sites are not feasible. In fact, Table 4.1 shows that our algorithm performs better than `dnaml` on the ENCODE data sets. Note that the measure used is the *symmetric distance* on trees, which counts the number of splits present in one tree that aren't present in the other. While neither algorithm constructed the correct tree a majority of the time, the SVD algorithm came much closer on average and constructed the correct tree much more often than `dnaml`, which almost never did (see Figure 4.6 for the correct tree and a common mistake).

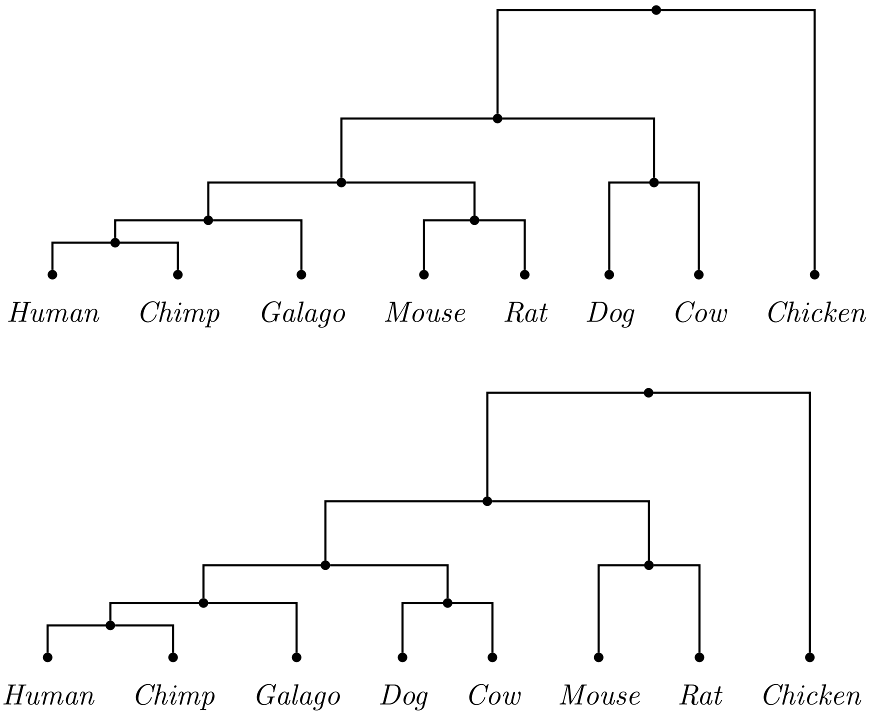

Figure 4.6: (Top) The accepted tree representing the evolution of our eight vertebrates. (Bottom) The tree commonly constructed from genomic data. Note the position of the rodent clade further up in the tree.

Chapter 5

Ultra-conserved elements in vertebrate and fly genomes

Ultra-conserved elements in an alignment of multiple genomes are consecutive nucleotides that are in perfect agreement across all the genomes. In this chapter, we examine ultra-conserved elements in aligned vertebrate and fly genomes. In Section 5.1, we describe the selected species and alignments. In Section 5.2, we give descriptive statistics of ultra-conserved elements, and in Section 5.3 we explain their biological relevance. Finally, in Section 5.4 we use the phylogenetic models introduced in Chapter 1 and studied in Chapters 3 and 4 to show that the existence of ultra-conserved elements is highly improbable in neutrally evolving regions.

The results in this chapter come from a book chapter [40] written with Mathias Drton and Garmay Leung. Many of our results mirror those of previous studies. However, these studies have considered long stretches of perfectly conserved regions across shorter evolutionary distances [14], or aligned regions above some relatively high threshold level of conservation [17, 84, 106]. We have focused on ultra-conserved elements across larger evolutionary distances. As a result, we have not captured all regions containing high levels of conservation, but have identified only those regions that appear to be under the most stringent evolutionary constraints.

5.1 The data

Our analyses of ultra-conserved elements are based on multiple sequence alignments produced by `MAVID` [18]. Prior to the alignment of multiple genomes, homology mappings (from Mercator [32]) group into bins genomic regions that are anchored together by neighboring homologous exons. A multiple sequence alignment is then produced for each of these alignment bins. `MAVID` is a global multiple alignment program, and therefore homologous regions with more than one homologous hit to another genome may not be found aligned together. Table 5.1 shows an example of Mercator's output for a single region along with the beginning of the resulting `MAVID` multiple sequence alignment.

Species	Chrom.	Start	End		Alignment
Dog	chrX	752057	864487	+	`A----AACCAAA---------`
Chicken	chr1	122119382	122708162	−	`TGCTGAGCTAAAGATCAGGCT`
Zebra fish	chr9	19018916	19198136	+	`------ATGCAACATGCTTCT`
Puffer fish	chr2	7428614	7525502	+	`---TAGATGGCAGACGATGCT`
Fugu fish	asm1287	21187	82482	+	`---TCAAGGG-----------`

Table 5.1: Mercator output for a single bin, giving the position and orientation on the chromosome. Notice that the Fugu fish genome has not been fully assembled into chromosomes.

The vertebrate dataset consists of 10,279 bins over 9 genomes (Table 5.2). A total of 4,368 bins (42.5%) contain alignments across all 9 species. The evolutionary relationships among these species (which first diverged about 450 million years ago) are shown in Figure 5.1. With the exception of the probability calculations in phylogenetic tree models, our subsequent findings on ultra-conserved elements do not depend on the form of this tree.

The fruit fly dataset consists of 8 *Drosophila* genomes (Table 5.3). Of the 3,731 alignment bins, 2,985 (80.0%) contain all 8 species, which reflects the smaller degree of evolutionary divergence. A phylogenetic tree for these 8 species, which diverged at least 45 million years ago, is shown in Figure 5.2.

The pilot phase of the ENCODE project [26] provides an additional dataset of vertebrate sequences homologous to 44 regions of the human genome. There are 14 manually selected regions of particular biological interest and 30 randomly selected

Species	Genome Size	Genome Release Date
Zebra fish (*Danio rerio*)	1.47 Gbp	11/27/2003
Fugu fish (*Takifugu rubripes*)	0.26 Gbp	04/02/2003
Puffer fish (*Tetraodon nigroviridis*)	0.39 Gbp	02/01/2004
Dog (*Canis familiaris*)	2.38 Gbp	07/14/2004
Human (*Homo sapiens*)	2.98 Gbp	07/01/2003
Chimp (*Pan troglogytes*)	4.21 Gbp	11/13/2003
Mouse (*Mus musculus*)	2.85 Gbp	05/01/2004
Rat (*Rattus norvegicus*)	2.79 Gbp	06/19/2003
Chicken (*Gallus gallus*)	1.12 Gbp	02/24/2004

Table 5.2: Genomes in the nine-vertebrate alignment with size given in billion base pairs.

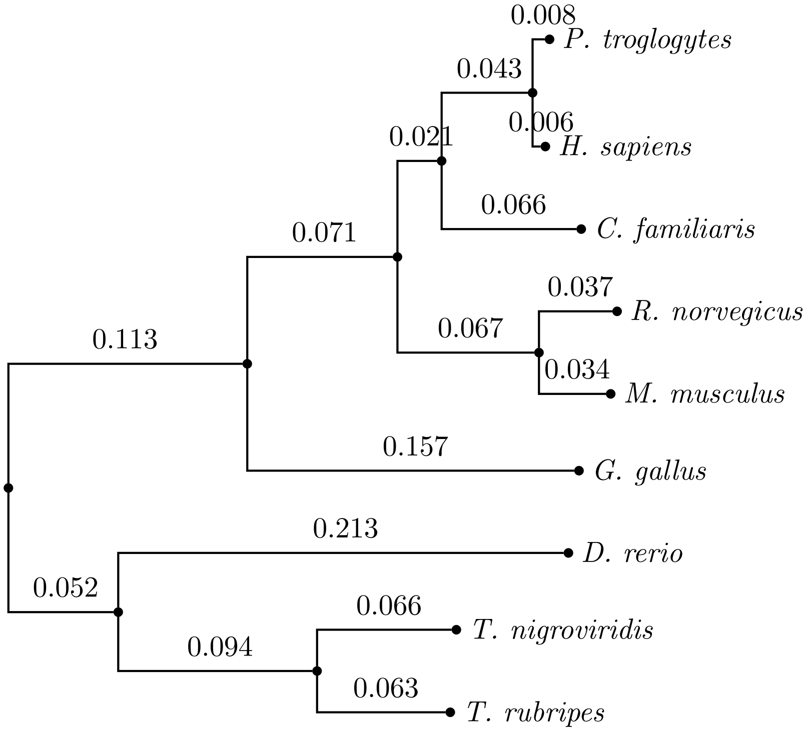

Figure 5.1: Phylogenetic tree for whole genome alignment of 9 vertebrates.

Species	Genome Size	Genome Release Date
D. melanogaster	118 Mbp	04/21/2004
D. simulans	119 Mbp	08/29/2004
D. yakuba	177 Mbp	04/07/2004
D. erecta	114 Mbp	10/28/2004
D. ananassae	136 Mbp	12/06/2004
D. pseudoobscura	125 Mbp	08/28/2003
D. virilis	152 Mbp	10/29/2004
D. mojavensis	177 Mbp	12/06/2004

Table 5.3: Genomes in the eight-*Drosophila* alignment with size given in million base pairs.

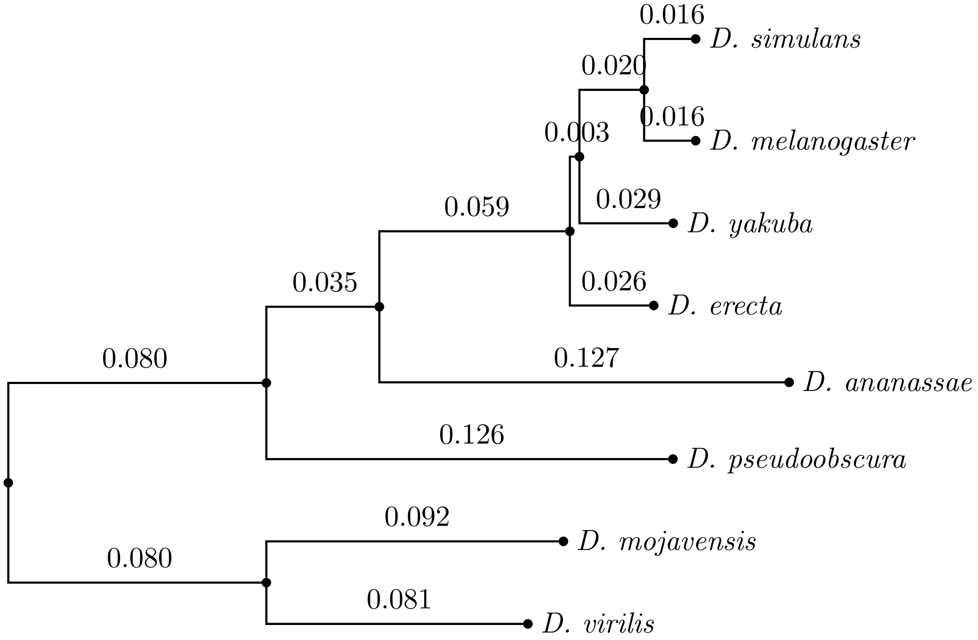

Figure 5.2: Phylogenetic tree for whole genome alignment of 8 *Drosophila* species.

regions with varying degrees of non-exonic conservation and gene density. Each manually selected region consists of 0.5–1.9 Mbp, while each randomly selected region is 0.5 Mbp in length. This gives a total of about 30 Mbp, approximately 1% of the human genome.

Varying with the region under consideration, a subset of the following 11 species is aligned along with the human genome in the preliminary October 2004 freeze: chimp, baboon (*Papiocynocephalus anubis*), marmoset (*Callithrix jacchus*), galago (*Otolemur garnettii*), mouse, rat, dog, armadillo (*Dasypus novemcintus*), platypus (*Ornithorhynchus anatinus*), and chicken. This collection of species lacks the three fish of the nine-vertebrate alignment. Armadillo and platypus sequences are only available for the first manually picked ENCODE region, and sequences for every region are only available for human, mouse, rat, dog and chicken. The number of species available for each region varies between 6 and 11 for manually selected regions, and between 8 and 10 for randomly selected regions. For each region, `Shuffle-LAGAN` [20] was applied between the human sequence and each of the other available sequences to account for rearrangements. Based on these re-shuffled sequences, a multiple sequence alignment for each region was produced with `MAVID`. The three sets of multiple alignments are available for download at `http://bio.math.berkeley.edu/ascb/chapter22/`.

5.2 Ultra-conserved elements

A position in a multiple alignment is *ultra-conserved* if for all species the same nucleotide appears in the position. An *ultra-conserved element* of length ℓ is a sequence of consecutive ultra-conserved positions $(n, n+1, \ldots, n+\ell-1)$ such that positions $n-1$ and $n+\ell$ are not ultra-conserved.

Example 5.1. Consider a subset of length 24 of a three-genome alignment:

```
G--ACCCAATAGCACCTGTTGCGG
CGCTCTCCA---CACCTGTTCCGG
CATTCT---------CTGTTTTGG
    *          *****  **
```

where ultra-conserved positions are marked by a star `*`. This alignment contains three ultra-conserved elements, one of length 1 in position 5, one of length 5 covering positions 16–20, and one of length 2 in positions 23–24.

5.2.1 Nine-vertebrate alignment

We scanned the entire nine-vertebrate alignment described in Section 5.1 and extracted 1,513,176 ultra-conserved elements, whose lengths are illustrated in Figure 5.3. The median and the mean length of an ultra-conserved element is equal to 2 and 1.918, respectively.

We will focus on the 237 ultra-conserved elements of length at least 20, covering 6,569 bp in sum. These 237 elements are clustered together; they are only found in 113 of the 4,368 bins containing all 9 species. The length distribution is heavily skewed toward shorter sequences as seen in Figure 5.3, with 75.5% of these regions shorter than 30 bp and only 10 regions longer than 50 bp.

The longest ultra-conserved element in the alignment is 125 bp long:

```
CTCAGCTTGT CTGATCATTT ATCCATAATT AGAAAATTAA TATTTTAGAT GGCGCTATGA
TGAACCCATT ATGGTGATGG GCCCCGATAT CAATTATAAC TTCAATTTCA ATTTCACTTA
CAGCC.
```

The next-longest ultra-conserved elements are two elements of length 85, followed by one element for each one of the lengths 81, 66, 62, 60, 59, 58, and 56. In particular, there is exactly one ultra-conserved element of length 42, which is the *"meaning of life"* element discussed in [74].

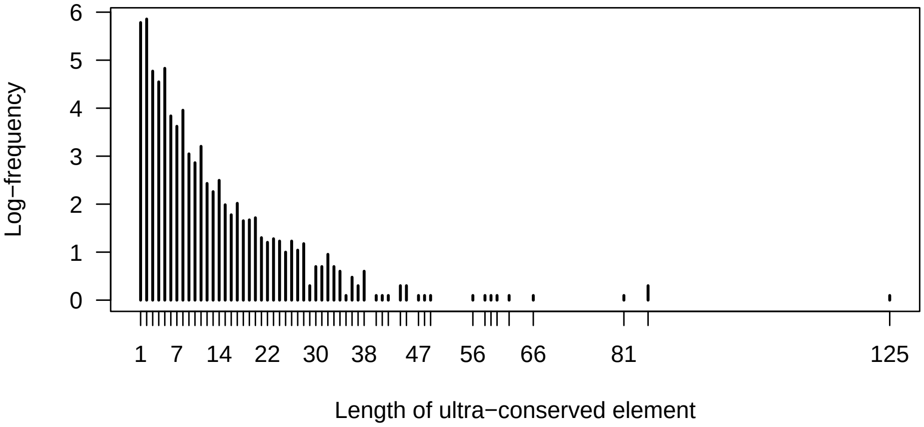

Figure 5.3: Frequencies of vertebrate ultra-conserved elements ($\log_{10}$-scale).

A number of the ultra-conserved elements are separated only by a few (less than 10), ungapped, intervening positions. In 18 cases, there is a single intervening position. Typically, these positions are nearly ultra-conserved, and display differences only between the fish and the other species. Collapsing the ultra-conserved elements separated by fewer than 10 bases reduces the number of ultra-conserved elements to 209, increases the base coverage to 6,636 bp, and brings the total number of regions greater than 50 bp in length to 26.

In the human genome, the GC-ratio (proportion of G and C among all nucleotides) is 41.0%. The ultra-conserved elements are slightly more AT-rich; for the 237 elements of length 20 or longer, the GC-ratio is 35.8%. However, GC-content and local sequence characteristics were not enough to identify ultra-conserved regions using data from only one genome.

5.2.2 ENCODE alignment

The 44 ENCODE regions contain 139,043 ultra-conserved elements, 524 of which are longer than 20 bp. These long elements cover 17,823 bp. By base coverage, 73.5% of the long elements are found in the manually chosen regions. The longest one is in region ENm012, of length 169 and consists of the DNA sequence:

```
AAGTGCTTTG TGAGTTTGTC ACCAATGATA ATTTAGATAG AGGCTCATTA CTGAACATCA
CAACACTTTA AAAACCTTTC GCCTTCATAC AGGAGAATAA AGGACTATTT TAATGGCAAG
GTTCTTTTGT GTTCCACTGA AAAATTCAAT CAAGACAAAA CCTCATTGA.
```

This sequence does not contain a subsequence of length 20 or longer that is ultra-conserved in the nine-vertebrate alignment, but the 169 bp are also ultra-conserved in the nine-vertebrate alignment if the three fish are excluded from consideration. The only overlap between the nine-vertebrate and ENCODE ultra-conserved elements occurs in the regions ENm012 and ENm005, where there are 3 elements that are extensions of ultra-conserved elements in the nine-vertebrate alignment.

Table 5.4 shows the number of species aligned in the 44 ENCODE alignments and the respective five longest ultra-conserved elements that are of length 20 or larger. Omitted randomly selected regions do not contain any ultra-conserved elements of length at least 20.

Manually selected			Randomly selected		
Region	Spec.	Ultra-lengths	Region	Spec.	Ultra-lengths
ENm001	11	$28, 27, 23, 20_2$	ENr122	9	22
ENm002	8	$39, 28, 27, 26_4$	ENr213	9	$30, 27, 26, 24, 23_2$
ENm003	9	$38, 28_2, 26, 25_2$	ENr221	10	$36_2, 32_2, 29$
ENm004	8	$35, 26_2, 25, 20$	ENr222	10	$29, 22$
ENm005	10	$114, 62, 38, 34, 32$	ENr231	8	$26, 23, 20$
ENm006	8	$-$	ENr232	8	$26, 25, 20$
ENm007	6	$-$	ENr233	9	$25, 24, 20$
ENm008	9	$23, 22$	ENr311	10	$42, 31, 25, 21$
ENm009	10	$-$	ENr312	9	$60, 31, 22, 20_4$
ENm010	8	$86, 68, 63, 61, 60_2$	ENr313	9	27
ENm011	7	$-$	ENr321	10	$68, 44, 38, 37, 35$
ENm012	9	$169, 159, 125_2, 123$	ENr322	9	$126, 80, 79, 61, 55$
ENm013	10	$30, 26, 23, 22$	ENr323	8	$53, 50, 45, 42, 29$
ENm014	10	$41_2, 39, 26_2$	ENr331	9	26
			ENr332	10	26
			ENr334	8	$79, 50, 44, 37, 32$

Table 5.4: Number of species and lengths of ultra-conserved elements in ENCODE alignments. Subindices indicate multiple occurrences.

5.2.3 Eight-*Drosophila* alignment

There are 5,591,547 ultra-conserved elements in the *Drosophila* dataset with 1,705 elements at least 50 bp long and the longest of length 209 bp. We focused on the 255 *Drosophila* ultra-conserved elements of length at least 75 bp, covering 23,567 bp total. These regions are also found clustered together, occurring over 163 bins out of the 2,985 bins with all 8 species aligned together. The shortest distance between consecutive ultra-conserved elements is 130 bp, and therefore regions were not collapsed for this dataset. The mean and median length of ultra-conserved elements are 2.605 and 2, respectively. The length distribution of all ultra-conserved elements is shown in Figure 5.4. This set of ultra-conserved elements is also somewhat more AT-rich, with a GC-ratio of 38.8% (for those elements of length at least 75 bp) compared with a GC-ratio of 42.4% across the entire *D. melanogaster* genome.

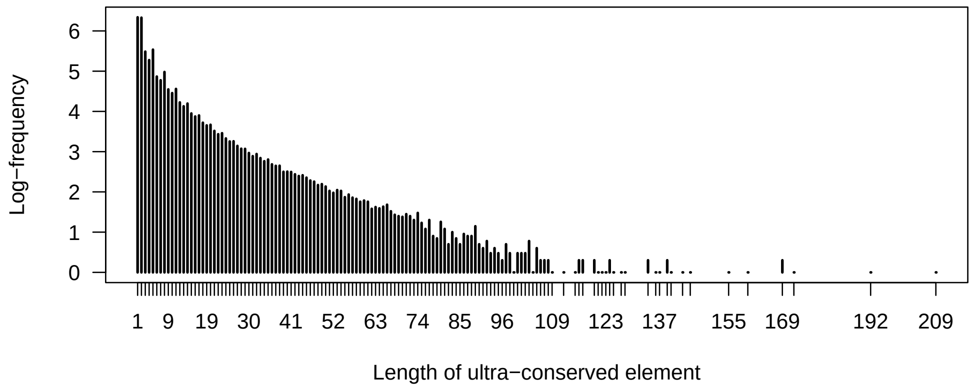

Figure 5.4: Frequencies of *Drosophila* ultra-conserved elements ($\log_{10}$-scale).

5.3 Biology of ultra-conserved elements

5.3.1 Nine-vertebrate alignment

Using the UCSC genome browser annotations of known genes for the July 2003 (hg16) release of the human genome, we investigated which ultra-conserved elements overlap known functional regions. Intragenic regions cover 62.6% of the bases of the 209 collapsed ultra-conserved elements described in Section 5.2.1. However, intragenic coverage increases to 67.6% for short elements (less than 30 bp) and drops to 56.3% for longer elements (at least 30 bp), as shown in Figures 5.5(a) and 5.5(b). While shorter ultra-conserved elements tend to correspond to exons, longer ones are generally associated with introns and unannotated regions. Nine ultra-conserved elements cover a total of 306 bp in the intronic regions of *POLA*, the alpha catalytic subunit of DNA polymerase. Six other genes are associated with more than 100 bp of ultra-conserved elements. Four of these genes are transcription factors involved in development (*SOX6*, *FOXP2*, *DACH1*, *TCF7L2*). In fact, elements near *DACH* that were highly conserved between human and mouse and also present in fish species have been shown to be *DACH* enhancers; see [68].

Among the 237 uncollapsed ultra-conserved elements of length at least 20, 151 are in intragenic regions of 96 genes. The remaining 86 elements did not overlap any annotated gene. However, by grouping together elements that have the same upstream and downstream flanking genes, there are only 27 super-regions to consider, with 51

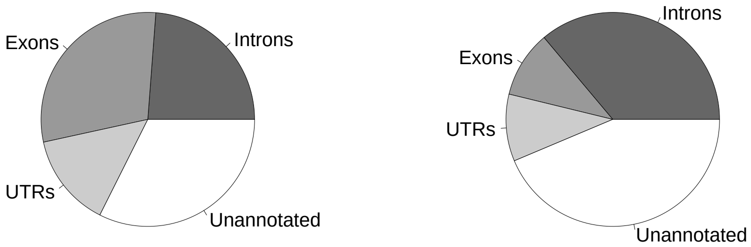

(a) 150 elements ≥ 20 and < 30 bp

(b) 59 elements ≥ 30 bp

Figure 5.5: Functional base coverage of collapsed vertebrate ultra-conserved elements based on annotations of known human genes.

unique flanking genes. There are 6 super-regions with at least 99 bp overlapping with ultra-conserved elements. At least one of the flanking genes for each of these 6 super-regions is a transcription factor located 1–314 kb away (*IRX3*, *IRX5*, *IRX6*, *HOXD13*, *DMRT1*, *DMRT3*, *FOXD3*, *TFEC*). The overall average distance to the closest flanking gene on either side is 138 kb and ranges from 312 bp to 1.2 Mbp.

It is a natural question whether the genes near or overlapping ultra-conserved elements tend to code for similar proteins. We divided the set of 96 genes with ultra-conserved overlap into 3 groups based on where in the gene the overlap occurred: exon, intron or untranslated region (UTR). If ultra-conserved elements overlap more than one type of genic region, then the gene is assigned to each of the appropriate groups. The 51 genes flanking ultra-conserved elements in unannotated regions form a fourth group of genes.

The Gene Ontology (GO) Consortium (`http://www.geneontology.org`) provides annotations for genes with respect to the molecular function of their gene products, the associated biological processes, and their cellular localization [5]. For example, the human gene *SOX6* is annotated for biological process as being involved in cardioblast differentiation and DNA-dependent regulation of transcription. Mathematically, each of the three ontologies can be considered as a partially ordered set (*poset*) in which the categories are ordered from most to least specific. For example, cardioblast differentiation is more specific than cardiac cell differentiation, which in turn is more specific than both cell differentiation and embryonic heart tube development. If a gene possesses a certain annotation, it must also possess all more general annotations; therefore GO consists of a map from the set of genes to order ideals in the three posets. We propose that this mathematical structure is important for analyzing the GO project.

In this study, we only considered molecular function and biological process annotations. These annotations are available for 46 of the 54 genes with exonic overlap, for all of the 28 with intronic overlap, for 14 of the 20 with UTR overlap, and for 30 of the 51 genes flanking unannotated elements. Considering one GO annotation and one of the 4 gene groups at a time, we counted how many of the genes in the group are associated with the considered annotation. Using counts of how often this annotation occurs among all proteins found in Release 4.1 of the Uniprot database (`http://www.uniprot.org`), we computed a p-value from Fisher's exact test for independence of association with the annotation and affiliation with the considered gene group. Annotations associated with at least 3 genes in a group and with an unadjusted p-value smaller than $3.0 \cdot 10^{-2}$ are reported in Table 5.5. DNA-dependent regulation of transcription and transcription factor activity are found to be enriched in non-exonic ultra-conserved elements, corresponding to previously reported findings [14, 17, 84, 106]. Conserved exonic elements tend to be involved in protein modification.

We scanned the human genome for repeated instances of these ultra-conserved elements and found that 14 of the original 237 elements have at least one other instance within the human genome. Generally, the repeats are not ultra-conserved except for some of the seven repeats that are found both between *IRX6* and *IRX5* and between *IRX5* and *IRX3* on chromosome 16. These genes belong to a cluster of Iroquois homeobox genes involved in embryonic pattern formation [75]. These repeated elements include two 32 bp sequences that are perfect reverse complements of each other and two (of lengths 23 bp and 28 bp) that are truncated reverse complements of each other. Overall, there are 5 distinct sequences within 226 bp regions on either side of *IRX5* that are perfect reverse complements of each other. The reverse complements are found in the same relative order (Figure 5.6). Furthermore, exact copies of the two outermost sequences are found both between *IRX4* and *IRX2* and between *IRX2* and *IRX1* on chromosome 5. Both of these regions are exactly 226 bp long. The repetition of these short regions and the conservation of their relative ordering and size suggests a highly specific coordinated

GO Annotation	p-value
Exons (14)	
protein serine/threonine kinase activity	$4.545 \cdot 10^{-3}$
transferase activity	$1.494 \cdot 10^{-2}$
neurogenesis	$1.654 \cdot 10^{-2}$
protein amino acid phosphorylation	$2.210 \cdot 10^{-2}$
Introns (10)	
regulation of transcription, DNA-dependent	$8.755 \cdot 10^{-4}$
transcription factor activity	$2.110 \cdot 10^{-3}$
protein tyrosine kinase activity	$4.785 \cdot 10^{-3}$
protein amino acid phosphorylation	$1.584 \cdot 10^{-2}$
protein serine/threonine kinase activity	$2.806 \cdot 10^{-2}$
UTRs (3)	
regulation of transcription, DNA-dependent	$1.403 \cdot 10^{-4}$
transcription factor activity	$3.971 \cdot 10^{-3}$
Flanking within 1.2 Mbp (4)	
transcription factor activity	$3.255 \cdot 10^{-11}$
regulation of transcription, DNA-dependent	$2.021 \cdot 10^{-8}$
development	$5.566 \cdot 10^{-3}$

Table 5.5: GO annotations of genes associated with vertebrate ultra-conserved elements. The number of GO annotations tested for each group are in parentheses. For each group, only GO annotations associated with at least 3 genes in the group were considered.

regulatory signal with respect to these Iroquois homeobox genes and strengthens similar findings reported by [84].

```
54102348 TGTAATTACAATCTTACAGAAACCGGGCCGATCTGTATATAAATCTCACCATCCAATTAC
54102408 AAGATGTAATAATTTTGCACTCAAGCTGGTAATGAGGTCTAATACTCGTGCATGCGATAA
54102468 TCCCCTCTGGATGCTGGCTTGATCAGATGTTGGCTTTGTAATTAGACGGGCAGAAAATCA
54102528 TTATTTCATGTTCAAATAGAAAATGAGGTTGGTGGGAAGTTAATTT

55002049 AAATTAACTTCCCACCAACCTAATTTTTTCCTGAACATGAAATAATGATTTTCTGCCCGT
55002109 CTAATTACAAAGCCAACATCTGATCAAGCCAGCATCCAGAGGGGATTATCGCATGCACGA
55002169 GTATTAGACCTCATTACCAGCTTGAGTGCAAAATTATTACATCTTGTAATTGGATGGTGA
55002229 GATTTATATACAGATCGGCCCGGTTTCTGTAAGATTGTAATTACA
```

Figure 5.6: Sequences found on either side of *IRX5*. Positions underlined with a thick line are ultra-conserved with respect to the nine-vertebrate alignment. Sequences underlined with a thin line are not ultra-conserved but their reverse complement is. Indices are with respect to human chromosome 16.

The longest ultra-conserved element that is repeated in the human genome is of length 35 and is found 18 additional times. None of these 18 instances are ultra-conserved, but this sequence is also found multiple times in other vertebrate genomes: 13 times in chimp, 10 times in mouse, 5 times in both rat and dog, 4 times in tetraodon, 3 times in zebra fish, and twice in both fugu and chicken. Of the 19 instances found in the human genome, two are found in well-studied actin genes, *ACTC* and *ACTG*, and the remainder are found in predicted retroposed pseudogenes with actin parent genes. These predictions are based on the retroGene track of the UCSC genome browser. Retroposed pseudogenes are the result of the reverse transcription and integration of the mRNA of the original functional gene. Actins are known to be highly conserved proteins, and β- and γ-actins have been shown to have a number of non-functional pseudogenes [67, 76]. The precise conservation of this 35 bp sequence across a number of human actin pseudogenes may suggest that these integration events may be relatively recent changes in the human genome.

5.3.2 ENCODE alignment

Based on the annotations of known human genes provided by the UCSC Genome Browser, 69.2% of the bases of the ultra-conserved elements of length at least 20 in the ENCODE alignment overlap intragenic regions. Shorter sequences (less than 50 bp) have far more overlap with exons and UTRs than longer sequences (at least 50 bp), as illustrated in Figures 5.7(a) and 5.7(b). These longer sequences are heavily biased towards intronic overlap, accounting for 67.7% of these sequences by base coverage.

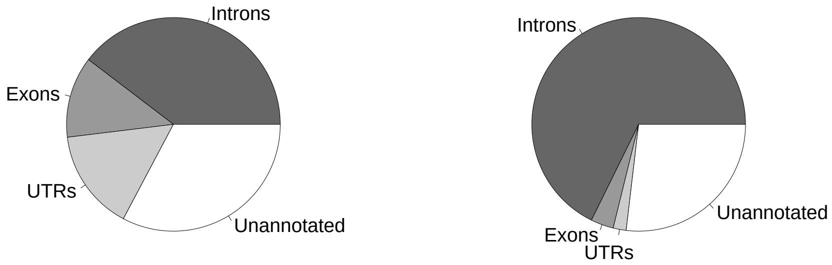

(a) 445 elements ≥ 20 and < 50 bp

(b) 79 elements ≥ 50 bp

Figure 5.7: Functional base coverage of ultra-conserved elements found in ENCODE regions based on annotations of known human genes.

Values for the gene density and non-exonic conservation level (human–mouse) are available for the randomly selected ENCODE regions [26]. For these regions, the base coverage by ultra-conserved elements is not correlated with gene density (Pearson correlation $= -0.0589$) and is moderately correlated with non-exonic conservation (Pearson correlation $= 0.4350$).

While we do not repeat the gene ontology analysis from the previous section, we note that the regions with the greatest number of ultra-conserved elements by base coverage are regions with well-known genes involved in DNA-dependent transcriptional regulation (Table 5.6). The elements in these 5 regions account for 80.3% of the bases of the ultra-conserved elements found in this dataset. The 35 longest ultra-conserved elements, of length at least 69 bp, are also all found in these 5 regions.

5.3.3 Eight-*Drosophila* alignment

We analyzed the 255 ultra-conserved elements of length at least 75 bp using the Release 4.0 annotations of *D. melanogaster*. These elements overlap 95 unique genes. Although the intragenic overlap for shorter elements (less than 100 bp) is only 42.9%, this proportion increases to 68.2% for the elements that are at least 100 bp in length (Figures 5.8(a)

	Ultra Coverage (bp)	Transcription Factor Genes	# Aligned Species
ENm012	9,086	*FOXP2*	9
ENr322	2,072	*BC11B*	9
ENm010	1,895	*HOXA1-7,9-11,13*; *EVX1*	8
ENm005	718	*GCFC*; *SON*	10
ENr334	549	*FOXP4*; *TFEB*	8

Table 5.6: ENCODE regions with the greatest number of ultra-conserved elements by base coverage and their associated transcription factor genes.

and 5.8(b)). Unlike the vertebrate dataset, longer regions are associated with exons, while shorter regions tend to correspond to unannotated elements.

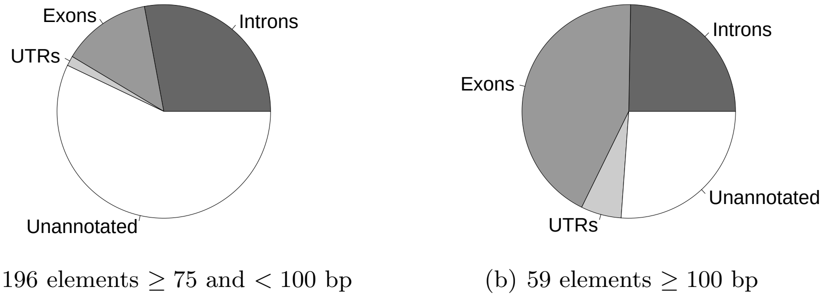

(a) 196 elements ≥ 75 and < 100 bp

(b) 59 elements ≥ 100 bp

Figure 5.8: Functional base coverage of ultra-conserved elements found in the *Drosophila* alignment based on annotations of known *D. melanogaster* genes.

The three genes with the greatest amount of overlap with ultra-conserved elements are *para* (765 bp), *nAcRα-34E* (426 bp) and *nAcRα-30D* (409 bp). All three of these genes are involved in cation channel activity, and the ultra-conserved elements correspond mostly with their exons. As with the nine-vertebrate dataset, the full set of 95 *D. melanogaster* genes is assessed for GO annotation enrichment, using all Release 4.0 *D. melanogaster* genes as the background set (Table 5.7). GO annotations exist for 78 of these 95 genes, which we did not differentiate further according to where in the gene overlap with an ultra-conserved element occurred. Genes involved in synaptic transmission are strongly over-represented in genes that have an ultra-conserved element overlap with their exons, introns and UTRs. These genes include those involved with ion channel activity, signal transduction and receptor activity, playing roles in intracellular signaling cascades, muscle contraction, development, and behavior. RNA binding proteins are also found to be over-represented. Another group of over-represented genes are those involved in RNA polymerase II transcription factor activity. These genes are strongly associated with development and morphogenesis.

The 130 ultra-conserved elements found in unannotated regions are grouped together into 109 regions by common flanking genes. These regions are flanked by 208 unique genes, 134 of which have available GO annotations. The distance from these ultra-conserved elements to their respective nearest gene ranges from 0.2–104 kb and is 16 kb on average. A number of transcription factors involved with development and morphogenesis are found within this set of genes. Five of the 10 flanking genes with ultra-conserved sequences both upstream and downstream are transcription factors (*SoxN*, *salr*, *toe*, *H15*, *sob*). In total, 44 unique transcription factors are found across the intragenic and flanking gene hits.

Ten of the original 255 ultra-conserved elements are repeated elsewhere in the *D. melanogaster* genome. However, all of these repeats correspond to annotated tRNA or snRNA, but not to homologous exons or regulatory regions. There are 10 ultra-conserved elements that overlap with tRNA (757 bp in sum), two that overlap with snRNA (191 bp in sum), and one that overlaps with ncRNA (81 bp). None of the ultra-conserved elements correspond to annotated rRNA, regulatory regions, transposable elements, or pseudogenes.

5.3.4 Discussion

We studied ultra-conserved elements in three very different datasets: an alignment of nine distant vertebrates, an alignment of the ENCODE regions in mammals, and an alignment of eight fruit flies. As Figures 5.5, 5.7, and 5.8 show, ultra-conserved elements overlap with genes very differently in the three datasets. In particular, in the *Drosophila* dataset, exonic conservation is much more substantial. This conservation at the DNA level is very surprising, as the functional constraint on coding regions is expected to be at the amino acid level. Therefore, the degeneracy of the genetic code should allow synonymous mutations to occur without any selective constraint.

The GO analysis showed that non-coding regions near or in genes associated

GO Annotation	p-value
Exons, Introns, and UTRs (41)	
synaptic transmission	$3.290 \cdot 10^{-9}$
specification of organ identity	$1.044 \cdot 10^{-6}$
ventral cord development	$3.674 \cdot 10^{-6}$
RNA polymerase II transcription factor activity	$4.720 \cdot 10^{-6}$
muscle contraction	$8.714 \cdot 10^{-6}$
voltage-gated calcium channel activity	$3.548 \cdot 10^{-5}$
RNA binding	$7.650 \cdot 10^{-5}$
synaptic vesicle exocytosis	$3.503 \cdot 10^{-4}$
leg morphogenesis	$3.503 \cdot 10^{-4}$
calcium ion transport	$6.401 \cdot 10^{-4}$
Flanking within 104 kb (58)	
regulation of transcription	$8.844 \cdot 10^{-7}$
neurogenesis	$5.339 \cdot 10^{-6}$
ectoderm formation	$8.285 \cdot 10^{-6}$
endoderm formation	$2.125 \cdot 10^{-5}$
salivary gland morphogenesis	$5.870 \cdot 10^{-5}$
Notch signaling pathway	$1.591 \cdot 10^{-4}$
leg joint morphogenesis	$1.788 \cdot 10^{-4}$
RNA polymerase II transcription factor activity	$2.381 \cdot 10^{-4}$
salivary gland development	$4.403 \cdot 10^{-4}$
signal transducer activity	$5.308 \cdot 10^{-4}$
foregut morphogenesis	$8.004 \cdot 10^{-4}$

Table 5.7: GO annotations of genes associated with *Drosophila* ultra-conserved elements. The number of GO annotations tested for each group are in parentheses. For each group, each tested GO annotation is associated with at least 3 genes in the group.

with transcriptional regulation tended to contain ultra-conserved elements in all datasets. In *Drosophila*, ultra-conserved elements overlapped primarily with genes associated with synaptic transmission. While the exonic conservation in *Drosophila* is due in part to a much shorter period of evolution, the exact conservation of exons whose gene products are involved in synaptic transmission may be fly-specific.

Non-coding regions that are perfectly conserved across all 9 species may be precise regulatory signals for highly specific DNA-binding proteins. In particular, repeated ultra-conserved elements such as those found near the Iroquois homeobox genes on chromosome 16 are excellent candidates for such regulatory elements. Of course, it is interesting to note that the degree of conservation in our ultra-conserved elements exceeds what is observed for other known functional elements, such as splice sites. We discuss the statistical significance of ultra-conservation in Section 5.4.

5.4 Statistical significance of ultra-conservation

Which ultra-conserved elements are of a length that is statistically significant? In order to address this question, we choose a model and compute the probability of observing an ultra-conserved element of a given length for the nine-vertebrate and *Drosophila*-alignments. First we consider phylogenetic tree models. These models allow for dependence of the occurrence of nucleotides in the genomes of different species at any given position in the aligned genomes, but make the assumption that evolutionary changes to DNA at one position in the alignment occur independently from changes at all other, and in particular, neighboring positions. Later we also consider a Markov chain, which does not model evolutionary changes explicitly but incorporates a simple pattern of dependence among different genome positions.

Before being able to compute a probability in a phylogenetic tree model, we must build a tree and estimate the parameters of the associated model. The tree for the nine-vertebrate alignment is shown in Figure 5.1. The topology of this tree is well-known, so we assume it fixed and use `PAML` [107] to estimate model parameters by maximum likelihood. As input to `PAML`, we choose the entire alignments with all columns containing a gap removed. The resulting alignment was 6,300,344 positions long for the vertebrates and 26,216,615 positions long for the *Drosophila*. Other authors (e.g., [74]) have chosen to focus only on synonymous substitutions in coding regions, since they are likely not selected for or against and thus give good estimates for neutral substitution rates. However, our independence model does not depend on the functional structure of the genome; that is, it sees the columns as i.i.d. samples. Thus, we believe that it is more appropriate to use all the data available to estimate parameters.

There are many phylogenetic tree models (cf. Section 1.4) and we concentrate here on the Jukes–Cantor and HKY85 models. With the parameter estimates from `PAML`, we can compute the probability p_{cons} of observing an ultra-conserved position in the alignment. Recall that the probability $p_{i_1 \dots i_s}$ of seeing the nucleotide vector $(i_1, \dots, i_s) \in \{\mathtt{A}, \mathtt{C}, \mathtt{G}, \mathtt{T}\}^s$ in a column of the alignment of s species is given by a polynomial in the entries of the transition matrices $P_e(t)$, which are obtained as $P_e(t) = \exp(Qt_e)$ where t_e is the length of the edge e in the phylogenetic tree and Q is a rate matrix that depends on the model selected.

Under the Jukes–Cantor model for the nine-vertebrate alignment, the maximum likelihood (ML) branch lengths are shown in Figure 5.1 and give the probabilities

$$p_{\mathtt{AAAAAAAAA}} = \cdots = p_{\mathtt{TTTTTTTTT}} = 0.01139...$$

Thus, the probability of a conserved column under this model is $p_{\text{cons}} = 0.0456$. If we require that the nucleotides are identical not only across present-day species but also across ancestors, then the probability drops slightly to 0.0434.

Under the HKY85 model for the nine-vertebrate alignment, the ML branch lengths are very similar to those in Figure 5.1 and the additional parameter is estimated as $\kappa = 2.4066$. The root distribution is estimated to be almost uniform. These parameters give the probabilities

$$p_{\mathtt{AAAAAAAAA}} = \cdots = p_{\mathtt{TTTTTTTTT}} = 0.00367,$$

which are much smaller than their counterpart in the Jukes–Cantor model. The HKY85 probability of a conserved column is $p_{\text{cons}} = 0.014706$. If we assume that nucleotides must also be identical in ancestors, this probability drops to 0.01234.

The binary indicators of ultra-conservation are independent and identically distributed according to a Bernoulli distribution with success probability p_{cons}. The probability of seeing an ultra-conserved element of length at least ℓ starting at a given position in the alignment therefore equals p_{cons}^{ℓ}. Moreover, the probability of seeing an ultra-conserved element of length at least ℓ anywhere in a genome of length N can be bounded above by Np_{cons}^{ℓ}. Recall that the length of the human genome is roughly 2.8 Gbp and the length of *D. melanogaster* is approximately 120 Mbp. Table 5.8 contains the evaluated probability bound for different values of ℓ.

	Nine-vertebrate (human)			*Drosophila* (*D. melanogaster*)	
	Jukes–Cantor	HKY85		Jukes–Cantor	HKY85
p_{cons}	0.0456	0.0147	p_{cons}	0.1071	0.05969
10	0.0001	$1.3 \cdot 10^{-9}$	15	$7.8 \cdot 10^{-6}$	$1.2 \cdot 10^{-9}$
20	$4.1 \cdot 10^{-18}$	$6.2 \cdot 10^{-28}$	75	$4.6 \cdot 10^{-64}$	$4.3 \cdot 10^{-83}$
125	$6.0 \cdot 10^{-159}$	$2.4 \cdot 10^{-220}$	209	$4.3 \cdot 10^{-194}$	$4.1 \cdot 10^{-247}$

Table 5.8: Probabilities of seeing ultra-conserved elements of certain lengths in an independence model with success probability p_{cons} derived from two phylogenetic tree models.

However, 46% of the ungapped columns in the nine-vertebrate alignment are actually ultra-conserved. This fraction is far greater than the 5% we would expect with the JC model and the 1% under the HKY85 model. This suggests that the model of independent alignment positions is overly simplistic. If we collapse the alignment to a sequence of binary indicators of ultra-conserved positions, then a very simple non-independence model for this binary sequence is a Markov chain model.

In a Markov chain model, the length of ultra-conserved elements is geometrically distributed. That is, the probability that an ultra-conserved element is of length ℓ equals $\theta^{\ell-1}(1-\theta)$, where θ is the probability of transitioning from one ultra-conserved position to another. The expected value of the length of an ultra-conserved element is equal to $1/(1-\theta)$. The probability that an ultra-conserved element is of length ℓ or longer equals

$$\sum_{k=\ell}^{\infty} \theta^{k-1}(1-\theta) = \theta^{\ell-1}.$$

Therefore, the probability that at least one of U ultra-conserved elements found in a multiple alignment is of length at least ℓ is equal to

$$1-(1-\theta^{\ell-1})^{U} \approx U \cdot \theta^{\ell-1} \quad \text{for large } \ell.$$

Restricting ourselves to the nine-vertebrate alignment (computations for the *Drosophila* alignment are qualitatively similar), we used the mean length of the ultra-conserved elements described in Section 5.3.1 to estimate the transition probability θ to 0.4785. Then the probability that at least one of the 1,513,176 ultra-conserved elements of the nine-vertebrate alignment is of length 25 or longer equals about 3%. The probability of seeing one of the U ultra-conserved elements being 30 or more bp long is just below 1/1000. However, the dependence structure in a Markov chain model cannot explain the longest ultra-conserved elements in the alignment. For example, the probability of one of the U elements being 125 or more bp long is astronomically small (0.3×10^{-33}). This suggests that the Markov chain model does not capture the dependence structure in the binary sequence of ultra-conservation indicators. At a visual level, this is clear from Figure 5.3. Were the Markov chain model true then, due to the resulting geometric distribution for the length of an ultra-conserved element, the log-scale frequencies should fall on a straight line, which is not the case in Figure 5.3. Modeling the process of ultra-conservation statistically requires more sophisticated models. The phylogenetic hidden Markov models that appear in [64, 87] provide a point of departure.

Despite the shortcomings of the calculations, it is clear that it is highly unlikely that the ultra-conserved elements studied in this chapter occur by chance. The degree of conservation strongly suggests extreme natural selection in these regions.

Chapter 6

Evolution on distributive lattices

In this chapter, we model the evolution of a population under strong selective pressure using a probabilistic model on a distributive lattice. We describe how the combinatorial structure of a distributive lattice arises naturally from both biology and algebraic statistics. The probability that the population develops an escape mutant before extinction is encoded in the algebraic combinatorics of the lattice.

Using methods from combinatorics and algebra, we analyze the problem of drug resistance in HIV under treatment with the protease inhibitors ritonavir and indinavir. We begin by explaining the problem of drug resistance in HIV in Section 6.1 and our mathematical formulation is Section 6.2. The material in this chapter comes from the paper [10] with Niko Beerenwinkel and Bernd Sturmfels.

The evolutionary fate of a population is determined by the replication dynamics of the ensemble and by the reproductive success of its individuals. We are interested in scenarios where most individuals have a low fitness, eventually leading to extinction, and only a few types of individuals ("escape mutants") can survive permanently. These situations often arise due to a significant change of the underlying fitness landscape. For example, a virus that has been transmitted to a new host is confronted with a new immune response. Likewise, medical interventions such as radiation therapy, vaccination, or chemotherapy result in altered fitness landscapes for the targeted agents, which may be bacteria, viruses, or cancer cells.

Given a population and such a hostile fitness landscape, the central question is whether the population will survive. In the case of medical interventions we wish to know the probability of successful treatment. Answering this question involves computing the risk of evolutionary escape, i.e., the probability that the population develops an escape mutant before extinction. In this chapter, we present a mathematical framework for computing such probabilities.

6.1 Drug resistance in HIV

Our primary application is the evolution of drug resistance during treatment of HIV infected patients [23]. Drug resistance is the consequence of mutations in the viral proteins which are targeted by antiretroviral drugs.

HIV is a retrovirus, which means that it uses RNA instead of DNA as its genetic material. Its genome is about 10000 nucleotides in length with nine open reading frames. Three of the precursor proteins that are produced, however, are cleaved by the viral protease enzyme, giving a total of 15 proteins which are produced by HIV.

The HIV virus binds to the CD4 receptor of a host cell with the aid of further cellular coreceptors and enters the cell. It then releases its genetic material (which is carried in the form of RNA). This RNA is transcribed into DNA using the HIV enzyme reverse transcriptase and enters the nucleus. There it is transcribed into mRNA and translated into proteins using the machinery of the host cell. This allows for many copies of the virus to be made in the host cell. These proteins have to be processed by the HIV protease enzyme into their functional form before the new copy of the virus can infect other cells. Different classes of drugs have been designed to attack the virus during every step of the above process with impressive success. There are currently 27 drugs approved by the FDA in four different classes. These drugs are typically taken in combinations of two to four drugs simultaneously from two different classes.

However, the reverse transcription step is notoriously error prone, producing on average one error in every replication of the genome. This high mutation rate can lead to the development of drug resistance. As many as 50 percent of patients receiving antiretroviral therapy are infected with viruses which are resistant to one of the available drugs [23]. Given this, it is key for doctors to have methods of determining the best possible combination of drugs to prescribe given the patients level of resistance and other factors.

In this chapter, we consider therapy with two different protease inhibitors (PIs). These compounds interfere with HIV particle maturation by inhibiting the viral protease enzyme. See Figure 6.1 for the structure of the protease enzyme and how the drugs bind to and inhibit it. This picture was created using the program `PyMOL` [29] with data from `http://www.chem.ucsb.edu/~molvisual/`.

The effectiveness of PI therapy is limited by the development of drug resistance. Rapid and highly error prone replication of a large virus population generates mutants that resist the selective pressure of drug therapy. PI resistance is caused by mutations in the protease gene that reduce the binding affinity of the drug to the enzyme. These mutations have been shown to accumulate in a stepwise manner [15]. For most PIs, no single mutation confers a significant level of resistance, but multiple mutations are required for escape from drug pressure. Quantitative predictions of the probability of successful PI treatment would help in finding effective antiretroviral combination therapies. Selecting a drug combination amounts to controlling the viral fitness landscape.

6.2 The model of evolution

We regard the directed evolution of a population towards an escape state as a fluctuation on a fitness landscape. The space of genotypes is modeled as follows. We start with a finite partially ordered set (poset) $\mathcal{E}$ whose elements are called *events*. The events are non-reversible mutations with some constraints on their order of occurrence. Such constraints are primarily due to epistatic effects between different loci in a genome [81]. The event constraints define the poset structure: $e_1 < e_2$ in $\mathcal{E}$ means that event e_1 must occur before event e_2 can occur. Each genotype g is represented by a subset of $\mathcal{E}$, namely, the set of all events that occurred to create g. Thus a genotype g is an *order ideal* in the poset $\mathcal{E}$. The space of genotypes $\mathcal{G}$ is the set of all order ideals in $\mathcal{E}$, which is a *distributive lattice* [90, Sec. 3.4]. The order relation on $\mathcal{G}$ is set inclusion and corresponds to the accumulation of mutations. This mathematical formulation is reasonable in the above situations, where a population is exposed to strong selective pressure.

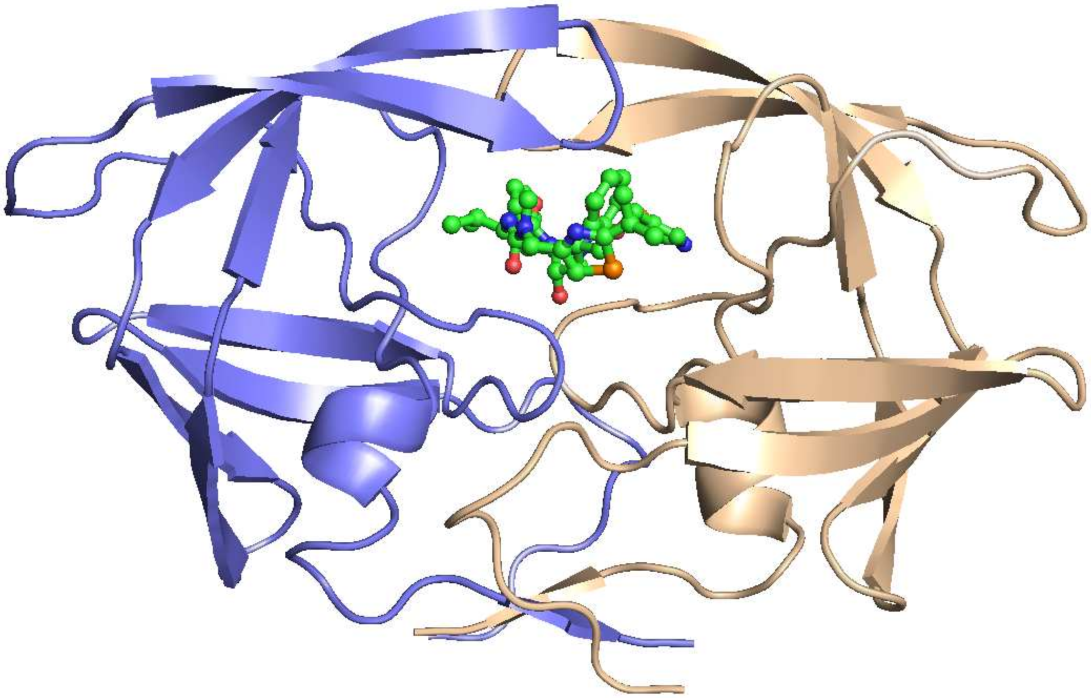

Figure 6.1: HIV protease enzyme with bound inhibitor.

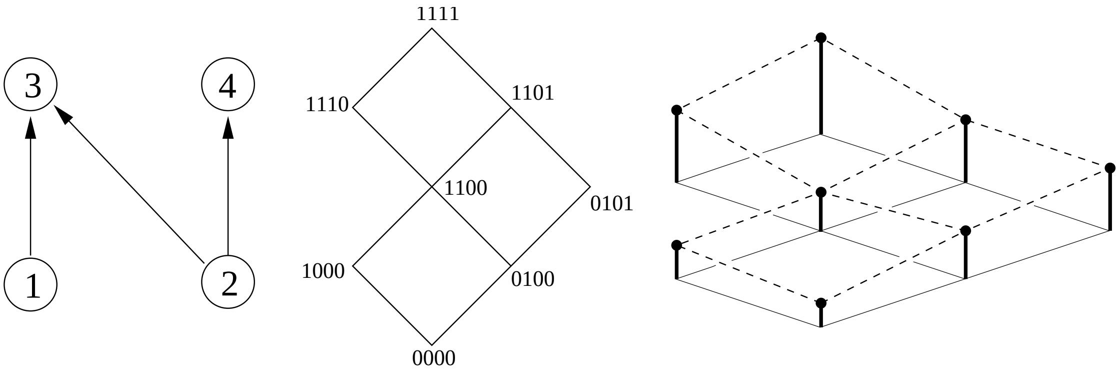

Figure 6.2: An event poset, its genotype lattice, and a fitness landscape.

The risk of escape is governed by the structure of $\mathcal{G}$, the fitness function on $\mathcal{G}$, and the population dynamics (such as the mutation rates and population size). Our focus is on the dependency of the risk of escape on the assigned fitness values for each genotype $g \in \mathcal{G}$. This leads us to the *risk polynomial*, which is shown to be equivalent to a well-known object in algebraic combinatorics. Indeed, one of the objectives of this work is to provide a bridge between algebraic combinatorics and evolutionary biology.

This chapter is organized as follows. In Section 6.3 we formalize our model of a static fitness landscape on the genotype lattice $\mathcal{G}$ derived from an event poset $\mathcal{E}$, and we discuss evolution on the lattice $\mathcal{G}$. In Section 6.4 we review the multistate branching process studied by Iwasa, Michor and Nowak [54, 55].

In Section 6.5 we study the Bayesian networks which arise from identifying the events in $\mathcal{E}$ with binary random variables. These statistical models can be used to infer the genotype space from given data. For conjunctive Bayesian networks we recover the distributive lattice of order ideals in $\mathcal{E}$. Of particular interest is the case where $\mathcal{E}$ is a directed forest: here the Bayesian network is a mutagenetic tree model [9, 12]. The application of our methods to the development of PI resistance in HIV is presented in Section 6.6.

Section 6.7 summarizes various representations of the risk polynomial in terms of structures from algebraic combinatorics. Efficient methods for computing the risk polynomial and their implementation are presented.

6.3 Fitness landscapes on distributive lattices

A partially ordered set (or poset) is a set $\mathcal{E}$ together with a binary relation, denoted "$\leq$", which is reflexive, antisymmetric, and transitive. Here we fix a finite poset $\mathcal{E}$ whose elements are called *events*. If the number of events is n then we often identify the set underlying $\mathcal{E}$ with the set $[n] = \{1, 2, \ldots, n\}$. In this way, the subsets of $\mathcal{E}$ are encoded by the 2^n binary strings of length n. The empty subset of $\mathcal{E}$ is encoded by the all-zero string $\hat{0} = 00\cdots0$ which represents the *wild type*, and the full set $\mathcal{E}$ is encoded by the all-one string $\hat{1} = 11\cdots1$ which represents the *escape state*.

An order ideal g in a poset $\mathcal{E}$ is a subset of $\mathcal{E}$ that is closed downward; that is, if $e_2 \in g$ and $e_1 \leq e_2$, then $e_1 \in g$. The set of all order ideals of $\mathcal{E}$ forms a distributive lattice $J(\mathcal{E})$ under inclusion. Birkhoff's Representation Theorem [90, Thm. 3.4.1] states that all distributive lattices have the form $J(\mathcal{E})$ for a poset $\mathcal{E}$. We write $\mathcal{G} = J(\mathcal{E})$, and we call $\mathcal{G}$ the *genotype lattice*.

Example 6.1. Let $\mathcal{E}$ be the trivial poset, where no two events are comparable, with $|\mathcal{E}| = n$. Then $\mathcal{G} = J(\mathcal{E})$ is the Boolean lattice consisting of all subsets of $\mathcal{E}$ ordered by inclusion. This means that all possible combinations of mutations are possible, and they can occur in any order. Each of the 2^n binary strings $g \in \{0,1\}^n$ represents a mutational pattern, or genotype.

In general, the event poset $\mathcal{E}$ does have non-trivial relations $e_1 < e_2$. The relation $e_1 < e_2$ excludes all genotypes g with $g_{e_1} = 0$ and $g_{e_2} = 1$ from $\mathcal{G}$. The remaining genotypes g form a sublattice of the Boolean lattice $\{0,1\}^n$, and this is precisely our distributive lattice $\mathcal{G} = J(\mathcal{E})$. Note that the lattice $\mathcal{G}$ is ranked, with the rank function given by $\mathrm{rank}(g) = |g|$.

Example 6.2. Consider a scenario with $n = 4$ mutation events, labeled $\mathcal{E} = \{1, 2, 3, 4\}$. Suppose that event 3 can only occur after events 1 and 2, and event 4 can only occur after event 2. This allows for precisely eight genotypes

$$\mathcal{G} \;=\; \big\{0000, 1000, 0100, 1100, 0101, 1110, 1101, 1111\big\}.$$

The event poset $\mathcal{E}$ and the genotype lattice $\mathcal{G}$ are shown in Figure 6.2.

A fitness landscape associates to each possible genotype a number which quantifies the reproductive capacity of an individual with that genotype [79]. We define a *fitness landscape* on the distributive lattice $\mathcal{G}$ to be any function $\mathbf{f}\colon \mathcal{G} \to \mathbb{R}$. The value $\mathbf{f}(g)$ at any $g \in \mathcal{G}$ is the *fitness* of the genotype g. Thus, the space of all fitness landscapes is the finite-dimensional vector space $\mathbb{R}^{\mathcal{G}}$.

We shall consider certain special models of fitness landscapes, which are represented by linear subspaces of $\mathbb{R}^{\mathcal{G}}$. In the following definitions, a genotype g is regarded as a subset of the event poset $\mathcal{E}$, where $|\mathcal{E}| = n$. A *constant fitness landscape* has the form $\mathbf{f}(g) \equiv a$ for some constant a. Thus the constant landscapes form a line through the origin in $\mathbb{R}^{\mathcal{G}}$. A *graded fitness landscape* is a landscape on $\mathcal{G}$ whose fitness values depend only on the rank. Equivalently, we have $\mathbf{f}(g) = a_{|g|}$ for constants $a_0, a_1, \ldots, a_n$. Thus, graded fitness landscapes form an $(n+1)$-dimensional linear subspace of $\mathbb{R}^{\mathcal{G}}$.

Our biological application in Section 6.6 uses the graded fitness landscape model, which means that the fitness of a virus type depends only on the number of mutations it harbors. We shall model situations where a virus escapes from a wild type $\hat{0}$ to a drug-resistant type $\hat{1}$. In this case, we assume a graded fitness landscape that is monotonically increasing with rank, i.e.,

$$a_0 \,<\, a_1 \,<\, a_2 \,<\, \cdots \,<\, a_n.$$

This implies that the fitness landscape $\mathbf{f}$ has a unique local (and global) maximum at the drug resistant type $\hat{1}$, which is the top element in $\mathcal{G}$.

We next introduce the mathematical framework for evolution on a fitness landscape. The general setup is as in the work of Reidys and Stadler [79], but this is adapted here to our specific situation, where the genotypes form a distributive lattice $\mathcal{G}$. The order relation on $\mathcal{G}$, which comes from inclusion of subsets of $\mathcal{E}$, induces a neighborhood structure on $\mathcal{G}$ where the neighbors of $g \in \mathcal{G}$ are the genotypes that strictly contain g,

$$N(g) \,:=\, \big\{h \in \mathcal{G} \;|\; g \subset h\big\}. \tag{6.1}$$

Unlike the typical situation considered in [79], this notion of neighborhood is not symmetric. To be precise, we have that $h \in N(g)$ implies $g \notin N(h)$.

This neighborhood structure implies that mutational changes are possible only upward in the genotype lattice. This structure models a directed evolutionary process from the wild type $\hat{0}$ towards the escape state $\hat{1}$. Typically, our configuration space $\mathcal{G}$ is a small subset of the Boolean lattice $\{0,1\}^n$ of all binary strings. Indeed, in the course of viral evolution, a population will visit only a small fraction of $\{0,1\}^n$, as most mutants are not viable.

Suppose that the number of genotypes in $\mathcal{G}$ is m. We wish to define dynamics between the states of $\mathcal{G}$. To this end, we fix a linear extension of $\mathcal{G}$, and we introduce an $m \times m$ matrix of transition rates, written $\mathbf{U} = (u_{gh})$, whose rows and columns are indexed by genotypes $g, h \in \mathcal{G}$. Each entry u_{gh} of the matrix $\mathbf{U}$ is a non-negative real number which is zero unless $h \in N(g)$. In the framework of algebraic combinatorics, it is convenient to think of the matrix $\mathbf{U}$ as an element in the incidence algebra of $\mathcal{G}$; see [90, Sec. 3.6].

We further assume that the non-zero mutation rates u_{gh} depend only on the events in $h \backslash g$. Equivalently, the rate at which a collection of mutation events occurs is independent of which other mutations have already occurred. With this assumption, there are only n free parameters $\mu_1, \ldots, \mu_n$ in the matrix $\mathbf{U}$, where μ_e is the mutation rate of event e. Then

$$u_{gh} = \begin{cases} \prod_{e \in h \backslash g} \mu_e & \text{if } g \subset h \\ 0 & \text{otherwise.} \end{cases} \tag{6.2}$$

In particular, if all rates are the same, say $\mu = \mu_1 = \cdots = \mu_n$, then the entries of $\mathbf{U}$ are $u_{gh} = \mu^{|h \backslash g|}$ if $g \subset h$ and $u_{gh} = 0$ otherwise.

Example 6.3. For the genotype lattice $\mathcal{G}$ in Figure 6.2, the matrix $\mathbf{U}$ equals

$$\begin{array}{c} \\ 0000 \\ 1000 \\ 0100 \\ 1100 \\ 0101 \\ 1110 \\ 1101 \\ 1111 \end{array} \begin{array}{c} \begin{array}{cccccccc} 0000 & 1000 & 0100 & 1100 & 0101 & 1110 & 1101 & 1111 \end{array} \\ \begin{pmatrix} 0 & \mu_1 & \mu_2 & \mu_1\mu_2 & \mu_2\mu_4 & \mu_1\mu_2\mu_3 & \mu_1\mu_2\mu_4 & \mu_1\mu_2\mu_3\mu_4 \\ 0 & 0 & 0 & \mu_2 & 0 & \mu_2\mu_3 & \mu_2\mu_4 & \mu_2\mu_3\mu_4 \\ 0 & 0 & 0 & \mu_1 & \mu_4 & \mu_1\mu_3 & \mu_1\mu_4 & \mu_1\mu_3\mu_4 \\ 0 & 0 & 0 & 0 & 0 & \mu_3 & \mu_4 & \mu_3\mu_4 \\ 0 & 0 & 0 & 0 & 0 & 0 & \mu_1 & \mu_1\mu_3 \\ 0 & 0 & 0 & 0 & 0 & 0 & 0 & \mu_4 \\ 0 & 0 & 0 & 0 & 0 & 0 & 0 & \mu_3 \\ 0 & 0 & 0 & 0 & 0 & 0 & 0 & 0 \end{pmatrix} \end{array}$$

Note that the entry in row g and column h of any power $\mathbf{U}^k$ equals u_{gh} times the number of paths of length k from g to h in $\mathcal{G}$. In particular, $\mathbf{U}^5 = 0$.

Let $\mathbf{f}$ be a fitness landscape on $\mathcal{G}$ and $\mathbf{F} = \operatorname{diag}\big(\mathbf{f}(g) \mid g \in \mathcal{G}\big)$ the $m \times m$ diagonal matrix whose entries are the fitness values. The entry of the matrix product $\mathbf{UF}$ in row g and column h represents the probability of genotype g transitioning into genotype h in one step. A precise probabilistic derivation and interpretation will be given in the next section.

We are interested in *all* mutational pathways that lead from the wild type $\hat{0}$ to the escape state $\hat{1}$. Towards this end, note that the entry (g, h) of the matrix $(\mathbf{UF})^k$ represents the probability of genotype g evolving to genotype h along any mutational pathway (chain) of length k in the genotype lattice $\mathcal{G}$. The chains from $\hat{0}$ to $\hat{1}$ in $\mathcal{G}$ are accounted for by the upper right hand entry of $(\mathbf{UF})^k$. Note that the matrix $(\mathbf{UF})^k$ is zero for $k > n$.

To account for chains of arbitrary length, we consider the matrix

$$(\mathbf{I} - \mathbf{UF})^{-1} - \mathbf{I} \;=\; \mathbf{UF} + (\mathbf{UF})^2 + (\mathbf{UF})^3 + \cdots + (\mathbf{UF})^n, \tag{6.3}$$

where $\mathbf{I}$ is the $m \times m$ identity matrix. We summarize our discussion in the following proposition, which is proved by elementary matrix algebra.

Proposition 6.4. *The entry of the matrix (6.3) in row g and column h is zero unless $g \subset h$, in which case it is $u_{gh} \cdot \mathbf{f}(h) \cdot P_{gh}(\mathbf{f})$ where P_{gh} is a polynomial function of degree $|h \backslash g| - 1$ on the space of all fitness landscapes $\mathbb{R}^{\mathcal{G}}$.*

The polynomial $P_{gh}(\mathbf{f})$ is the generating function for all chains from g to h in $\mathcal{G}$. This will be made precise in the following corollary. We shall restrict ourselves to the most important case when $g = \hat{0}$ is the wild type and $h = \hat{1}$ is the escape state. Studying $P_{\hat{0}\hat{1}}(\mathbf{f})$ only is no loss of generality because any interval of a distributive lattice is again a distributive lattice.

Proposition 6.4 tells us that $P_{\hat{0}\hat{1}}(\mathbf{f})$ is a polynomial of degree $n - 1$ in the unknown fitness values $\mathbf{f}(g)$, which are also written as f_g, where $g \in \mathcal{G}$.

Corollary 6.5. *The polynomial* $P_{\hat{0}\hat{1}}(\mathbf{f})$ *in the upper-right entry of (6.3) equals*

$$P_{\hat{0}\hat{1}}(\mathbf{f}) \quad = \sum_{\hat{0}=g_0\subset g_1\subset\cdots\subset g_k=\hat{1}} f_{g_1}f_{g_2}\cdots f_{g_{k-1}}, \tag{6.4}$$

where the sum runs over all chains from $\hat{0}$ *to* $\hat{1}$ *in the genotype lattice* $\mathcal{G}$.

6.4 The risk of escape

For a poset of events $\mathcal{E}$ and the corresponding distributive lattice $\mathcal{G} = J(\mathcal{E})$, the *risk polynomial* of $\mathcal{G}$ is defined as the polynomial (6.4), which we denote by $\mathcal{R}(\mathcal{G};\mathbf{f})$. The risk polynomial was introduced in [54, 55]. In this section we review the evolutionary dynamics model proposed in these papers, and we discuss the probabilistic meaning of the risk polynomial.

Example 6.6. Let $\mathcal{G}$ be the genotype lattice in Figure 6.2. Then the risk polynomial $\mathcal{R}(\mathcal{G};\mathbf{f})$ is the following polynomial of degree three in six unknowns:

$$\begin{gathered}1 + f_{1000} + f_{0100} + f_{1100} + f_{0101} + f_{1110} + f_{1101}\\ +f_{1000}f_{1100} + f_{0100}f_{1100} + f_{0100}f_{0101} + f_{1000}f_{1110} + f_{0100}f_{1110}\\ +f_{1000}f_{1101} + f_{0100}f_{1101} + f_{1100}f_{1110} + f_{1100}f_{1101} + f_{0101}f_{1101}\\ +f_{1000}f_{1100}f_{1110} + f_{0100}f_{1100}f_{1110} + f_{1000}f_{1100}f_{1101}\\ +f_{0100}f_{1100}f_{1101} + f_{0100}f_{0101}f_{1101}.\end{gathered}$$

If we restrict the fitness landscape $\mathbf{f}$ to lie in a linear subspace of $\mathbb{R}^{\mathcal{G}}$, then $\mathcal{R}(\mathcal{G};\mathbf{f})$ specializes to a polynomial in fewer unknowns. For example, the risk polynomial for graded fitness landscapes is obtained from the specialization $\mathbf{f}(g) = a_{|g|}$. That risk polynomial has degree $n-1$ and is denoted by $\mathcal{R}(\mathcal{G};a_1,\ldots,a_{n-1})$. For instance, $\mathcal{R}(\mathcal{G};\mathbf{f})$ in Example 6.6 specializes to

$$\mathcal{R}(\mathcal{G};a_1,a_2,a_3) = 1 + 2a_1 + 2a_2 + 2a_3 + 3a_1a_2 + 4a_1a_3 + 3a_2a_3 + 5a_1a_2a_3.$$

For constant fitness landscapes $\mathbf{f} \equiv a$, the risk polynomial is a polynomial in one unknown a. It is denoted $\mathcal{R}(\mathcal{G};a)$. In our running example,

$$\mathcal{R}(\mathcal{G};a) \;=\; 1 + 6a + 10a^2 + 5a^3.$$

We now make precise the notion of *risk of escape*, which will justify our definition of the risk polynomial. Our derivation is based on the model for the dynamics of a replicating population on a fitness landscape studied by Iwasa, Michor and Nowak [54, 55]. See also the work of Wilke [105] and the references given therein for approaches to computing fixation probabilities.

A *multistate branching process* [6] consists of a set of genotypes along with a fitness landscape and mutation rates between genotypes. We assume a discrete time process, where in one generation an individual with genotype g has a random number of offspring following a Poisson distribution with mean R_g. Some of these offspring may be mutants according to the mutation rates u_{gh}. The parameter R_g is the *basic reproductive ratio* [69, Chap. 3].

We assume there is no interaction between individuals; each reproduces at a rate independent of the distribution of the population. Let $\rho^k_{g,h}$ be the probability that one individual of genotype g has k children of type h. Then,

$$\rho^k_{g,h} = \frac{(u_{gh}R_g)^k \cdot e^{-u_{gh}R_g}}{k!}. \tag{6.5}$$

The *reproductive fitness* f_g is related to the reproductive ratio R_g by

$$f_g = \frac{R_g}{1-R_g} \qquad \text{and} \qquad R_g = \frac{f_g}{1+f_g}. \tag{6.6}$$

Let ξ_g be the probability of escape starting with one individual of genotype g, so $1-\xi_g$ is the probability of extinction. In particular, $\xi_{\hat{1}}$ is the probability that one resistant virus will not become extinct. Each of these probabilities is a function of the mutation rates u_{gh} and the reproductive ratios R_g. We assume that the u_{gh} are as in (6.2), but with $u_{gg} = 1$. Thus, each escape probability ξ_g can be expressed as a function of the μ_e for $e \in \mathcal{E}$ and (using the relation (6.6)) the fitness values f_g for $g \in \mathcal{G}$.

Theorem 6.7. *If $\xi_g \ll 1$ for $g \neq \hat{1}$, then the probability of escape on the fitness landscape $\mathbf{f} \in \mathbb{R}^{\mathcal{G}}$ starting with one individual of wild type $\hat{0}$, satisfies*

$$\xi_{\hat{0}} \quad \approx \quad \xi_{\hat{1}} \cdot f_{\hat{0}} \cdot \prod_{e\in\mathcal{E}} \mu_e \cdot \mathcal{R}(\mathcal{G};\mathbf{f}). \tag{6.7}$$

Proof. The probability of extinction satisfies the recursive formula

$$1 - \xi_g \quad = \quad \prod_{h \supseteq g} \sum_{k=0}^{\infty} (1 - \xi_h)^k \cdot \rho_{g,h}^k. \tag{6.8}$$

Using (6.5), the right hand side of (6.8) can be rewritten as follows:

$$\prod_{h \supseteq g} \exp((1 - \xi_h) u_{gh} R_g) \cdot \exp(-u_{gh} R_g) \quad = \quad \exp\left(\sum_{h \supseteq g} -\xi_h u_{gh} R_g \right).$$

We conclude that

$$\log(1 - \xi_g) \quad = \quad -\sum_{h \supseteq g} \xi_h u_{gh} R_g \qquad \text{for all } g \in \mathcal{G}.$$

Under the assumption that $\xi_g \ll 1$ for $g \neq \hat{1}$, we can linearize the logarithms using the relation $\log(1 - \xi_g) \approx -\xi_g$. This implies, for $g \in \mathcal{G} \backslash \{\hat{1}\}$,

$$\begin{aligned} \xi_g \quad &\approx \quad R_g \cdot \textstyle\sum_{h \supseteq g} \xi_h u_{gh} \\ &= \quad \tfrac{R_g}{1 - R_g u_{gg}} \cdot \textstyle\sum_{h \supset g} \xi_h u_{gh} \\ &= \quad f_g \cdot \textstyle\sum_{h \supset g} \xi_h u_{gh}. \end{aligned}$$

The theorem now follows by setting $g = \hat{0}$ and expanding the last equation recursively. Here we are using the fact from (6.2) that the product of the u_{gh} over any chain from $\hat{0}$ to $\hat{1}$ in $\mathcal{G}$ equals $\prod_{e \in \mathcal{E}} \mu_e$. □

The typical situation of interest is a fitness landscape for which only the escape state has a basic reproductive ratio greater than one, i.e.,

$$R_{\hat{1}} > 1 \qquad \text{and} \qquad R_g < 1 \quad \text{for all} \quad g \neq \hat{1}.$$

When the positive numbers R_g are very small for $g \in \mathcal{G} \backslash \{\hat{1}\}$ then the approximation (6.7) is valid, and it shows the crucial role that the risk polynomial $\mathcal{R}(\mathcal{G}; \mathbf{f})$ plays in assessing the risk of escape from the wild type $\hat{0}$ to the escape state $\hat{1}$. The theorem implies that the risk of escape of a population of N wild type viruses is $(1 - \xi_{\hat{0}})^N$. In Section 6.8 we discuss the situation in which the population is not homogeneous at the time of intervention.

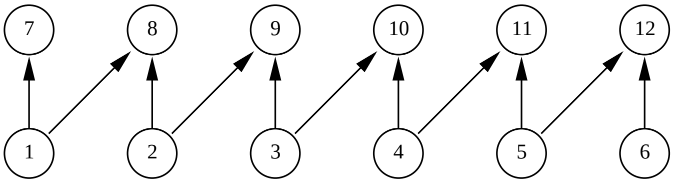

Figure 6.3: An event poset whose general risk polynomial is of degree 11 in 375 unknowns.

The risk of escape is an important quantity in analyzing the invasiveness of pathogens and in assessing the success probability of medical interventions such as chemotherapy. However, putting this concept into practice depends on our ability to actually compute the risk polynomial. It turns out that methods from algebraic combinatorics lead to efficient algorithms for this task. We present several methods in detail in Section 6.7.

Our method of choice from a practical perspective relies on computing linear extensions of the event poset $\mathcal{E}$ (Theorem 6.15). Our software implementation is available at `http://bio.math.berkeley.edu/riskpoly/`. For an example of the efficiency of the software, let $\mathcal{E}$ be the poset in Figure 6.3 on $n = 12$ events with cover relations $i < 6 + i$ for $1 \leq i \leq 6$ and $i < 7 + i$ for $1 \leq i \leq 5$. Here the genotype lattice $\mathcal{G}$ consists of 375 genotypes. The risk polynomial $\mathcal{R}(\mathcal{G}; \mathbf{f})$ is a polynomial of degree 11 in 375 unknowns f_g. This polynomial has 224,750,298 monomials in the 375 unknowns, but we represent it as a sum of 2,702,765 products, one for each linear extension of the event poset $\mathcal{E}$. Our software takes about ten seconds to compute this representation of $\mathcal{R}(\mathcal{G}; \mathbf{f})$. The result takes up 200MB of disk space.

The univariate risk polynomial for this example is

$$1 + 375a + 19088a^2 + 324498a^3 + 2610169a^4 + 11729394a^5 + 32080336a^6 + \\ 55597909a^7 + 61448965a^8 + 42020208a^9 + 16216590a^{10} + 2702765a^{11}.$$

Thus, exact symbolic computations, as opposed to numerical approximations, may be necessary and feasible when one is interested in assessing the risk of escape in applications like the one described in Section 6.6 below.

6.5 Distributive lattices from Bayesian networks

In this section, we present a family of statistical models that naturally gives rise to distributive lattices. This statistical interpretation provides a method for deriving the genotype lattice $\mathcal{G}$ directly from data. The basic idea is to estimate the poset structure on $\mathcal{E}$ from observed genotypes, by applying model selection techniques to a range of Bayesian networks, and to define $\mathcal{G}$ as the set of all genotypes with non-zero probability in the model.

We first make precise the derivation of a genotype space from a statistical model. Let $\mathcal{E}$ be an unordered set of n genetic events. The events are labeled by $1, 2, \ldots, n$. Subsets of $\mathcal{E}$ are identified with binary strings $g \in \{0,1\}^n$. They are the possible genotypes. We consider binary random variables $X_{\mathcal{E}} = (X_1, \ldots, X_n)$, where $X_e = 1$ indicates the occurrence of event e. Let Δ denote the $(2^n - 1)$-dimensional simplex of probability distributions on $\{0,1\}^n$. A *statistical model* for $X_{\mathcal{E}}$ is a map $p\colon \Theta \to \Delta$, where Θ is some parameter space. The g-th coordinate of p, denoted p_g, is the probability of genotype $g \in \{0,1\}^n$ under the model p. The *induced genotype space* of the model $p\colon \Theta \to \Delta$ is the set $\mathcal{G}_p$ of all strings $g \in \{0,1\}^n$ such that p_g is not the zero function on Θ. We regard $\mathcal{G}_p$ as a poset ordered by inclusion.

Now consider a directed acyclic graph on the set of events $\mathcal{E}$. We will also call this graph $\mathcal{E}$. The *Bayesian network model*, or directed acyclic graphical model, defined by $\mathcal{E}$ is the family of joint distributions that factor as

$$\Pr(X_1, \ldots, X_n) \quad = \quad \prod_{e \in \mathcal{E}} \Pr(X_e \mid X_{\mathrm{pa}(e)}),$$

where $\mathrm{pa}(e)$ denotes the set of parents of e in $\mathcal{E}$. Equivalently, a Bayesian network is specified by a set of conditional independence statements. Each node is independent of its ancestors given its parents. See [61] for an introduction to the relevant statistical theory and [51] for an algebraic perspective.

The parameters for a Bayesian network are specified by providing, for each event $e \in \mathcal{E}$, a $2^{|\mathrm{pa}(e)|} \times 2$ matrix θ^e. The matrix entries are

$$\theta^e_{g_{\mathrm{pa}(e)}, g_e} \quad = \quad \Pr\left(X_e = g_e \mid X_{\mathrm{pa}(e)} = g_{\mathrm{pa}(e)}\right),$$

for $g_{\mathrm{pa}(e)} \in \{0,1\}^{\mathrm{pa}(e)}$, $g_e \in \{0,1\}$. These conditional probabilities satisfy

$$\theta^e_{g_{\mathrm{pa}(e)},0} \geq 0\,,\ \ \theta^e_{g_{\mathrm{pa}(e)},1} \geq 0 \quad \text{and} \quad \theta^e_{g_{\mathrm{pa}(e)},0} + \theta^e_{g_{\mathrm{pa}(e)},1} \ = \ 1. \tag{6.9}$$

Set $d = \sum_{e\in\mathcal{E}} 2^{|\mathrm{pa}(e)|}$ and $\Theta = [0,1]^d$. The points in the cube Θ are identified with n-tuples of matrices $\theta = (\theta^e \,|\, e \in \mathcal{E})$ as above. The *general Bayesian network* is the polynomial map $p\colon \Theta \to \Delta$ whose coordinates are

$$p_g(\theta) \ = \ \prod_{e\in\mathcal{E}} \theta^e_{g_{\mathrm{pa}(e)},g_e}. \tag{6.10}$$

The general Bayesian network on $\mathcal{E}$ induces the genotype space $\mathcal{G}_p = \{0,1\}^n$, the Boolean lattice on $\mathcal{E}$. Indeed, the factorization (6.10) implies that no genotype $g \in \{0,1\}^n$ has probability zero for all parameter values.

To obtain other genotype spaces, we replace the cube $\Theta = [0,1]^d$ by one of its faces, as follows. For each event $e \in \mathcal{E}$ consider a Boolean function $\beta_e\colon \{0,1\}^{\mathrm{pa}(e)} \to \{0,1\}$. If $\beta_e(g_e) = 0$ then the row of the $2^{|\mathrm{pa}(e)|} \times 2$-matrix θ^e indexed by the genotype g is fixed to be the vector $(1,0)$; otherwise that row remains indeterminate subject to the constraints (6.9). Let Θ^β denote the face of Θ determined by these requirements and $p^\beta\colon \Theta^\beta \to \Delta$ the restriction of the polynomial map p to Θ^β. The resulting model is the Bayesian network on $\mathcal{E}$ constrained by the Boolean functions β^e.

If all Boolean functions β^e are disjunctions then we get the *disjunctive Bayesian network* on $\mathcal{E}$. In this model, an event e can only occur if at least one of its parent events has already occurred. If all Boolean functions β^e are conjunctions then we get the *conjunctive Bayesian network* on $\mathcal{E}$. In this model, an event e can only occur if all of its parent events have already occurred. These restricted Bayesian network models induce interesting genotype spaces. Our main result in this section concerns the conjunctive case.

We regard the given directed acyclic graph $\mathcal{E}$ as a poset by setting $e_1 \leq e_2$ if there exists a path from e_1 to e_2. We write $p^{\mathrm{conj}}\colon [0,1]^n \to \Delta$ for the conjunctive Bayesian network on $\mathcal{E}$, since it has precisely n free parameters.

Theorem 6.8. *The genotype space induced by the conjunctive Bayesian network on $\mathcal{E}$ is the distributive lattice of order ideals in $\mathcal{E}$, i.e., $\mathcal{G}_{p^{\mathrm{conj}}} = J(\mathcal{E})$.*

Proof. The possible genotypes g are binary strings whose coordinates g_e indicate whether or not the event e has occurred. If p is any of the Bayesian network models discussed above, then (6.10) implies that $g \in \mathcal{G}_p$ if and only if each $\theta^e_{g_{\mathrm{pa}(e)},g_e}$ is non-zero. Consider now the conjunctive model $p = p^{\mathrm{conj}}$. Here, the conditional probability $\theta^e_{g_{\mathrm{pa}(e)},g_e}$ is non-zero if and only if $g_e = 1$ implies $g_{\mathrm{pa}(e)} = (1,\ldots,1)$. This is precisely the condition for g to be an order ideal in $\mathcal{E}$. Thus $\mathcal{G}_p$ is the distributive lattice of order ideals of $\mathcal{E}$. □

The following example illustrates Theorem 6.8, and it compares the genotype spaces induced by the disjunctive and the conjunctive Bayesian network. The former is not a distributive lattice, but the latter always is.

Example 6.9. Let $\mathcal{E}$ be the event poset in Figure 6.2. The general Bayesian network model defined by $\mathcal{E}$ is parametrized by the following four matrices:

$$\begin{array}{l} \theta^1 = \begin{pmatrix} a & 1-a \end{pmatrix}, \\[2ex] \theta^2 = \begin{pmatrix} b & 1-b \end{pmatrix}, \end{array} \qquad \theta^3 = \begin{pmatrix} c_{00} & 1-c_{00} \\ c_{01} & 1-c_{01} \\ c_{10} & 1-c_{10} \\ c_{11} & 1-c_{11} \end{pmatrix}, \qquad \theta^4 = \begin{pmatrix} d_0 & 1-d_0 \\ d_1 & 1-d_1 \end{pmatrix}.$$

The map $p\colon [0,1]^8 \to \Delta$ has coordinates

$$\begin{aligned}
p_{0000} &= abc_{00}d_0, & p_{0001} &= abc_{00}(1-d_0),\\
p_{0010} &= ab(1-c_{00})d_0, & p_{0011} &= ab(1-c_{00})(1-d_0),\\
p_{0100} &= a(1-b)c_{01}d_1, & p_{0101} &= a(1-b)c_{01}(1-d_1),\\
p_{0110} &= a(1-b)(1-c_{01})d_1, & p_{0111} &= a(1-b)(1-c_{01})(1-d_1),\\
p_{1000} &= (1-a)bc_{10}d_0, & p_{1001} &= (1-a)bc_{10}(1-d_0),\\
p_{1010} &= (1-a)b(1-c_{10})d_0, & p_{1011} &= (1-a)b(1-c_{10})(1-d_0),\\
p_{1100} &= (1-a)(1-b)c_{11}d_1, & p_{1101} &= (1-a)(1-b)c_{11}(1-d_1),\\
p_{1110} &= (1-a)(1-b)(1-c_{11})d_1, & p_{1111} &= (1-a)(1-b)(1-c_{11})(1-d_1).
\end{aligned}$$

This model induces the Boolean lattice $\{0,1\}^4$ as the genotype space.

The disjunctive Bayesian network is the six-dimensional submodel obtained by setting $c_{00} = 1$ and $d_0 = 1$. This substitution implies

$$p_{0001} = p_{0010} = p_{0011} = p_{1001} = p_{1011} = 0.$$

The genotype space $\mathcal{G}_{p^{\mathrm{disj}}}$ consists of the remaining eleven strings in $\{0,1\}^4$. Note that $\mathcal{G}_{p^{\mathrm{disj}}}$ is not a lattice because it is not closed under intersections. For instance, 1010 and 0110 are in $\mathcal{G}_{p^{\mathrm{disj}}}$ but $0010 = 1010 \cap 0110 \notin \mathcal{G}_{p^{\mathrm{disj}}}$.

The conjunctive Bayesian network is the four-dimensional submodel obtained by setting $c_{00} = c_{01} = c_{10} = d_0 = 1$. The remaining eight non-zero probabilities are indexed by the eight genotypes in Figure 6.2:

$$\begin{aligned} p_{0000} &= ab\,, & p_{0100} &= a(1-b)d_1\,, \\ p_{0101} &= a(1-b)(1-d_1)\,, & p_{1000} &= (1-a)b\,, \\ p_{1100} &= (1-a)(1-b)c_{11}d_1\,, & p_{1101} &= (1-a)(1-b)c_{11}(1-d_1)\,, \\ p_{1110} &= (1-a)(1-b)(1-c_{11})d_1\,, & p_{1111} &= (1-a)(1-b)(1-c_{11})(1-d_1). \end{aligned}$$

If $\mathcal{E}$ is a directed forest, i.e., if every $e \in \mathcal{E}$ has at most one parent, then we can augment $\mathcal{E}$ to a tree $\mathcal{E}^T$ by adding an auxiliary root node 0 which points to the roots (edges with no parents) of the forest. On the resulting tree $\mathcal{E}^T$ we consider the *mutagenetic tree model* of [12, 31].

Proposition 6.10. *If $\mathcal{E}$ is a directed forest then the following three statistical models coincide: the disjunctive Bayesian network on $\mathcal{E}$, the conjunctive Bayesian network on $\mathcal{E}$, and the mutagenetic tree model on $\mathcal{E}^T$.*

Proof. The disjunctive and the conjunctive networks coincide because they are defined by the same specializations of the parameters θ^e. The identification with the mutagenetic tree model follows from [9, Thm. 14.6]. □

Mutagenetic tree models can be learned from observed data by an efficient combinatorial algorithm. With appropriate edge weights that depend on the pairwise probabilities of events, a mutagenetic tree can be obtained as the maximum weight branching rooted at 0 in the complete graph on $\{0,\ldots,n\}$; see [31]. This gives an efficient method for learning the poset $\mathcal{E}$, and hence the genotype lattice $\mathcal{G} = J(\mathcal{E})$, from data. It would be interesting to extend this model selection technique to arbitrary conjunctive Bayesian networks.

6.6 Applications to HIV drug resistance

We investigate the development of resistance during treatment of HIV infected patients with two different PIs. Consider the seven genetic events

$$\mathcal{E} = \{\text{K20R, M36I, M46I, I54V, A71V, V82A, I84V}\},$$

where K20R stands for the amino acid change from lysine (K) to arginine (R) at position 20 of the protease chain, etc. The occurrence of these mutations confers broad cross-resistance to the entire class of PIs. Appearance of the virus with all 7 mutations renders most of the PIs ineffective for subsequent treatment. We analyze the risk of reaching this escape state under therapy with the PIs ritonavir (RTV) and indinavir (IDV) [25, 66].

We use mutagenetic trees for estimating preferred mutational pathways and for defining genotype lattices. For both drugs, a tree $\mathcal{E}^T$ is learned from genotypes derived from patients under the respective therapy. We used 112 and 691 samples from the Stanford HIV Drug Resistance Database [80] for ritonavir and indinavir, respectively. Figure 6.4 shows the inferred mutagenetic trees. The models indicate that the evolution of ritonavir resistance is partly a linear process, whereas indinavir resistance develops in a less ordered fashion. This is consistent with previous studies [25, 66]. The genotype lattices $\mathcal{G}$ have size 16 for ritonavir and 45 for indinavir. We study the risk polynomials on these lattices under different fitness landscape models.

For the constant fitness landscape on $\mathcal{G}\backslash\{\hat{0}, \hat{1}\}$, we obtain

$$\begin{aligned}
\mathcal{R}_{\text{RTV}}(a) &= 15a^6 + 70a^5 + 131a^4 + 124a^3 + 61a^2 + 14a + 1, \\
\mathcal{R}_{\text{IDV}}(a) &= 420a^6 + 1470a^5 + 1970a^4 + 1250a^3 + 372a^2 + 43a + 1.
\end{aligned}$$

Thus, the risk of developing all seven PI resistance mutations is higher under indinavir therapy than under ritonavir: $\mathcal{R}_{\text{IDV}}(a) > \mathcal{R}_{\text{RTV}}(a)$ for $a > 0$. Intuitively, the risk under ritonavir is lower because the mutations must occur in a certain order. Likewise, the high risk under indinavir results from many mutations occurring independently, which gives rise to a large genotype lattice and to many mutational pathways from the wild type to the escape state.

More realistic fitness landscapes may be derived by modeling viral fitness as a function of drug concentration. We follow the approach pursued in [94] and use a simple

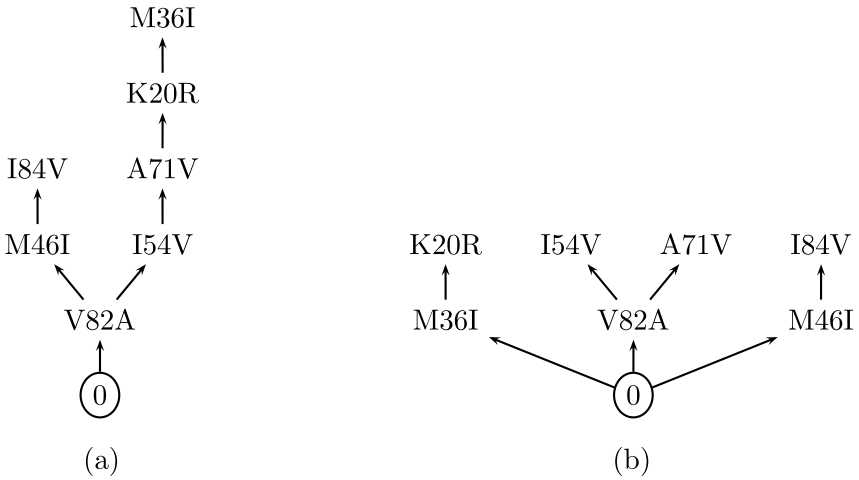

Figure 6.4: Mutagenetic trees $\mathcal{E}^T$ for the development of resistance to (a) ritonavir and (b) indinavir in the HIV-1 protease. The event poset $\mathcal{E}$ is obtained by removing the root node "0".

saturation function for this dependency. Specifically, we assume viral fitness to be the following function of drug concentration D,

$$f_g(D) \quad = \quad \frac{\phi_g}{1 + D/r_g}, \tag{6.11}$$

where ϕ_g denotes the fitness of genotype g in the absence of drug and r_g the IC$_{50}$ value of g, i.e., the drug concentration necessary to inhibit viral replication *in vitro* by 50%. The IC$_{50}$ value is a measure of resistance. We will assume throughout that all $\phi_g \equiv \phi$ are equal. If we assume, in addition, that the resistance landscape is constant on $\mathcal{G} \backslash \{\hat{0}, \hat{1}\}$, with $r_g \equiv r$, then the substitution (6.11) turns the risk polynomial into a rational function in ϕ, D, and r. For example, for ritonavir, this rational function is

$$\frac{(15\phi^2 r^2 + 10\phi D r + 10\phi r^2 + D^2 + 2Dr + r^2)(\phi r + D + r)^4}{(D + r)^6}.$$

In general, the IC$_{50}$ values r_g are distinct and can be determined experimentally for some genotypes by phenotypic resistance testing [103], and may be predicted for all genotypes using regression techniques [8]. PI phenotypic resistance data suggests a graded resistance landscape; see [15] and [25, Tab. 3]. Hence, we estimate the resistance $r \in \mathbb{R}^8$ for ritonavir and indinavir by defining r_k as the mean predicted IC$_{50}$ of all genotypes of rank k. The resulting resistance landscapes are shown in Figure 6.5.

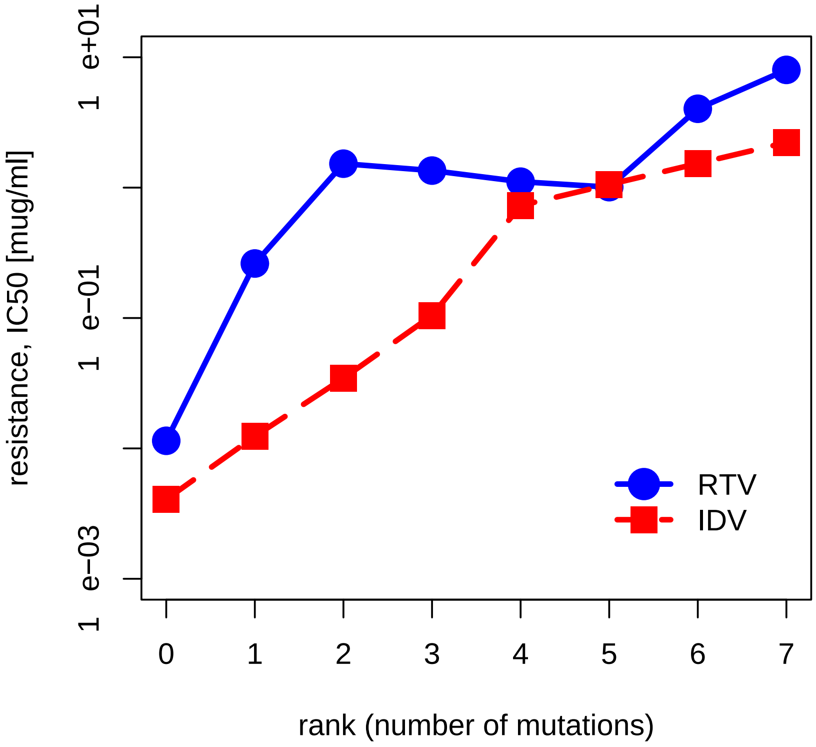

Figure 6.5: Graded resistance landscapes for ritonavir (RTV, bullets) and indinavir (IDV, squares). Resistance is quantified as the drug concentration necessary to inhibit viral replication *in vitro* by 50% (IC_{50}).

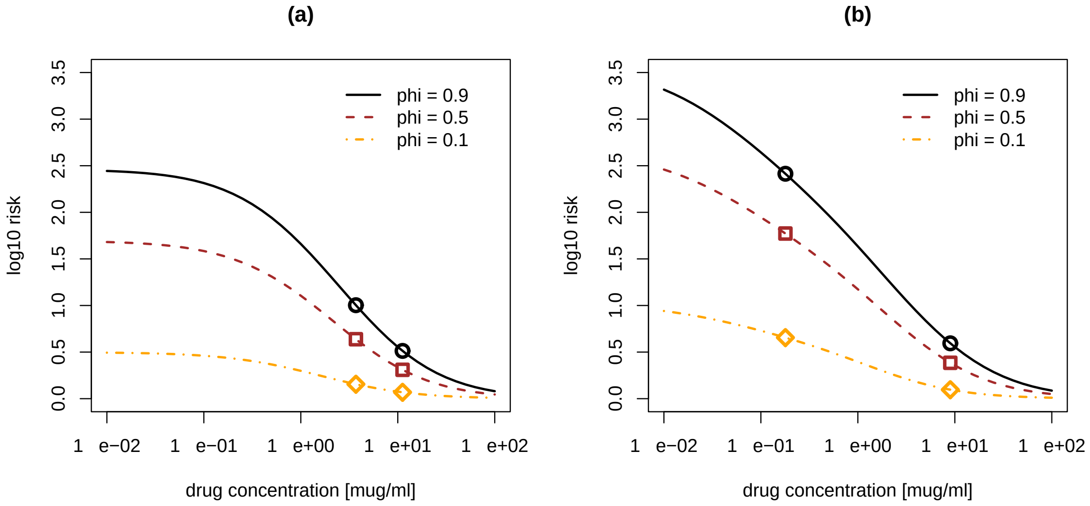

Figure 6.6: Drug dependent risk. The log of the risk polynomial for ritonavir (a) and indinavir (b) is displayed as a function of plasma drug concentration D. Marked values denote mean trough ($C_{\min}$) and peak ($C_{\max}$) levels observed in clinical studies. The parameter ϕ is the relative fitness of mutants as compared to the wild type in the absence of drug.

The graded risk polynomials $\mathcal{R}(a_1, a_2, a_3, a_4, a_5, a_6)$ have 64 terms. After substituting $a_k = \phi/(1 + D/r_k)$, we obtain rational risk functions in D with parameter ϕ. Figure 6.6 illustrates the dependency of the risk on drug concentration for three different values of ϕ. For both drugs we indicate published mean plasma trough ($C_{\min}$) and peak ($C_{\max}$) levels observed in clinical settings.

This example illustrates how the risk polynomial can be used to study viral escape as a function of different parameters. For instance, given a pharmacokinetics model of antiretroviral drug therapy, we can compute the risk of developing resistance after a patient has missed a dose. Thus, our mathematical framework may help in designing robust drug combinations.

6.7 Mathematics and computation of the risk polynomial

Here we discuss in more detail mathematical properties of the risk polynomial and we present several methods for computing it. The given data consists of an n element poset

$\mathcal{E}$ and its induced genotype lattice $\mathcal{G}$, which is the distributive lattice of order ideals in $\mathcal{E}$. We assume that $\mathcal{G}$ has m elements, which are encoded either as subsets of $\mathcal{E}$ or as binary strings in $\{0,1\}^n$. The risk polynomial is the polynomial $\mathcal{R}(\mathcal{G};\mathbf{f})$ in the m unknowns $f_g = \mathbf{f}(g)$, one for each genotype g. We are also interested in specializations of $\mathcal{R}(\mathcal{G};\mathbf{f})$ obtained by setting some (or all) of the unknowns equal to each other, such as the graded risk polynomial and the univariate risk polynomial.

Stanley's linear algebra method

A direct method for computing the risk polynomial is given in Section 6.4. Namely, we can set all μ_e equal to one in the matrix $\mathbf{U}$ and then compute the upper right entry of the matrix $(\mathbf{I} - \mathbf{UF})^{-1} - \mathbf{I}$ of equation (6.3). In practice, one would compute this entry by a dynamic program which runs in time $O(m^2)$. That dynamic program is easily derived by resolving the recursion in the last equation of the proof of Theorem 6.7.

The following alternative linear algebra technique for computing polynomials similar to our risk polynomials was given by Stanley in [89]. Let $\mathcal{G}' = \mathcal{G}\backslash\{\hat{0},\hat{1}\}$ denote the genotype lattice with the top element $\hat{1}$ and the bottom element $\hat{0}$ removed. We define $\mathbf{A}$ to be the *anti-adjacency matrix* of the truncated genotype lattice $\mathcal{G}'$. Thus $\mathbf{A}$ is the $(m-2)\times(m-2)$-matrix with rows and columns indexed by $\mathcal{G}'$, and whose entry in row g and column h is 0 if $g \subset h$ and is 1 otherwise. We write $\mathbf{I}$ for the $(m-2)\times(m-2)$ identity matrix and $\mathbf{F}' = \mathrm{diag}\big(\mathbf{f}(g)\,|\, g \in \mathcal{G}'\big)$ for the $(m-2)\times(m-2)$-diagonal matrix whose entries are the fitness values. Stanley's result reads as follows.

Theorem 6.11 (Stanley [89]). *The risk polynomial* $\mathcal{R}(\mathcal{G};\mathbf{f})$ *equals the determinant of the* $(m-2)\times(m-2)$*-matrix* $\mathbf{I} + \mathbf{F}'\cdot\mathbf{A}$.

Example 6.12. Let $\mathcal{G}$ be the genotype lattice in Figure 6.2. Then $m = 8$ and $\mathbf{I} + \mathbf{F}'\cdot\mathbf{A}$

is the 6×6-matrix

$$\begin{array}{c|cccccc}
 & 1000 & 0100 & 1100 & 0101 & 1110 & 1101 \\
\hline
1000 & 1+f_{1000} & f_{1000} & 0 & f_{1000} & 0 & 0 \\
0100 & f_{0100} & 1+f_{0100} & 0 & 0 & 0 & 0 \\
1100 & f_{1100} & f_{1100} & 1+f_{1100} & f_{1100} & 0 & 0 \\
0101 & f_{0101} & f_{0101} & f_{0101} & 1+f_{0101} & f_{0101} & 0 \\
1110 & f_{1110} & f_{1110} & f_{1110} & f_{1110} & 1+f_{1110} & f_{1110} \\
1101 & f_{1101} & f_{1101} & f_{1101} & f_{1101} & f_{1101} & 1+f_{1101}
\end{array}.$$

The determinant of this matrix is the risk polynomial of Example 6.6.

The Hilbert series method

A more conceptual way of thinking about the risk polynomial is based on the following algebraic construction. The *Stanley-Reisner ideal* $I_{\mathcal{G}'}$ of $\mathcal{G}'$ is the ideal generated by all quadratic monomials $f_g \cdot f_h$ where g and h are genotypes that are incomparable, i.e., neither $g \subseteq h$ nor $h \subseteq g$ holds. The ambient polynomial ring $S = \mathbb{R}[\mathbf{f}]$ is generated by the unknowns f_g where $g \in \mathcal{G}'$. The *Hilbert series* of $I_{\mathcal{G}'}$ is the formal sum over all monomials $\mathbf{f}^u = \prod_{g \in \mathcal{G}'} f_g^{u_g}$ which are not in the ideal $I_{\mathcal{G}'}$. This is a formal generating function which can be written as a rational function of the following form

$$H(S/I_{\mathcal{G}'}; \mathbf{f}) \quad = \quad \frac{K_{\mathcal{G}}(\mathbf{f})}{\prod_{g \in \mathcal{G}'}(1 - f_g)}.$$

Here $K_{\mathcal{G}}(\mathbf{f})$ is a polynomial in the unknowns f_g with integer coefficients. The polynomial $K_{\mathcal{G}}(\mathbf{f})$ is known as the *K-polynomial* of the ideal $I_{\mathcal{G}'}$. We refer to [65] for an introduction to Stanley-Reisner ideals and their K-polynomials.

If $\mathcal{E}$ is a directed forest (and we identify $f_g = p_g$) then Proposition 6.10 and [9, Thm. 14.11] imply that the ideal $I_{\mathcal{G}'}$ is an initial monomial ideal of the conjunctive Bayesian network on $\mathcal{E}$. In a forthcoming paper we shall prove that this initial ideal property holds for all event posets (not just trees).

Example 6.13. Let $\mathcal{G}$ be the genotype lattice in Figure 6.2. Then

$$I_{\mathcal{G}'} \quad = \quad \langle\, f_{0101} f_{1110},\ f_{1101} f_{1110},\ f_{0101} f_{1100},\ f_{0101} f_{1000},\ f_{0100} f_{1000} \rangle$$

is indeed the initial monomial ideal of the conjunctive Bayesian network in Example 6.9. The K-polynomial $K_{\mathcal{G}}(\mathbf{f})$ equals

$$\begin{gathered} 1 - f_{0101}f_{1110} - f_{1101}f_{1110} - f_{0101}f_{1100} - f_{0101}f_{1000} - f_{0100}f_{1000} \\ +f_{0100}f_{1000}f_{0101} + f_{1000}f_{0101}f_{1100} + f_{1000}f_{0101}f_{1110} + f_{0101}f_{1100}f_{1110} \\ +f_{0101}f_{1110}f_{1101} + f_{0100}f_{1000}f_{1110}f_{1101} \\ -f_{1000}f_{0101}f_{1100}f_{1110} - f_{0100}f_{1000}f_{0101}f_{1110}f_{1101}. \end{gathered}$$

Again using Proposition 6.10 and Theorem 14.11 in [9] we see that the risk polynomial $\mathcal{R}(\mathcal{G};\mathbf{f})$ is the sum of all squarefree monomials in the expansion of the Hilbert series $H(S/I_{\mathcal{G}'};\mathbf{f})$. Equivalently, $\mathcal{R}(\mathcal{G};\mathbf{f})$ is the reduction of $H(S/I_{\mathcal{G}'};\mathbf{f})$ modulo the ideal generated by the squares f_g^2 of the unknowns. Since $1/(1-f_g)$ equals $1+f_g$ modulo $\langle\, f_g^2 \,\rangle$, we have the following result.

Proposition 6.14. *The risk polynomial $\mathcal{R}(\mathcal{G};\mathbf{f})$ of the genotype lattice $\mathcal{G}$ is the sum of all squarefree terms in the expansion of*

$$K_{\mathcal{G}}(\mathbf{f}) \cdot \prod_{g\in\mathcal{G}'} (1+f_g),$$

where $K_{\mathcal{G}}(\mathbf{f})$ is the K-polynomial of the Stanley-Reisner ideal $I_{\mathcal{G}'}$.

The univariate risk polynomial $\mathcal{R}(\mathcal{G};a)$ is derived from $\mathcal{R}(\mathcal{G};\mathbf{f})$ by replacing each f_g by the scalar unknown a. We have

$$\mathcal{R}(\mathcal{G};a) \quad = \quad c_0 + c_1a + c_2a^2 + \cdots + c_{n-1}a^{n-1},$$

where c_i is the number of chains of length i in $\mathcal{G}'$. Thus, $(c_0,\ldots,c_{n-1})$ is the f-vector of the simplicial complex of chains in $\mathcal{G}'$. Likewise, we get the graded risk polynomial from $\mathcal{R}(\mathcal{G};\mathbf{f})$ by replacing each f_g by $a_{|g|}$. We note that the graded risk polynomial is related to Ehrenborg's quasi-symmetric function encoding [42] of the flag f-vector of the chain complex of $\mathcal{G}'$.

The linear extensions method

One advantage of both Theorem 6.11 and Proposition 6.14 is that these formulas do not actually depend on the fact that $\mathcal{G}$ is a distributive lattice. They also apply if the set $\mathcal{G}$

of genotypes is an arbitrary poset. This is relevant for our discussion of the statistical models in Section 6.5, where we introduced a more general class of posets $\mathcal{G}_p \subseteq \{0,1\}^n$.

This advantage is also a disadvantage: Theorem 6.11 and Proposition 6.14 do not give the most efficient methods for computing $\mathcal{R}(\mathcal{G};\mathbf{f})$ when $\mathcal{G}$ is the distributive lattice induced by an event poset $\mathcal{E}$. In what follows we present a specialized and more efficient algorithm for the risk polynomial. The input to this algorithm consists of the event poset $\mathcal{E}$. It is not necessary to compute the genotype lattice $\mathcal{G}$ as this will be done as a byproduct of our approach, which is to compute the risk polynomial $\mathcal{R}(\mathcal{G};\mathbf{f})$ directly from $\mathcal{E}$.

As before, we assume that $\mathcal{E}$ has n elements, and we write $[n]$ for the linearly ordered set $\{1,2,\ldots,n\}$. A *linear extension* of $\mathcal{E}$ is an order-preserving bijection $\pi\colon \mathcal{E} \to [n]$. This means that $e < e'$ in $\mathcal{E}$ implies $\pi(e) < \pi(e')$. Every linear extension $\pi\colon \mathcal{E} \to [n]$ gives rise to an ordered list of $n-1$ genotypes $g^{(1)}, g^{(2)}, \ldots, g^{(n-1)}$ in $\mathcal{G}' = \mathcal{G}\backslash\{\hat{0},\hat{1}\}$ as follows. The genotype $g^{(i)}$ is the subset of $\mathcal{E}$ consisting of all events whose image under π is among the first i positive integers. In symbols, $g^{(i)} = \pi^{-1}(\{1,2,\ldots,i\})$. The sequence $g^{(1)}, g^{(2)}, \ldots, g^{(n-1)}$, derived from π, represents a mutational pathway in $\mathcal{G}$.

We now fix one distinguished linear extension of $\mathcal{E}$, that is, we identify the set underlying $\mathcal{E}$ with $[n]$ itself. Then a linear extension is simply any permutation π of $[n]$ which preserves the order relations in $\mathcal{E}$. We define

$$\mathbf{f}(\pi) \quad = \quad \prod_{i:\pi(i)<\pi(i+1)} (f_{g^{(i)}} + 1) \cdot \prod_{i:\pi(i)>\pi(i+1)} f_{g^{(i)}}, \tag{6.12}$$

where i runs over $\{1,2,\ldots,n-1\}$. Our algorithm amounts to evaluating the risk polynomial by means of the following explicit summation formula.

Theorem 6.15. *The risk polynomial $\mathcal{R}(\mathcal{G};\mathbf{f})$ equals the sum of the products $\mathbf{f}(\pi)$ where π runs over all linear extensions of the event poset $\mathcal{E}$.*

Proof. The relationship between chains in $\mathcal{G}$ and linear extensions of $\mathcal{E}$ is the content of [90, Prop. 3.5.2]. The distributive lattice $\mathcal{G}$ has a canonical *R-labeling* [90, Sec. 3.13] which assigns to each edge of the Hasse diagram of $\mathcal{G}$ the corresponding element of $\mathcal{E}$. In view of this R-labeling, Exercise 59d in [90, Chap. 3] tells us that the poset $\mathcal{G}' = \mathcal{G}\backslash\{\hat{0},\hat{1}\}$ is *chain-partitionable.* Each product $\mathbf{f}(\pi)$ as in (6.12) is the generating function for all the chains in precisely one part of that chain partition of $\mathcal{G}'$. Adding up all products gives the generating function for all chains, which is the risk polynomial. □

Example 6.16. The event poset $\mathcal{E}$ in Figure 6.2 has five linear extensions π:

π	$\mathbf{f}(\pi)$
$(1,2,3,4)$	$(1+f_{1000})(1+f_{1100})(1+f_{1110})$
$(1,2,4,3)$	$(1+f_{1000})(1+f_{1100})f_{1101}$
$(2,1,3,4)$	$f_{0100}(1+f_{1100})(1+f_{1110})$
$(2,1,4,3)$	$f_{0100}(1+f_{1100})f_{1101}$
$(2,4,1,3)$	$(1+f_{0100})f_{0101}(1+f_{1101})$

The sum of these five products equals the risk polynomial $\mathcal{R}(\mathcal{G};\mathbf{f})$.

Implementation

Pruesse and Ruskey [77] showed that the linear extensions of a poset $\mathcal{E}$ can be computed in time linear in the number of linear extensions. Thus, their algorithm computes $\mathcal{R}(\mathcal{G};\mathbf{f})$ in time linear in the size of the output of Theorem 6.15. That output is in factored form (6.12) and is always more compact than the expanded risk polynomial. In this manner, we compute the risk polynomial in time sublinear in the size of the expanded risk polynomial.

To obtain the univariate risk polynomial, we take the sum of the terms $(1+a)^{n-1-\delta}a^{\delta}$, where $\delta=\delta(\pi)$ is the number of descents of the linear extension π. Similarly, the graded risk polynomial $\mathcal{R}(\mathcal{G};a_1,\ldots,a_{n-1})$ is found by keeping track of the descent set of each linear extension π. We believe that this method is best possible for general posets $\mathcal{E}$. Notice that the leading term of the univariate risk polynomial is the number of linear extensions of $\mathcal{E}$, and it is #P-complete to count linear extensions [19].

When $\mathcal{E}$ is a directed forest, the recursive structure can be used to help compute the risk polynomial. In this case, $\mathcal{E}$ is built up by the operations of disjoint union and ordinal sum from the one element poset. For example, in the univariate case, the zeta polynomial [90, Sec. 3.11] of $\mathcal{G}$ behaves nicely under these operations and can be used to write down the risk polynomial. Based on these considerations, we can design an efficient algorithm for computing the univariate risk polynomial of a directed forest.

Using the method of Theorem 6.15, we have developed software for computing risk polynomials. The input to our program is an arbitrary event poset $\mathcal{E}$, and the output is the risk polynomial, the graded risk polynomial or the univariate risk polynomial. Optionally, the user can also input either exact fitness values or upper and lower bounds for each fitness value. The output in this case is either the exact risk of escape or upper and lower bounds for the risk. It is designed to integrate with the package `Mtreemix` [13], allowing the user to start with data, infer a mutagenetic tree, and then easily compute the risk polynomial. Our software is available at `http://bio.math.berkeley.edu/riskpoly/` We use the algorithm of [101] for computing linear extensions. Although this algorithm isn't asymptotically optimal (see [77]), it is simple to implement and efficient in practice.

6.8 Discussion

We have presented a computational framework for assessing the risk of escape of an evolving population of pathogens. The risk of escape is the probability that the population reaches an escape state before extinction. In virus transmissions, for example, this probability is the chance of survival in the new host. In the situation of antiretroviral therapy, the risk of escape is the probability of therapy failure due to the development of drug resistance.

The general setup we consider for computing the risk of escape includes an event poset, a fitness landscape on its induced genotype lattice, and a branching process on this lattice. The event poset $\mathcal{E}$ consists of all mutational events that can occur and encodes the constraints which apply to their order of occurrence. From this structure the genotype space $\mathcal{G}$ is obtained by considering all mutational pathways that respect the order constraints. This natural construction endows $\mathcal{G}$ with the mathematical structure of a distributive lattice. The risk polynomial, the crucial factor in computing the risk of escape, turns out to coincide with the chain polynomial of the genotype lattice. We have presented methods from algebraic combinatorics that exploit this connection and that result in efficient algorithms.

The space of genotypes may also be inferred from observed genotype data using statistical model selection tools. We have identified a class of Bayesian network models, the conjunctive Bayesian networks, whose support induces a genotype lattice. Mutagenetic tree models arise as important special cases. Here, both statistical model selection and risk computation are particularly efficient, and readily available with existing software [13] coupled with our implementation of the linear extensions method (Theorem 6.15).

We have focused on the dependency of the risk polynomial on the fitness landscape and considered throughout a homogeneous wild type population prior to intervention. However, the risk of escape is calculated similarly for a quasispecies distribution at the time of intervention. In fact, this involves computing the risk polynomial of the prior fitness landscape [54]. In contrast, the branching process model can not account for recombination, horizontal gene transfer, or frequency dependent selection, since evolution is assumed to take place in multiple lineages independently.

The main challenge in using our method to compute the risk of escape from antiretroviral therapy lies in accurately modeling the fitness landscape. The dependency (6.11) of the fitness on drug concentration may be improved by experimentally determined viral replicative capacities in the absence of drugs. An alternative approach to derive a fitness landscape for HIV-1 proteases is based on estimating the binding affinity of the drug to the mutant protease, and the mutant's ability to cleave its natural substrates [82]. These calculations are based on simplified molecular modeling techniques. The resulting fitness landscape does not account for different drug levels, but it is independent of experimental resistance and fitness data.

Escape from indinavir and ritonavir therapy may in some cases involve mutations other than the seven we considered, although those are the most frequent mutations observed after therapy failure [25, 66]. On the other hand, viral escape might be accomplished with genotypes that harbor fewer than all of the mutations. Thus it would be desirable to compute the risk of reaching any of several escape states, rather than only the $11\cdots1$ type. This computation will involve similar techniques to those presented in Sections 6.4 and 6.7.

Finally, the PIs form only one out of four distinct classes of antiretroviral drugs that are in current clinical use. The standard of care is combination therapy with at least three different drugs from two different drug classes. Modeling the fitness landscape of combination therapy in terms of viral drug resistance and drug exposure is even more challenging, but can eventually help in designing optimal antiretroviral therapies. Algebraic combinatorics offers tools for the mathematical analysis of these biomedical problems.

Bibliography

[1] Jameel Al-Aidroos and Sagi Snir. Analysis of point mutations in vertebrate genomes. In L. Pachter and B. Sturmfels, editors, *Algebraic Statistics for Computational Biology*, chapter 21, pages 375–386. Cambridge University Press, Cambridge, UK, 2005.

[2] ES Allman and JA Rhodes. Phylogenetic invariants for the general Markov model of sequence mutation. *Mathematical Biosciences*, 186(2):113–144, 2003.

[3] ES Allman and JA Rhodes. Phylogenetic ideals and varieties for the general Markov model. `http://arxiv.org/abs/math.AG/0410604`, 2004.

[4] ES Allman and JA Rhodes. Quartets and parameter recovery for the general Markov model of sequence mutation. *AMRX Applied Mathematics Research Express*, 2004(4):107–131, 2004.

[5] M Ashburner, CA Ball, JA Blake, D Botstein, H Butler, JM Cherry, K Dolinski, SS Dwight, JT Eppig, MA Harris, et al. Gene Ontology: tool for the unification of biology. The Gene Ontology Consortium. *Nature Genetics*, 25:25–29, 2000.

[6] K.B. Athreya and P.E. Ney. *Branching processes*. Dover, Mineola, New York, 1972.

[7] Matthias Beck and Dennis Pixton. The Ehrhart polynomial of the Birkhoff polytope. *Discrete Comput. Geom.*, 30(4):623–637, 2003.

[8] Niko Beerenwinkel, Martin Däumer, Mark Oette, Klaus Korn, Daniel Hoffmann, Rolf Kaiser, Thomas Lengauer, Joachim Selbig, and Hauke Walter. Geno2pheno:

Estimating phenotypic drug resistance from HIV-1 genotypes. *Nucleic Acids Res*, 31(13):3850–3855, Jul 2003.

[9] Niko Beerenwinkel and Mathias Drton. Mutagenetic tree models. In L. Pachter and B. Sturmfels, editors, *Algebraic Statistics for Computational Biology*, chapter 14, pages 278–290. Cambridge University Press, Cambridge, UK, 2005.

[10] Niko Beerenwinkel, Nicholas Eriksson, and Bernd Sturmfels. Evolution on distributive lattices. *Journal of Theoretical Biology*, 2006.

[11] Niko Beerenwinkel, Lior Pachter, and Bernd Sturmfels. Epistasis and shapes of fitness landscapes. http://www.arxiv.org/abs/q-bio.PE/0603034, 2006.

[12] Niko Beerenwinkel, Jörg Rahnenführer, Martin Däumer, Daniel Hoffmann, Rolf Kaiser, Joachim Selbig, and Thomas Lengauer. Learning multiple evolutionary pathways from cross-sectional data. *J Comput Biol*, 12(6):584–598, 2005. RECOMB 2004.

[13] Niko Beerenwinkel, Jörg Rahnenführer, Rolf Kaiser, Daniel Hoffmann, Joachim Selbig, and Thomas Lengauer. Mtreemix: a software package for learning and using mixture models of mutagenetic trees. *Bioinformatics*, 21(9):2106–2107, May 2005.

[14] G Bejerano, M Pheasant, I Makunin, S Stephen, WJ Kent, JS Mattick, and D Haussler. Ultraconserved elements in the human genome. *Science*, 304:1321–1325, 2004.

[15] B. Berkhout. HIV-1 evolution under pressure of protease inhibitors: Climbing the stairs of viral fitness. *J. Biomed. Sci.*, 6:298–305, 1999.

[16] Louis J. Billera, Susan P. Holmes, and Karen Vogtmann. Geometry of the space of phylogenetic trees. *Adv. in Appl. Math.*, 27(4):733–767, 2001.

[17] D Boffelli, MA Nobrega, and EM Rubin. Comparative genomics at the vertebrate extremes. *Nature Reviews Genetics*, 5:456–465, 2004.

[18] Nicolas Bray and Lior Pachter. MAVID: constrained ancestral alignment of multiple sequences. *Genome Research*, 14(4):693–9, 2004.

[19] Graham Brightwell and Peter Winkler. Counting linear extensions. *Order*, 8(3):225–242, 1991.

[20] M Brudno, S Malde, A Poliakov, C Do, O Couronne, I Dubchak, and S Batzoglou. Global alignment: finding rearrangements during alignment. *Special issue on the Proceedings of the ISMB 2003, Bioinformatics*, 19:54i–64i, 2003.

[21] Marta Casanellas, Luis David Garcia, and Seth Sullivant. Catalog of small trees. In L. Pachter and B. Sturmfels, editors, *Algebraic Statistics for Computational Biology*, chapter 15, pages 291–304. Cambridge University Press, Cambridge, UK, 2005.

[22] J.A. Cavender and J. Felsenstein. Invariants of phylogenies: A simple case with discrete states. *J. Classif.*, 4:57–71, 1987.

[23] Franois Clavel and Allan J. Hance. HIV drug resistance. *N. Engl. J. Med.*, 350(10):1023–1035, Mar 2004.

[24] S. Collart, M. Kalkbrener, and D. Mall. Converting bases with the Gröbner walk. *J. Symbolic Comput.*, 24(3-4):465–469, 1997. Computational algebra and number theory (London, 1993).

[25] J.H. Condra, D.J. Holder, W.A. Schleif, O.M. Blahy, R.M. Danovich, L.J. Gabryelski, D.J. Graham, D. Laird, J.C. Quintero, A. Rhodes, H.L. Robbins, E. Roth, M. Shivaprakash, T. Yang, J.A. Chodakewitz, P.J. Deutsch, R.Y. Leavitt, F.E. Massari, J.W. Mellors, K.E. Squires, R.T. Steigbigel, H. Teppler, and E.A. Emini. Genetic correlates of in vivo viral resistance to indinavir, a human immunodeficiency virus type 1 protease inhibitor. *J. Virol.*, 70(12):8270–8276, 1996.

[26] ENCODE Project Consortium. The ENCODE (ENCyclopedia Of DNA Elements) Project. *Science*, 306(5696):636–40, 2004.

[27] David Cox, John Little, and Donal O'Shea. *Ideals, varieties, and algorithms.* Undergraduate Texts in Mathematics. Springer-Verlag, New York, second edition, 1997. An introduction to computational algebraic geometry and commutative algebra.

[28] J.A. De Loera, D. Haws, R. Hemmecke, P. Huggins, J. Tauzer, and R. Yoshida. A user's guide for latte v1.1. Available at `http://www.math.ucdavis.edu/~latte/`, 2003.

[29] W.L. DeLano. The PyMOL molecular graphics system. Available at `http://www.pymol.org`, 2002.

[30] JW Demmel. *Applied Numerical Linear Algebra.* Society for Industrial and Applied Mathematics (SIAM), Philadelphia, PA, 1997.

[31] R Desper, F Jiang, O-P Kallioniemi, H Moch, CH Papadimitriou, and AA Schäffer. Inferring tree models for oncogenesis from comparative genome hybridization data. *Journal of Computational Biology*, 6(1):37–51, 1999.

[32] C Dewey. MERCATOR: multiple whole-genome orthology map construction. Available at `http://hanuman.math.berkeley.edu/~cdewey/mercator/`, 2005.

[33] Colin Dewey, Peter Huggins, Kevin Woods, Lior Pachter, and Bernd Sturmfels. Parametric alignment of drosophila genomes. *PLoS Computational Biology*, 2006. To appear.

[34] Persi Diaconis. *Group Representations in Probability and Statistics*, volume 11 of *IMS Lecture Series.* Institute of Mathematical Statistics, 1988.

[35] Persi Diaconis. A generalization of spectral analysis with application to ranked data. *Ann. Statist.*, 17(3):949–979, 1989.

[36] Persi Diaconis and Bradley Efron. Testing for independence in a two-way table: new interpretations of the chi-square statistic. *Ann. Statist.*, 13(3):845–913, 1985.

[37] Persi Diaconis and Nicholas Eriksson. Markov bases for noncommutative Fourier analysis of ranked data. *J. Symbolic Comput.*, 41(2):182–195, 2006.

[38] Persi Diaconis and D. Freedman. Partial exchangeability and sufficiency. In J.K. Ghosh and J. Roy, editors, *Statistics: Applications and New Directions*, pages 205–236, Calcutta, 1984. Indian Statistical Institute.

[39] Persi Diaconis and Bernd Sturmfels. Algebraic algorithms for sampling from conditional distributions. *Ann. Statist.*, 26(1):363–397, 1998.

[40] Mathias Drton, Nicholas Eriksson, and Garmay Leung. Ultra-conserved elements in vertebrate and fly genomes. In L. Pachter and B. Sturmfels, editors, *Algebraic Statistics for Computational Biology*, chapter 22, pages 387–402. Cambridge University Press, Cambridge, UK, 2005.

[41] Rick Durrett. Genome rearrangement. In *Statistical methods in molecular evolution*, Stat. Biol. Health, pages 307–323. Springer, New York, 2005.

[42] Richard Ehrenborg. On posets and Hopf algebras. *Adv. Math.*, 119(1):1–25, 1996.

[43] Nicholas Eriksson. Toric ideals of homogeneous phylogenetic models. In *ISSAC 2004*, pages 149–154. ACM, New York, 2004.

[44] Nicholas Eriksson. Tree construction using singular value decompsition. In L. Pachter and B. Sturmfels, editors, *Algebraic Statistics for Computational Biology*, chapter 19, pages 347–358. Cambridge University Press, Cambridge, UK, 2005.

[45] Nicholas Eriksson, Kristian Ranestad, Bernd Sturmfels, and Seth Sullivant. Phylogenetic algebraic geometry. In C. Ciliberto, A. Geramita, B. Harbourne, R-M. Roig, and K. Ranestad, editors, *Projective varieties with unexpected properties*, pages 237–255. Walter de Gruyter GmbH & Co. KG, Berlin, 2005.

[46] Joseph Felsenstein. *Inferring Phylogenies.* Sinauer Associates, Sunderland, 2003.

[47] Joseph Felsenstein. Phylip (phylogeny inference package) version 3.6. Available at `http://evolution.genetics.washington.edu/phylip.html`, 2005.

[48] Ronald A. Fisher. *Statistical methods for research workers.* Hafner Publishing Co., New York, 1973.

[49] A Frieze, R Kannan, and S Vempala. Fast Monte Carlo algorithms for low rank approximation. In *39th Symposium on Foundations of Computing*, pages 370–378, 1998.

[50] William Fulton. *Introduction to toric varieties*, volume 131 of *Annals of Mathematics Studies*. Princeton University Press, Princeton, NJ, 1993. The William H. Roever Lectures in Geometry.

[51] Luis David Garcia, Michael Stillman, and Bernd Sturmfels. Algebraic geometry of Bayesian networks. *Journal of Symbolic Computation*, 39/3-4:331–355, 2004. Special issue on the occasion of MEGA 2003.

[52] G.-M. Greuel, G. Pfister, and H. Schönemann. SINGULAR 3.0. A Computer Algebra System for Polynomial Computations, Centre for Computer Algebra, University of Kaiserslautern, 2005. `http://www.singular.uni-kl.de`.

[53] Raymond Hemmecke and Ralf Hemmecke. 4ti2 version 1.1—computation of Hilbert bases, Graver bases, toric Gröbner bases, and more. Available at `www.4ti2.de`, September 2003.

[54] Yoh Iwasa, Franziska Michor, and Martin A. Nowak. Evolutionary dynamics of escape from biomedical intervention. *Proc Biol Sci*, 270(1533):2573–2578, Dec 2003.

[55] Yoh Iwasa, Franziska Michor, and Martin A. Nowak. Evolutionary dynamics of invasion and escape. *J Theor Biol*, 226(2):205–214, Jan 2004.

[56] Anders N. Jensen. Gfan, a software system for Gröbner fans. Available at `http://home.imf.au.dk/ajensen/software/gfan/gfan.html`.

[57] Anders N. Jensen. Cats, a software system for toric state polytopes. Available at `http://www.soopadoopa.dk/anders/cats/cats.html`, 2003.

[58] Eric Kuo. Geometry of Markov chains. In L. Pachter and B. Sturmfels, editors, *Algebraic Statistics for Computational Biology*, chapter 10, pages 226–236. Cambridge University Press, 2005.

[59] JA Lake. A rate-independent technique for analysis of nucleaic acid sequences: evolutionary parsimony. *Molecular Biology and Evolution*, 4:167–191, 1987.

[60] J. M. Landsberg and L. Manivel. On the ideals of secant varieties of Segre varieties. *Found. Comput. Math.*, 4(4):397–422, 2004.

[61] SL Lauritzen. *Graphical models*, volume 17 of Oxford Statistical Science Series. The Clarendon Press Oxford University Press, New York, 1996. Oxford Science Publications.

[62] Jun Liu. *Monte Carlo techniques in scientific computing.* Springer, New York, 2001.

[63] J. Marden. *Analyzing and modeling rank data.* Chapman and Hall, London, 1995.

[64] Jon D. McAuliffe, Lior Pachter, and Michael I. Jordan. Multiple-sequence functional annotation and the generalized hidden Markov phylogeny. *Bioinformatics*, 20(12):1850–60, 2004.

[65] Ezra Miller and Bernd Sturmfels. *Combinatorial commutative algebra*, volume 227 of *Graduate Texts in Mathematics.* Springer-Verlag, New York, 2005.

[66] A. Molla, M. Korneyeva, Q. Gao, S. Vasavanonda, P. J. Schipper, H. M. Mo, M. Markowitz, T. Chernyavskiy, P. Niu, N. Lyons, A. Hsu, G. R. Granneman, D. D. Ho, C. A. Boucher, J. M. Leonard, D. W. Norbeck, and D. J. Kempf. Ordered accumulation of mutations in HIV protease confers resistance to ritonavir. *Nat Med*, 2(7):760–766, Jul 1996.

[67] SY Ng, P Gunning, R Eddy, P Ponte, J Leavitt, T Shows, and L Kedes. Evolution of the functional human beta-actin gene and its multi-pseudogene family: conservation of noncoding regions and chromosomal dispersion of pseudogenes. *Molecular and Cellular Biology*, 5:2720–2732, 1985.

[68] MA Nobrega, I Ovcharenko, V Afzal, and EM Rubin. Scanning human gene deserts for long-range enhancers. *Science*, 302(5644):413, 2003.

[69] M.A. Nowak and R.M. May. *Virus dynamics.* Oxford University Press, 2000.

[70] S Ota and WH Li. Njml: A hybrid algorithm for the neighbor-joining and maximum likelihood methods. *Molecular Biology and Evolution*, 17(9):1401–1409, 2000.

[71] Lior Pachter and Bernd Sturmfels. Parametric inference for biological sequence analysis. *Proc. Natl. Acad. Sci. USA*, 101(46):16138–16143 (electronic), 2004.

[72] Lior Pachter and Bernd Sturmfels. Tropical geometry of statistical models. *Proc. Natl. Acad. Sci. USA*, 101(46):16132–16137 (electronic), 2004.

[73] Lior Pachter and Bernd Sturmfels. *Algebraic Statistics for Computational Biology.* Cambridge University Press, Cambridge, UK, 2005.

[74] Lior Pachter and Bernd Sturmfels. The mathematics of phylogenomics. *SIAM Review*, 2006.

[75] T Peters, R Dildrop, K Ausmeier, and U Ruther. Organization of mouse iroquois homeobox genes in two clusters suggests a conserved regulation and function in vertebrate development. *Genome Research*, 10:1453–1462, 2000.

[76] TD Pollard. Genomics, the cytoskeleton and motility. *Nature*, 409:842–843, 2001.

[77] Gara Pruesse and Frank Ruskey. Generating linear extensions fast. *SIAM J. Comput.*, 23(2):373–386, 1994.

[78] A Rambaut and NC Grassly. Seq-Gen: An application for the Monte Carlo simulation of DNA sequence evolution along phylogenetic trees. *Comput. Appl. Biosci.*, 13:235–238, 1997.

[79] Christian M. Reidys and Peter F. Stadler. Combinatorial landscapes. *SIAM Review*, 44:3–54, 2002.

[80] Soo-Yon Rhee, Matthew J Gonzales, Rami Kantor, Bradley J Betts, Jaideep Ravela, and Robert W Shafer. Human immunodeficiency virus reverse transcriptase and protease sequence database. *Nucleic Acids Res*, 31(1):298–303, Jan 2003.

[81] Ruy M. Ribeiro and Sebastian Bonhoeffer. Production of resistant HIV mutants during antiretroviral therapy. *PNAS*, 97(14):7681–7686, 2000.

[82] C.D. Rosin, R.K. Belew, G.M. Morris, A.J. Olson, and D.S. Goodsell. Coevolutionary analysis of resistance-evading peptidomimetic inhibitors of HIV-1 protease. *Proc. Natl. Acad. Sci. U.S.A.*, 96:1369–1374, 1999.

[83] N Saitou and M Nei. The neighbor-joining method: a new method for reconstructing phylogenetic trees. *Mol Biol Evol*, 4:406–425, 1987.

[84] A Sandelin, P Bailey, S Bruce, PG Engström, JM Klos, WW Wasserman, J Ericson, and B Lenhard. Arrays of ultraconserved non-coding regions span the loci of key developmental genes in vertebrate genomes. *BMC Genomics*, 5:99, 2004.

[85] D Sankoff and M Blanchette. Comparative genomics via phylogenetic invariants for Jukes-Cantor semigroups. In *Stochastic models (Ottawa, ON, 1998)*, volume 26 of *Proceedings of the International Conference on Stochstic Models*, pages 399–418. American Mathematical Society, Providence, RI, 2000.

[86] Charles Semple and Mike Steel. *Phylogenetics*, volume 24 of *Oxford Lecture Series in Mathematics and its Applications*. Oxford University Press, Oxford, 2003.

[87] A Siepel and D Haussler. Combining phylogenetic and hidden markov models in biosequence analysis. *Journal of Computational Biology*, 11:413–428, 2004.

[88] A. Silverberg. Statistical models for q-permutations. *Proc Biopharm. Sec. Amer. Statist. Assoc.*, pages 107–112, 1984.

[89] Richard P. Stanley. A matrix for counting paths in acyclic digraphs. *J. Combin. Theory Ser. A*, 74(1):169–172, 1996.

[90] Richard P. Stanley. *Enumerative combinatorics. Vol. 1*, volume 49 of *Cambridge Studies in Advanced Mathematics*. Cambridge University Press, Cambridge, 1997.

[91] M. Steel, L. Székely, P. Erdös, and P. Waddell. A complete family of phylogenetic invariants for any number of taxa under Kimura's 3st model. *New Zealand Journal of Botany*, 31:289–296, 1993.

[92] M A Steel and Y X Fu. Classifying and counting linear phylogenetic invariants for the Jukes-Cantor model. *J Comput Biol*, 2(1):39–47, Spring 1995.

[93] H. Stern. Probability models on rankings and the electoral process. In M. Fligner and J. Verducci, editors, *Probability models and statistical analyses for ranking data*, pages 173–195. Springer, 1993.

[94] N.I. Stilianakis, C.A. Boucher, M.D. De Jong, R. Van Leeuwen, R. Schuurman, and R.J. De Boer. Clinical data sets of human immunodeficiency virus type 1 reverse transcriptase resistant muatnts explained by a mathematical model. *J. Virol.*, 71(1):161–168, 1997.

[95] V Strassen. Rank and optimal computation of generic tensors. *Linear Algebra Appl.*, 52/53:645–685, 1983.

[96] K Strimmer and A von Haeseler. Quartet puzzling: A quartet maximum likelihood method for reconstructing tree topologies. *Molecular Biology and Evolution*, 13:964–969, 1996.

[97] B Sturmfels and S Sullivant. Toric ideals of phylogenetic invariants. *Journal of Computational Biology*, 12:204–228, 2005.

[98] Bernd Sturmfels. *Gröbner bases and convex polytopes*, volume 8 of *University Lecture Series*. American Mathematical Society, Providence, RI, 1996.

[99] Bernd Sturmfels. Equations defining toric varieties. In *Algebraic geometry—Santa Cruz 1995*, volume 62 of *Proc. Sympos. Pure Math.*, pages 437–449. Amer. Math. Soc., Providence, RI, 1997.

[100] J. H. van Lint and R. M. Wilson. *A course in combinatorics*. Cambridge University Press, Cambridge, second edition, 2001.

[101] Yaakov L. Varol and Doron Rotem. An algorithm to generate all topological sorting arrangements. *Comput. J.*, 24(1):83–84, 1981.

[102] J. Verducci. *Discriminating between two probabilities on the basis of ranked preferences*. PhD thesis, Stanford University, 1982.

[103] H. Walter, B. Schmidt, K. Korn, A. M. Vandamme, T. Harrer, and K. Überla. Rapid, phenotypic HIV-1 drug sensitivity assay for protease and reverse transcriptase inhibitors. *J. Clin. Virol.*, 13:71–80, 1999.

[104] Michael S. Waterman. Applications of combinatorics to molecular biology. In *Handbook of combinatorics, Vol. 1, 2*, pages 1983–2001. Elsevier, Amsterdam, 1995.

[105] C.O. Wilke. Probability of fixation of an advantageous mutant in a viral quasispecies. *Genetics*, 163:467–474, 2003.

[106] A Woolfe, M Goodson, DK Goode, P Snell, GK McEwen, T Vavouri, SF Smith, P North, H Callaway, K Kelly, et al. Highly conserved non-coding sequences are associated with vertebrate development. *PLoS Biology*, 3:7, 2005.

[107] Z Yang. PAML: A program package for phylogenetic analysis by maximum likelihood. *CABIOS*, 15:555–556, 1997.